NOVEL OPTICAL DEVICES BASED ON SILICONE OPTICAL TECHNOLOGY (SOT) AND THEIR APPLICATIONS FOR CHEMICAL AND BIOLOGICAL ANALYSIS

チャクリヤ, マラスク

NOVEL OPTICAL DEVICES BASED ON SILICONE OPTICAL TECHNOLOGY (SOT) AND THEIR APPLICATIONS FOR CHEMICAL AND BIOLOGICAL ANALYSIS

CHACRIYA MALASUK

2020

九州大学
KYUSHU UNIVERSITY

Novel optical devices based on Silicone Optical Technology (SOT) and their applications for chemical and biological analysis

By

Chacriya Malasuk

A thesis submitted to Kyushu University
for the degree of Doctor of Engineering

Department of Electrical and Electronic Engineering
Graduate School of Information Science and Electrical Engineering
Kyushu University
Fukuoka, Japan

September 2020

Abstract

Nowadays, small, portable, low cost and fast fabricated analytical devices have been interested because of their availability and flexibility for on-demand and on-site chemical and biological applications. The measurement instrumentation in analytical chemistry has also been developed to a new design which is emphasized on small detection system using photometric instruments and portable instrument due to the drawbacks of traditional optical system as expensive and unwieldy. Novel method for fabrication of optical system was proposed to be compact, tiny, lightweight, and easy prototype for use in chemical and biological analysis. In addition, potential optical properties of low noise detection and high sensitivity has been required to improve in optical devices for determination of chemical and biological compound in real samples.

In **chapter 1**, the introduction, including principle of analytical chemistry, a pleasing modern analytical technique termed flow injection analysis (FIA), three-dimensional (3D) printing technique for analytical chemistry, the background of novel fabrication technique for the optical device termed silicone optical technology (SOT), and chemical and biological applications in this study were explained. In addition, objectives of this work were also described in this chapter.

In **chapter 2**, materials, 3D printing process and optical detector in this work were described.

Abstract

In **chapter 3**, a quasi-spatial filter that was previously demonstrated based on silicone optical technology (SOT) was combined with a light source of light emitting diode (LED), 24-well microplate (6 × 4 wells), and color sensors (Red-Green-Blue-Infrared) called of the SOT compact microplate reader to use for the continuous cell monitoring. This chapter presents a compact microplate reader that can measure cell activity and cell environment in a 24-well microplate continuously using the detection of optical absorption. The proposed compact microplate reader provided benefits of upkeep and control of cell production and discrimination. The SOT-spatial filter which showed an excellent effect of noise reduction was embedded in similar size with the cell culture microwell plates that is convenience for use to monitor cell state. Light reflection or light scattering can be absorbed by the special optical filter and only straight light can be transmitted. The fabricated compact microplate reader allows real-time cell monitoring during cell cultivation and culture medium condition in the clean room by uniting with the SOT spatial filter. In addition, this proposed device was possible to investigate concentration continuously and pH of cell culture in real time. A cell activity was also detected using the proposed device. These results showed that the newly developed device is a warranting tool for monitoring of cell conducts for quality control of cell without altering the cell culture surroundings.

In **chapter 4**, The new compact and flexible optical module using fast digital fabrication was proposed based on a concept of silicone optical technology (SOT) using in analytical technique of flow-injection analysis (FIA). A mold free optical module with additive planting of quasi-spatial filter (QSF) for straightforward optical detection was demonstrated. In this work, 3D printed silicone rough-frame was embedding SOT-QSF

simple injecting and coating method for trapping unwanted light signal. The simple coaxial structure of SOT-QSF using clear PDMS core and carbon black doped PDMS clad was fabricated by injecting and coating of carbon-dispersed-PDMS on an optical channel of the 3D printed optical module. The coating properties as optical trapping layer and optical trapping efficiency was performed. These embedding technique and method development that is a rapid on-demand-fabrication will be beneficial for the application in analytical chemistry with general FIA research.

In **chapter 5**, currently, trend of devices in analytical chemistry has become low cost, portable, and tiny due to the adjustability and accessibility for on-site measurement applications. In this work, a fully flexible compact optical device using digital fabrication of 3D printing was demonstrated based on the concept of SOT for flow injection analysis (FIA) system as SOT-FIA optical device. A simple core and cladding structure using optical core of clear polydimethylsiloxane (PDMS) and a cladding of carbon black doped PDMS performs as a simple and tiny optical filter that can trap the tilted incident light as noise signal. A simple injection coating method was used to embed the structure of SOT optical filter. The coating properties and the optical properties of the proposed device were evaluated. The results show that the developed optical module successfully provided a 99.8% trapping efficiency of unexpected light and noise level was lower than 0.5% demonstrating the low noise level detection of the developed optical module. This proposed optical module was combined with FIA system and absorbance sensor of Ushio picoExplorer™ using for colorimetric determination of iron in natural water samples. An outstanding linearity, a broad chemical analysis range, and acceptable percentage recovery performance were observed.

Moreover, the results of iron contents in real water samples using the proposed optical device were validated with the results from the traditional spectrophotometric method. This inexpensive, movable, simple, adjustable, and highly sensitive optical device was potentially useful for on-site chemical analysis measurements.

In **chapter 6**, a proposed SOT-FIA optical device was used for light absorption in a flow enzyme-linked immunosorbent assay (ELISA) method by enzymatic reaction of polyaniline using aniline, H_2O_2 and horseradish peroxidase (HRP) enzyme. A radical polymerization of aniline to polyaniline is rapidly formed via the enzymatic reaction. This rapid reaction rate provides a benefit for flow ELISA. In this work, the flow competitive ELISA for determination of 3-phenoxybenzoic acid (3PBA) was investigated by an anti-3-phenoxybenzoic acid monoclonal antibody (mAb). The competitive ELISA was performed on a Y-shaped channel acrylic plate. An acrylonitrile butadiene styrene (ABS) resin beads with 1 mm diameter were filled in the Y channel to enhance the surface area for the mAb immobilization. The SOT-FIA optical device fabricated by a 3D printing and injection coating method which was made of polydimethylsiloxane (PDMS) as optical core and PDMS containing carbon black as cladding of optical trapping layer can significantly decrease light scattering. The acrylic flow chip and the SOT-FIA optical device was connected by the flow tube and combined with a blue LED as a light source for the flow ELISA. The results of flow response showed that the absorbance changes were related to the enzymatic reaction and the flow competitive ELISA with the proposed optical device was achieved for quantitative analysis of 3PBA in the range of 3PBA concentration from 0.2 to 2 ppm. Also, the proposed

FIA competitive ELISA was applied in real sample of an artificial urine that showed no significant matrix effect of the artificial urine on the ELISA.

In **chapter 7**, based on concept of silicone optical technology (SOT) advantages in optical properties for low noise detection with compact package, use of common matrix of polydimethylsiloxane (PDMS), and easy integrated optical equipment, thus, in this work, a rapid design and digital fabrication of SOT optical modules was proposed for chemical analysis via flow injection analysis technique and a compact absorbance meter picoExplorer™. A rapid digital fabrication of 3D printing method was used to create the 3D printed mold or frame. A simple structure based on SOT concept which optical core used transparent PDMS mixed with rutile particle of titanium dioxide (TiO_2) as W-PDMS and a cladding used carbon black dispersed PDMS (K-PDMS) was fabricated by casting the PDMS on the 3D printed mold/frame. This structure acts as a spatial filter which is small and simply fabricated showing the ability of trapping the tilted incident light. The TiO_2 dispersed into PDMS provided a special benefit in optical properties for enhancing of the optical sensitivity due to increasing the amount of scattered light by the white pigment of TiO_2. This optical module was designed to directly mount on a LED light source and the absorbance color sensors of red-green-blue (RGB) at 45 degrees to the flow channel to increase the detection length. The effects of the percentage of white pigment of TiO_2 (%wt. of W-PDMS) and the effect of the detection length were investigated an improvement of optical sensitivity. The enhancement of 35 to 45 times of the sensitivity of detection was achieved compared to the calculation from the Beer-Lambert's law theory. In addition, the optical property of reduction noise effect was observed with lower than 1% of different percentage of RGB signal between

dark room and light room. The proposed optical module integrated with a FIA system with compact LED detection system was achieved to determine iron in drinkable tap water samples. An outstanding linearity, a broad dynamic range, low limit of detection, good percentage recovery, and high precision were observed to confirm the usefulness of the proposed optical system. The results from our proposed method also agreed well with the traditional spectrophotometric method. The design of the proposed optical device shows newly developed and evaluated.

In **chapter 8**, the conclusions of all chapters were summarized.

Contents

List of tables

List of figures

Chapter 1

Introduction

Chapter 1

1.1 Analytical chemistry

Analytical chemistry studies and uses instruments and methods used to separate, identify, and quantify matter [1]. It is science involved with qualitative analysis which identifies desired compound or analytes in the sample, and quantitative analysis which determines the numerical amount or concentration of analytes in the sample by using instrumentation and robots specifically developed to prepare and analyze the sample. Practically, the entire analysis in analytical chemistry composed of separation, identification or quantification. Analytical chemists need to use their understanding of chemistry, computer, instrumentation, and statistics to fix problems in almost every area of chemistry. Thing that analytical chemists do is to prepare appropriate sample by specific method, measure sample using proper instrument and interpret read out data in appropriate contexts and outcomes. There are two difference method in analytical chemistry as classical method or wet chemical methods and modern method or instrumental method. The classical methods are extraction, and distillation precipitation for qualitative analysis of classical methods. The color, odor, radioactivity, reactivity, melting point or boiling point were observed, and the changes of volume or mass were observed in term of quantitative analysis of the classical method. The flow injection analysis, chromatography, electrophoresis or field flow fractionation were used to separate and quantify the amount of chemical compounds by the instrumental method. Thus, the new instrumental method is very convenient to investigate the compounds in qualitative and quantitative analysis. In addition, the other instruments used the ability of electric fields, magnetic fields, heat interaction, and light interaction were commonly utilized for many application in analytical chemistry area. Analytical chemistry has applications

including in environmental analysis, materials analysis, bioanalysis, clinical analysis and forensic science [2].

The case of quantitative analysis in analytical chemistry, important analytical characteristics are required to report for considering of the utilization of the developed method for useful applications. These analytical parameters are the factors that guarantee the quality of the chemical analysis using the developed methods from analytical chemists. The significant parameters are described the meaning and the importance below;

1. Calibration curve, linearity of the method; a detector response (signal response) observed by many detection systems used for measuring the chemical compound or analyte; for example, an optical signal as absorbance, the electrical signal as voltage, i.e., is investigated in function of relative concentration of analyte. The relationship between the signal responses and concentrations of the analytes is then plotted as calibration curve. The linearity is presented in the regression equation. This equation is used for investigation of the analyte concentration in the sample, which is the result of quantitative analysis.

2. Linear range is a range of linear relationship between detector responses and the analyte concentrations. The linear range is sometimes called working range which is the range that is reliable for investigation the analyte concentration is the sample.

3. Dynamic range is the ratio between the largest and smallest values that a certain quantity or in the linear range can assume. It is often used in the circumstance of signals, for example sound, volt, light. It is measured either as a ratio or as a base-10 (decibel) or base-2 (doublings,

bits or stops) logarithmic value of the difference between the smallest and largest signal values [3].

4. Sensitivity is the smallest change of quantity or analyte concentration which the instrument or detector can detect by a measurement.

5. Selectivity is the selective chemical reaction of the analyte to the specific reagent. Other chemicals cannot be reacted to the reagent except the analyte.

6. Detection limit or limit of detection (LOD) is the lowest quantity/concentration of analyte that can be distinguished from a blank value with a stated confidence level [4]. The LOD is defined as the probability density function for normally distributed measurements at the blank of 3 times of standard deviation of the blank.

7. Quantitation limit is the lowest quantity/concentration of analyte that can be reliably measure by the detector. It is defined as 10 times of standard deviation of the blank.

8. Accuracy is a measurement of the closeness of the experimental value to the actual amount of the substance or analyte in the matrix [5]. Commonly, the spiked recovery is used to investigate the accuracy of the analytical method, which is defined as the percentage of the amount of observed analyte concentration recovered from the matrix compared to the nominal concentration of analyte.

9. Precision is measurement of how close individual measurements are to each other [5], which is defined as the deviation of the results from each replicates of the measurement.

Normally, the deviation can be calculated represented as %RSD, equals to the percentage of the standard deviation (SD) divided by mean or average value of the result.

10. Robustness is the tolerances of the analytical method to the chemical and physical interferences, for example heat, light, basic-acid condition i.e.

11. Sample throughput is the speed of the measurement of sample per hour (the amount of samples that can measure in an hour).

Analytical chemistry research is largely developed by investigation of the analytical performance including linear range, dynamic range, selectivity, sensitivity, detection limit, accuracy, precision, robustness, and speed or sample throughput. The cost which sums up of purchase, operation, training, time, and space is also one of the factors that was concerned in analytical chemistry application. Also, development in new determinations method for trace chemical compounds or difficultly observed compounds is one role of the analytical chemists.

1.2 Flow injection analysis

Flow injection analysis (FIA) is one of the analytical chemistry techniques. It is a highly efficiently automated method of chemical analysis referred the injection of sample into carrier stream or reagent stream in tubing closed system. The principle of the FIA method was injecting a plug of sample into a flowing carrier stream that mixes with reagents and then mixed solution of sample and reagent will transport to reach a detector for measurement and data analysis. FIA was developed in the mid-1970s by Ruzicka and Hansen in Denmark and Stewart and coworkers in United States as a new effective technique for the automated

analyses of samples and this technique allows for the rapid with an unlimited number of samples of sequential analysis. FIA is the modern technique in analytical chemistry with benefits of versatile, simple, and fast analysis for use in various application for quantitative analysis of chemical compounds [6]. In addition, it can be highly repeated, adapt to micro-miniaturization, limit chemicals in close system, reduce waste chemicals, and use small amount of reagent economically in the level of microliter. The main point of FIA is the formation of well-defined concentration gradient when an analyte or sample is injected into the reagent stream. Thus, this phenomenon offers a highly reproducible analyte to reagent ratios. Also, and the accurate time of flow operation is provided from excellent control over the reaction conditions [7].

1.2.1 The phenomenon of flow injection analysis system

The main phenomenon occurred in flow injection analysis system is laminar flow. As normal, the sample is injected into the carrier stream providing the rectangular flow profile of width (w) as shown in Fig. 1.1-part a. After the plug of sample moving through the mixing and reaction zone, the width of the sample plug is increased because of dispersion of the sample into the carrier stream. The dispersion is from two processes, one is convection due to the flow of the carrier stream and two is diffusion due to the concentration gradient between the sample and the carrier stream. Convection occurs by laminar flow. Because the difference of the linear velocity of the sample at the tube's walls and at the center (a linear velocity of the sample at the tube wall is zero whereas the linear velocity of the sample at the center is twice time of carrier stream), it provides a parabolic flow profile occurred in FIA

system (Fig. 1.1-part b). Then, the different linear velocity at the center and the edge of tubing was occurred by radial diffusion. At the edge of tubing, the velocity was higher than at the center and diffusion can maintain the integrity of the flow profile of the sample (Fig. 1.1-part c). Both convection and diffusion make magnificent effect on dispersion from approximately 3–20 sec which is the normal time scale for a FIA after the sample's injection. After approximately 25 secs, flow profile was affected by the diffusion which can observe as Figure 1.1-part d [8].

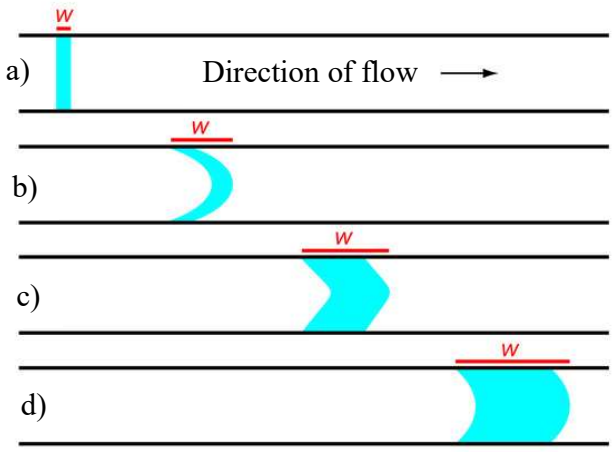

Fig. 1.1 Effect of dispersion on the sample flow profile at various time of flowing solution in FIA system a) at the time of injection, b) the convection overcomes the dispersion, c) the convection and the diffusion conduct to dispersion, and d) the diffusion overcomes the dispersion [8].

1.2.2 Basic component of flow injection analysis system

The basic components of a flow injection analysis system include reservoir for storing of reagent as the carrier stream, propelling unit uses for moving of carrier stream and maintaining a constant flow of the carrier. Normally, the peristatic pump or syringe pump was used as propelling unit in FIA system for transport the stream. The propelling unit possibly controls the flow rates from 0.0005–40 mL/min which is more than adequate to meet the needs of FIA (0.5–2.5 mL/min in common). The FIA system also has the tubing that comprises the transport system, the sample injector part as injection value for injecting the sample into carrier stream, the mixing coil using for mixing the sample with reagent stream and providing reaction zones before reaching the flow-cell of detector for measurement the signal of target compound reaction/assay. The electrochemical and optical detectors are the most common detectors used in FIA system. Fig. 1.2 presents the schematic of simplest design of flow injection analysis system consisting of a single channel and one reagent reservoir call single channel manifold. The reagent stream is set independent each other line stream. All line stream must be merged before the carrier stream gets to the detector. The complete transport system is called a manifold. Nowadays, the FIA system has been developed to dual and multi-channel FIA system for complicated chemical analysis. These complicated FIA systems can transport two or more reagent streams with the complex transported line for mixing the standard analyte or sample. The manifold can design for many applications in chemical and biological analysis. Thus, the design of manifold is very important in the research of analytical chemistry.

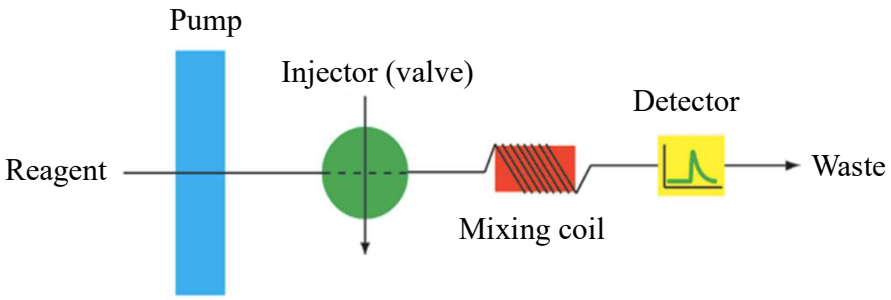

Fig. 1.2 Illustration of a simple flow injection analysis system showing its basic components. The sample is injected into the carrier stream of the reagent and then mixed and reacted to provide the sample signal before reaching to the detector. The reacted solution was flow to waste and next injection can continue to measure next sample [8].

1.2.3 The flow injection analysis results

The response signal from detector when is plotted as function of the time provides the FIA curves or FIAgram. Example of typical FIAgram shows in Fig. 1.3 for conditions in which both convection and diffusion leads the dispersion of the sample. Also, several parameters for characterizing a FIAgram of the sample are described as following;

t_a = Travel time, time between the sample injection and the arrival of its leading edge at the detector

T = Residence time, the time required to obtain the maximum signal of detector response

t' = the time difference between travel time and residence time

Δt = time between the arrival of the leading edge to the departure of its tailing edge

T' = The elapsed time between the maximum signal and its return to the baseline is the return time

h = sample peak height related to the analyte concentration in sample

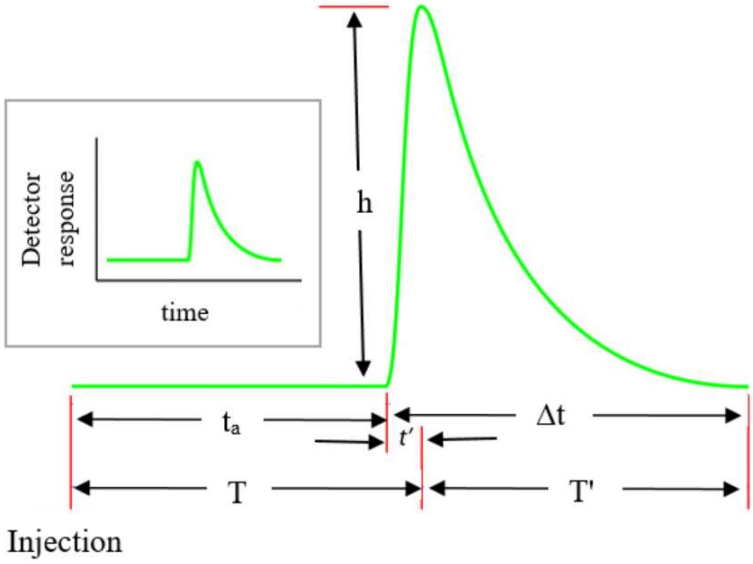

Fig. 1.3 Typical FIAgram for flow injection analysis showing the detector [8]

For development of FIA for variety of applications, the parameters of time need to optimize due to highly sensitive measuring of sequentially chemical analysis of FIA system. The quantitative analysis of FIA system can be obtained from linear calibration curve plotted from the relationship between external standards (containing known concentrations of analyte) peak heights of detector responses and the known nominal concentrations. For example, the format of calibration curve can be plotted between absorbance versus concentration in case of optical detector, and potential versus concentration in case of electrochemical detector, which is depended on the method of detection. Then the sample

peak height is used for calculation of analyte concentration in the sample from linear regression of calibration curve. The precision and accuracy of the FIA method can be comparable with conventional method. Also, the selectivity is often better than the related traditional method of analysis, because the kinetic nature of the measurement process cause slow reaction of other potential interferents compared to reaction of analyte and the close system of FIA from storage of samples and reagents in closed reservoir and their transportation in tubing cause low contamination from external sources.

A calibration curve is investigated by injecting a series of known concentrations of analyte as external standards for quantitative analysis in flow injection method. The formats of calibration curve exemplify plots of the response of light absorption as absorbance versus concentration or electrochemical detection as potential versus concentration which it is depended on the method of detection. Over past three decades, FIA techniques evolved into a wide impressive display of applications as clinical, environmental, pharmaceutical, agricultural, and industrial applications using spectrophotometry, fluorescence spectroscopy, mass spectrometry, atomic absorption spectroscopy, and other methods of instrumental analysis for detection [9].

1.2.4 Detection system in flow injection analysis system; absorption spectroscopy

The goal of the analytical method is to apply the developed method for determination of the target analyte in the real samples that have different matrices. Thus, the selective detection system in FIA is required towards a given target analyte. The common detection system in flow injection analysis is absorptive molecular spectrophotometry in the UV/Vis

range because it is widely available and usually low cost than other kinds of instruments for detection. There are many optical equipment using in the FIA system. Traditionally, the spectrophotometers coupled with flow cuvettes was used. Then the fiber optics, light emitting diode (LED)-based optoelectronic detectors [10] were developed for miniaturizing the detection system using in FIA system. The sensitivity of the absorption spectroscopic detection in FIA system can be essentially enhanced by the light waveguide capillary cell [11]. For example, trace determination of iron in water [12] or wine [13] samples, and trace determination of Copper [14].

In the last 20 years ago, a miniaturization of instruments with photometric detection has been developed in design of analytical measuring instrumentation as portable instruments for on-site measurements. The light-emitting diodes (LED) was particularly used as use as light sources [15]. in the 1980s, the LED detector was used for absorptive measurements in first applications in detection systems [16]. It was used in capillary electrophoresis, chromatographic detectors, and microfluidics analysis. The other applications of the LED as luminescence and spectro-electrochemical measurements were applicable because of ability to use in deep-UV region to the mid-IR region [17]. LEDs has sufficient for use in photometric analytical because of the width of the emission bands, however the unavoidable nonlinearity of Lambert–Beer's law can be observed depended on the matching of the absorbance band of the analytes and the LED emission spectra. The LEDs detector was successfully utilized in FIA system with linear response presented in recently applications For example, the blue LED at λ = 470 nm was used for iron determination using isothiocyanate [18], and LED-based detector at $\lambda = 540 \pm 10$ nm was used for determination

of chromium with 1,5-diphenylcarbazide that were presented a good precision results with better LOD values compared to the common spectrophotometric method using a diode array [19].

The LED based flow cell was recently reported with use of light-dependent resistor for light absorption detection. It was used for determination of pesticide paraquat by using sodium dithionite as a reducing agent. The results in natural water samples showed no matrix interference of other herbicides [20]. For further complex detection system, the LED-based photometric detectors which a fused-LED sensor and an optical probe integrating two optoelectronic components were achieved [21,22]. The application of LED-based photometric detector was published as the FIA system for enzymatic determination of urea [23]. A pH changes resulting from an enzymatic reaction with use of bromothymol blue dye was demonstrated with photometric detection of a two LED-based flow cell that incorporated with tubular PVC reactor with triacetate cellulose membrane/ immobilized urease that united both urease and Bromothymol Blue. Other application was applied for determinations of nitrate in water based on the chromotropic acid [24]. The 3D printed LEDs flow cell was used for absorbance measurements. The use of silicon photodiodes and LEDs as detectors was compared and the LED photocurrents were ten times lower, and generally, the faster setting times of photodiode provided better signals and precision [25].

Even though the selective detector for specific analyte is required for using in the real applications of flow injection analysis system, the development of new improved flow-through detectors and optimization of conditions for their applications, together with

permanent simplify of sample-processing steps is also needed when the detector response is not sufficient. Thus, the improvement of sensitivity of the detection is very important for chemical and biological applications since the ability for determination of some trace analyte compounds is requested.

1.3 3D printing technique

3D printing is an additive manufacturing (AM) process defined as the process of joining materials to make 3D objects via computer control of 3D model design. The process formed the object layer by layer which is deducts the step of fabrication of traditional machining [26,27]. Because the design and control of the 3D printing is digital process by 3D computer aids design (CAD) program as computer aids design and the printer program, the 3D printed material can be fabricated in many complex and sophisticated geometries without need of post-processing. The users can freely design their unique products and create for their specific desire of use. Firstly, a CAD file which is the sketch of the structure or device is prepared in 3D virtual model of the object for the printing process. Next, the process converted a 3D CAD through a digital standard tessellation language (STL) file into a physical product is required. The 3D CAD sketch file is broken down into a series of horizontal layers. The computer controls the printer to print one layer at time. The layers are stacked in the vertical (z axis) direction which each layer relates to the print resolution in the z direction. To achieve a coherent build of previous layer to another layer, supporting structures which bonding the layers to make the object without the fall of layers by gravity was built by the printing software. The supporting layers can be removed after the object is

completely printed. Then the last process is printing process or making product. The STL file is sent to the 3D printer. The printer need setting before the final part is fabricated. The fabricated process of 3D printing can be divided into seven unique methods as described below [28-31];

1. Material extrusion – the process that selectively dispense materials through a nozzle or orifice called fused deposition modelling (FDM), and robocasting/direct ink writing (DIW). The material used in the process is thermoplastic polymers and composite materials, such as glass and carbon- reinforced composites.

2. Binder jetting - the process that selectively deposit a liquid bonding agent to join powder materials called 3D printing (3DP), and binder jetting (BJG). The material used in the process is metals composites, including alloys based on Al, Cu, Fe, Ni and Co, as well as silica, glass and graphite- based ceramics.

3. Material jetting - the process that selectively deposit droplets of build material called continuous inkjet printing (CIJ), drop-on-demand (DoD), multijet modelling (MJM), and polyjet modelling (PJM). The material used in the process is UV- curable photopolymers, typically acrylates, epoxides, or urethanes.

4. Directed energy deposition - the process that use focused thermal energy to fuse materials by melting as they are being deposited called laser engineered net shaping (LENS), directed light fabrication (DIF), and direct metal deposition (DMD). The material used in the process

is metal powders, including aluminium, stainless steel, nickel- based alloys, titanium, copper, and cobalt.

5. Powder bed fusion - the process that selectively fuses regions of a powder bed by thermal energy called direct metal laser sintering (DMLS), electron- beam melting (EBM), laser sintering (LS), and selective heat sintering (SHS). The material used in the process is metal alloys, polymers, such as nylon-12, polypropylene (PP) and PEEK, some experimental ceramics, and reinforced composites.

6. Sheet lamination - the process that bond sheets of material to form an object called laminated object manufacturing (LOM), and ultrasonic additive manufacturing (UAM). The material used in the process is sheets of paper, thermoplastics such as PVC and softer metals such as aluminium or copper.

7. Vat photopolymerization - the process that selectively cure liquid photopolymer in a vat by light- activated polymerization called two- photon polymerization (2PP), continuous liquid interface production (CLIP), digital light processing (DLP), and stereolithography (SL). The material used in the process is UV- curable photopolymers, typically acrylates, epoxides or urethanes.

Each process is unique in the method and material used in the printing process. However, all processes are based on the sequential layer- by-layer deposition of print material. Due to many processes of the 3D printing technique, various applications of chemical and biological analysis can be succeeded using 3D printing technique with simple and easy prototyping as a main advantage.

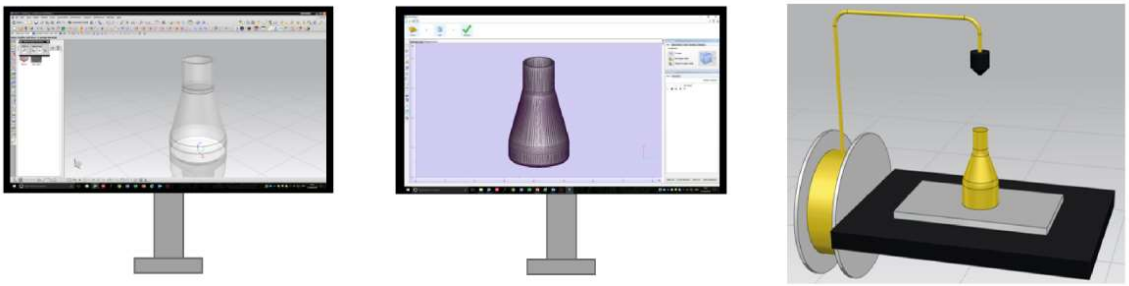

Fig. 1.4 Schematic of the 3D printing process from the first step (design the 3D CAD) to the printing by 3D printer [32]

The 3D printing technique has been used in Chemical, Material, and Biological application since 2012 and growing availability of affordable desktop printer can gain the attention of the use of the 3D printing since then. The 3D printing was popular due to its lots of advantages; explore the newly useful designs, embed the sensor technologies, rapid repeat process, easy to make simple device components. However, its drawbacks were the comparable with the solvents, the printing resolution, cost of some printing materials, and specific for some chemical application.

Versatile applications of 3D printing technique have been reported in analytical chemistry. Highlight future research directions and the challenges in chemistry need to be overcome. The research of 3D printing in applications of analytical chemistry were divided in important sorts of fabrication of common laboratory hardware, bespoke analytic instrumentation, custom micro-or milli-fluidic devices and teaching aids to illustrate complex scientific concepts.

1.3.1 Laboratory equipment

Use of 3D printing technique for fabrication of common equipment in laboratories can reduce the cost of research and teaching laboratories. Due to the demands of repairing, customizing, or developing bespoke laboratory equipment, the 3D printing is increased to use for convenient fabrication and saving cost compared to commercial alternatives. Nowadays, it is very convenient to use the 3D printing laboratory hardware in chemical and biochemical applications because there are free downloaded sources of various 3D printing designs or printing resources for fabrication of general laboratory equipment [32]. The common laboratory equipment is designed to meet the objectives of the experiments. The 3D printed equipment was presented in many types, for a mixer and shaker [33], a syringe pump [34], a miniature peristatic pump [35], the microfluidic pumping [36], i.e. The common printing materials, including polypropylene (PP), polylactic acid (PLA), polyethylene terephthalate glycol (PETG), and acrylonitrile butadiene styrene (ABS) have been tested the solvent compatibility and permeability especially in alcohol solvent to prove the ability of use of 3D printed laboratory hardware.

1.3.2 Analytical equipment

Analytical instrumentations have special properties which are needed the complex design to meet the desire of usage in chemical applications. Use of 3D printing to prototype and manufacture bespoke devices can reduce the costs and associated production times. The first demonstration of 3D printed analytical device was the temperature- stable and pressure-stable high-performance liquid chromatography (HPLC) column using selective laser

melting from Ti-6Al-4V titanium alloy [37]. The channels of the HPLC column were internally functionalized post- print with a poly(butyl methacrylate- co-ethyleneglycoldimethacrylate) stationary phase for proteins separation of the complex mixtures. A 3D printed single- piece photometric detector body with a slit was printed by FDM process. It is used for quantitative photometric detection when integrated with a commercial light- emitting diode (LED) and a photodiode on either side of the capillary tube [38]. Other demonstrations of printed analytical hardware have included devices for UV–visible (UV–vis) spectroscopy as 3D printed cuvette and open-source colorimeter [39,40], and LED array detection as 3D printed detector [41]. In flow injection analysis system, the 3D printed flow-through cuvette fluorescence measurements [42], One-step 3D printed flow cells using single transparent material [43], 3D-printed flow system for determination of lead in natural waters [44], and 3D printed radial flow-cell for chemiluminescence detection [45] were also demonstrated for application in FIA system. Thus, 3D printing technique plays an important role in development of FIA system to become simple, easily fabricated, low cost, and on-demand devices used in various analytical chemistry application.

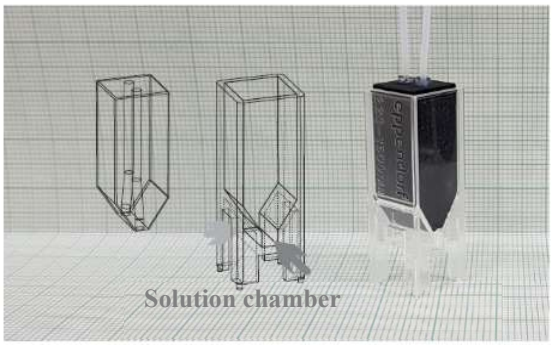

Fig. 1.5 Schematic illustration of 3D-printed flow-through cuvette fluorescence measurements [42]

1.3.3 Chemical and biological fluidic devices

The use of 3D printed fluidic devices have been popularly demonstrated for preparation, synthesis and analysis of small volumes of chemical reagents that are the advantage of this kind of devices [46]. The traditionally manufactured processes of fluidic devices referred as microfluidics or millifluidics, lab- on-a- chip (LOC) or miniaturized total analysis systems (μTAS) are photolithography, soft lithography, injection molding, chemical etching, laser ablation, micromachining, thermoforming and hot embossing [47]. These processes are used a template or master to fabricate the fluidic devices. Commonly, polydimethylsiloxane (PDMS) is used as the molding material for fabrication of the template or master. Because of the advantages of low cost, transparency, biocompatibility, gas permeability, simple integration with flow components, the PDMS favored for fluidic applications. However, its drawbacks are chemical swelling in many organic solvents, deformation at relatively low pressures ($>1\times10^5$ Pa), and absorption of hydrophobic compounds. Furthermore, at final step of the fluidic device's fabrication by PDMS master, the casting form the master pattern can be uncompleted final piece because some part of the final piece device was bonded chemically with the master [48]. Other disadvantages of these traditionally manufactured processes are the restriction of the design of fluidic devices, the complex mixing pathways, the analytical functionality, and accessible geometries mostly only can only fabricate to 2D planar channel networks, the high cost of clean room facilities, requirement of specialist equipment, time consuming and complex processing. Thereafter, the product costs heighten with increase in complex design, waste of costs when reproducing designs, and the post-production prolonged [49].

Recently, high- resolution and cost- effective 3D printing have approached to print the micro or milli fluidic devices. Although the resolution of the 3D printing is not equal to the photolithography of gold-standard approaches. However, the process overcomes the simple fabrication in one step [32]. In addition, the 3D printing technique can overcome the limitation of complex designs with rapid fabrication compared with other manufacturing approaches. 3D printing provided an easy accessibility of fabrication fluidic devices and is driving considerable innovation in many research areas.

The FDM techniques of 3D printing was used to produce chemical reactors in preparative chemistry as reactionware [49,50]. It facilitated advanced analytical approaches to monitor the reactions by electrochemical detection and UV- vis spectroscopy. The reactionware has been adopted to produce valuable pharmaceutical compounds such as ibuprofen [52,53]. The 3D printing applications in flow chemistry were achieved. The potentially 3D printed reactors were demonstrated to integrate with accessible analytical instrumentation for inline UV–vis and attenuated total reflectance infrared (ATR- IR) spectroscopy, and/or electrospray ionization mass spectrometry (ESI- MS) to rapidly produce experimental data [54–56]. Even though the 3D printed devices showed simplicity of fabrication, however the accuracy of determination of the printing process for example, chemical compatibilities, printing parameters and material properties need to achieve a working device.

The issues of design elements to the success of the 3D printed fluidic devices were reported [57, 58] and the results showed that the complexation of printing geometry can affect

the mixing of chemicals in the fluidic devices. The layer thickness, density and part orientation of the print parameters needed to be optimized for a desirable mixing effect due to the layer-by-layer nature of FDM-type printing. The different printing techniques were compared and assessed them for the fabrication of flow devices [59].

The increase in functionalities of the flow reactors was able to integrate by using 3D printing technology. The optical detector as fiber optics can be successfully embedded into 3D printed structures [60,61]. The complex design of the 3D printed fluidic devices with good alignment of the fibres, light source and detector are required for successful application. Other designs were also proposed to make 3D printed microfluidic device embed with the flow cell of the diode array detector of an HPLC instrument to achieve online reaction monitoring [62].

In biological applications, 3D printing technologies shows the achievable goal to produce the devices that can integrate chemical reaction optimization and investigation of the biological responses to the compounds. The increase in biological applications of 3D printed devices has been raised due to the effective cost of the printed system with drug development and pharmaceutical screening. Complicated microfluidic devices for pharmaceutical testing was fabricated by 3D printing and the suitably complicated design based on biological response to various engineering alterations provided the simplicity to researchers for development in biological applications. The efficacy of 3D printing in bio-microfluidics has previously been discussed extensively [63]. However, the biocompatibility of 3D printed material for using in biological system is required to assess for the 3D printed

devices. Many 3D printed devices that feature biological functionality have been produced [64,65]. To duplicate a biological fluid such as blood system, the fluid perfusion devices was fabricated and used in many biological applications [66-68]. Although, a print resolution of the advances 3D printing technology can reach in level of 100 μm which in the scale of microfluidic devices. In addition, the speed of printing process and replicate production were the benefits of 3D printing over the conventional techniques [69].

1.3.4 Teaching aids

The most common applications of 3D printing are the production of teaching aids. The 3D printed models of the laboratory items or the scientific models used in undergraduate teaching assist the students to illustrate more or less complex concepts. The increase in accessibility of printable educational material and affordability of printing technology provided potentially reduction of the teaching costs and stimulated the innovative teaching methods. The students can more understand about the concepts of complex scientific phenomena via the manufacture of 3D model kits, which visualize molecular structures, orbitals, and symmetry [70–72]. Also, the fabrication of 3D diagrams to represent spectroscopic data was reported in a more engaging format [73]. In flow chemistry, the 3D printed models illustrated principles of continuous flow synthesis through simplistic mixing devices [74]. The teachers can use 3D printed instrumentation to describe innovation and potential of this technology to the students.

1.4 Silicone Optical Technology (SOT)

An optical system was traditionally configured optical components in a space to provide the robust optical light path for stable signal and be flexible for optical intensity tuning. The optical components and fundamental base need to be durable and black optical coverage generally render to the fundamental base to obtain the good ability of the optical system. These make the drawbacks of traditional optical system as heavy, hard, expensive and hard to carry. Thus, optical system which the light path was filled with transparent and solid-state medium called “filled path” optical system [75-77] was demonstrated to replace the blank space in transitional optical system. This replacement showed ability of reducing in fundamental base and increase in stability, but a tunability was decreased. A small cross section of an optical fiber proposes a significant concept of the filled path optical system [78] with simultaneously longitudinal robustness and transverse flexibility. Then, waveguide technology such as Wavelength-Division Multiplexing or WDM has been studied [79] for using in network applications. However, in some applications of filled path optical system as in case of lab on a chip device [80], The simple optical system as an absorption cell was integrated in the flow-injection system consisting of glass, the problem of high background noise was occurred due to multiple internal scattering of glass substrate. Thus, some external optical component as optical filter is needed for sensitive measurement. Because of the problem mentioned above, in 2017, Nomada et. al. was demonstrated novel optical system using soft materials for spectroscopic analysis of laser-induced fluorescence (LIF) detection [81]. The soft matrix used for fabrication was polydimethylsiloxane (PDMS). Because PDMS has suitable optical properties as flexibility for tuning signal, high chemical stability,

low fluorescence, and transparency in the UV region, this research studied the use of PDMS for optical system design for special optical properties. A core of transparent PDMS and clad of black particle dispersed PDMS structure was proposed for reducing of internal stray light. The refractive index matching of core/clad structure provides the suppression of intense background radiation due to multiple internal scatting in a transparent material. This presents the special optical properties as a quasi-spatial filter (QSF) and carbon micro particles and carbon nanotubes dispersed PDMS can attain to absorb the stray light 99-99.7 %.

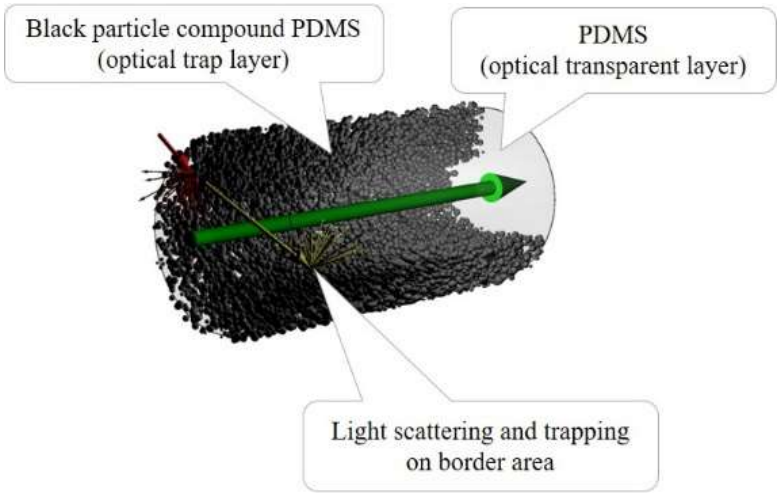

Fig. 1.6 Schematic of light propagation through the SOT quasi-spatial filter

Comparison to the previous researches using metallic (Al, Ag, Au, Cu) layer have been be used as optical trapping layer or sub wavelength scatterers [81-83], The SOT -QSF provided benefits of inexpensive, flexible, and simple fabrication overwhelming the metal trapping layer. The Nomada's proposed compact optical system was cigarette box size which composed of laser light source (532 nm), PDMS sample chamber (black PDMS of carbon particle doped PDMS), hole for critical reflection, transparent PDMS as light channel, dye

PDMS wavelength filter (Sudan-II), and photodetector. This is the first time of the optical system developed to be tiny size, light weight, no shall or frame, and portable by using fabrication of soft material.

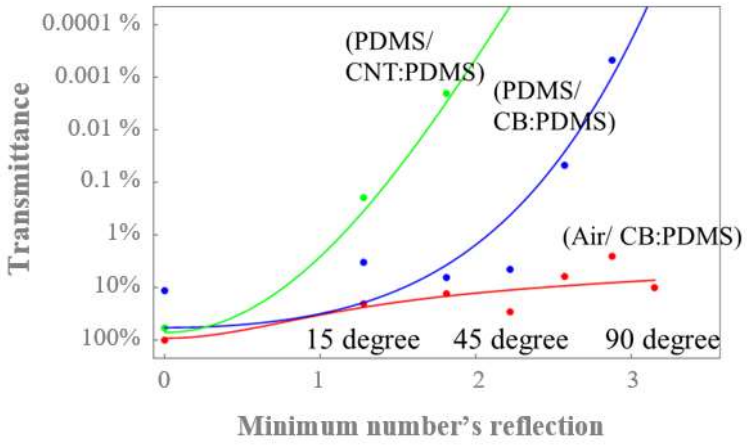

Fig. 1.7 Trapping performance measurement of the SOT optical filter [84] described that the SOT filter can trap the stray light providing decrease in noise signal.

The boundary of black PDMS cladding and the transparent PDMS core seemed to effect to the trapping of scattering light which can provide the low blank signal level. According to the results of trapping performance by observing the transmittance of the flexible PDMS core/black PDMS clad light channel as a function of the bending angle (Fig. 1.7), the sample of optical QSF as straight light guides (cross section of 1-2 mm^2, length of 50 mm) were prepared to evaluate trapping performance. The black PDMS were prepared by using 10% wt. of carbon black (CB) doped PDMS and 0.83% wt. of carbon nanotubes (CNTs) to cover the transparent PDMS core. These results of trapping performance of the light guides show the function of straight filter that only light propagating along the axis of

core channel can pass to the photodetector. The scattering light can be absorbed via black particle diffused PDMS as optical trap layer. Thus, the noise signal can be suppressed to~0% and 99-99.7% of trapping performance was observed. This presented the novel idea of fabrication of the optical system with low noise level detection that can provide the advantages in many areas of research.

1.5 Chemical application: Colorimetric determination of iron (II)

Iron is a metal that belongs to the first transition series and group 8 of the periodic table. It is present in many material and commonly, has oxidation states of iron(II) and iron(III). The iron (II) solution can react with 1,10-phenanthroline ($C_{12}H_8N_2$, ortho-phenanthroline or *o*-Phen) is a tricyclic nitrogen heterocyclic compound to form colored complexes of a deeply red color. This property provides an excellent and sensitive method for determining these metal ions in aqueous solution called colorimetric analysis which the concentration of the analyte is based on the change in the intensity of the color of solution. Colorimetric methods represent the simplest form of absorption analysis that normally use the spectrophotometric method for determination of the analyte. In case of iron (II) reacts with *o*-Phen, the colored solution is formed following below equation [85];

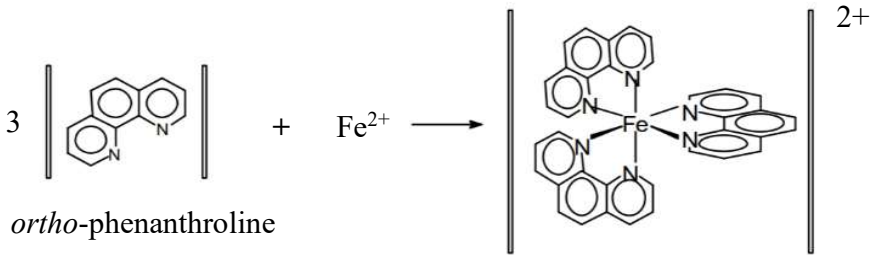

ortho-phenanthroline

Ferrous tris-*o*-phenanthroline

For the quantitative analysis of iron (II). The Fe(II)-*o*-Phen complex provided the red color solution which it absorbed the visible light as λ_{max} at 510 nm. Based on the Beer-Lambert's Law, is a very simple relationship: $A = \varepsilon cl$ while A is the absorbance of an analyte at a specified wavelength λ in nanometer range, normally used in electromagnetic region of the ultraviolet (UV) and visible (Vis); the molar absorptivity (ε) of the ferrous complex, $[(C_{12}H_8N_2)_3Fe]^{2+}$, is 11,100 M^{-1} cm^{-1} at the λ_{max}, c is the concentration in molarity as M, and l is the length of the light path through the sample, usually in cm. For Fe(II)-*o*-Phen complex, the intensity of the color is independent of pH in the range 2 to 9 and complex is very stable that the intensity of the complex color does not change for long analysis time. The applications of colorimetric determination of iron using *o*-Phen were widely used for determination of iron in vitamin tablet, milk, urine and i.e. Also, the determination of iron in water samples is usually carried out for routine quality control because the legislation limited the iron content in drinking water of lower 200 µg L^{-1} [86]. In case of iron analysis in the seawater, river, tap water or other source of natural water, the matrix effects and trace concentration levels of iron contents are the main issue for quantitative analysis. Thus, increase in sensitivity, preconcentration, and good separation are required in spectrophotometric method. The FIA system with increase in precision, accuracy and sample throughput was successfully used for determination of iron in natural water by *o*-Phen [87], however the method need the long-pathlength liquid core waveguide as the additional equipment to improve the sensitivity of the method. Thus, the determination of iron by *o*-Phen can be developed to improve the sensitivity by development of the detection system.

1.6 Biological applications

1.6.1 Continuous monitoring of the cell

In industry of cell culture and regeneration of medicine, a monitoring of the cell is very significant which development of controlling cell environment is needed. Normally, the management of cell culture environment is involved management of the conditions of the cell culture medium such as the pH, humidity, and temperature [88,89]. Because nutritive supply for the cell is the culture medium, it is important to monitor the culture medium continuously for the management of cell conditions. Generally, processes of controlling a regular exchange with fresh medium or monitoring pH values were used for investigation of culture medium conditions [90]. However, the expert operators who experience in the fields of biological analysis are required for these approaches [91]. Thus, a continuous monitoring device was developed for the quantitative analysis of culture medium and cell [92]. Microdevices used for continuous measurement of the cell state have been demonstrated [93–95]. Functional microdevices were able to control and measure single cells, however the devices are not aimed to investigate the culture state of a cell population. Methods used the recovery of medium and assessing of the production of oxygen, proteins, and amino acids for investigation of the cell state have been proposed [96]. However, a removal of the culture dish from the incubator was required and opening the lid for recovery of the culture medium was needed that provided disadvantage of changing in the culture cell environment. An alternative approach was use of imaging data to measure cell morphology [97,98] but the method uses expensive instrument requested skillful workers.

1.6.2 Determination of 3-Phenoxybenzoic Acid with Anti-3-Phenoxybenzoic Acid Monoclonal Antibody

3-phenoxybenzoic acid (3PBA) that phenoxy group is meta to the carboxy group is a major metabolite of pyrethroid insecticides. It acts as a human xenobiotic metabolite and a marine xenobiotic metabolite which is neurotoxin and toxic to aquatic life [99]. Figure 1.8 presented the molecular structure of several synthetic pyrethroid insecticides. Commonly, pyrethroid insecticides are used for crops, and diet in worldwide. After we take these products from the crops and diet as the primary route of the 3PBA, it can be exposed in general population [100]. The enzyme in human body as esterase can hydrolyze pyrethroid compounds after absorbing in the human body. The compounds are change into 3-phenoxybenzyl alcohol or 3-phenoxybenzaldehyde in the liver (half-lives between 2.5 and 12 h) and then, they are rapidly converted to 3PBA [101]. 3PBA is conjugated to glucuronic acid that become to the xenobiotic which is more hydrophilic. After that, it can facilitate via excretion in the urine. Thus, 3PBA is potential to use as a marker of synthetic pyrethroid insecticide exposure [102–107]. Previously, the detection of 3PBA using anti-3PBA antibodies [102–106] and nanobodies [107] have been proposed showing the important of determination of 3PBA or pyrethroid insecticides.

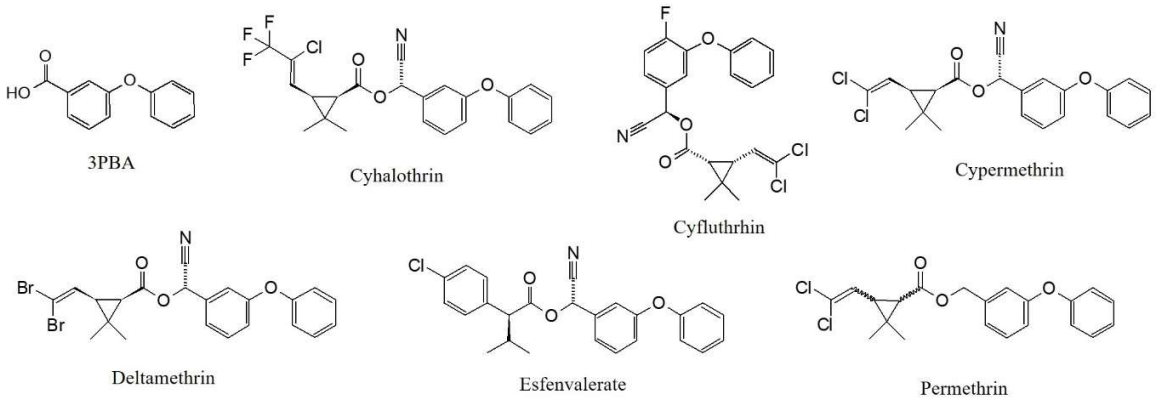

Fig. 1.8 Molecular structures of 3PBA and several pyrethroid insecticides.

1.7 Objectives

The objectives of the work presented in this thesis are:

In **chapter 3**, the portable optical device according to silicone optical technology (SOT) was developed to apply for biological analysis. A compact microplate reader was performed continuously and quantitatively monitoring of the cell state without altering the culture surroundings in a 24-wells plate that embedded the SOT spatial filter. The optical properties of the proposed device were investigated the special properties of an excellent noise reduction effect. Moreover, the newly developed device for biological application was confirmed.

In **Chapter 4**, the optical device based on the SOT concept with a small, light-weighted, and flexible properties was fabricated by combining 3D printing and SOT-QSF planting using in analytical Chemistry. The use of 3D printed silicone as flexible frame and

the SOT-QSF embedding by simple injecting and blowing method for coating black PDMS (carbon dispersed PDMS) and injecting transparent PDMS was developed to investigate the novel fabrication method of the optical device.

In **Chapter 5**, the SOT optical device was newly fabricated to couple with FIA system with suitable design for using as compact on-demand optical device for on-site measurement. The proposed SOT optical device integrated with FIA system and a simple and compact LED detection (SOT-FIA optical system) was used for chemical analysis applications. The chemical application for determination of iron content in real samples was examined using the proposed optical system. The analytical characteristics and the validation of the developed optical system using a traditional spectrophotometer were evaluated to confirm its beneficial in chemical analysis applications for on-site and on-demand measurement.

In **Chapter 6**, the SOT optical device coupling with FIA system using for a flow enzyme-linked immunosorbent assay (ELISA) was demonstrated. The ELISA method using enzymatic reaction of polyaniline using aniline, H_2O_2, and horseradish peroxidase (HRP) was proposed based on light absorption. The SOT-FIA optical device used a blue LED (470 nm) as the light source and photomultiplier tube (PMT) was performed as a detector of competitive flow ELISA for biological application of determination of 3-phenoxybenzoic acid (3PBA) with anti-3-phenoxybenzoic acid monoclonal antibody (mAb). The results of determination of 3PBA in artificial urine was investigated for using in the real application.

In **Chapter 7**, the newly SOT optical device was developed using white PDMS as TiO_2 dispersed in PDMS for enhancing the sensitivity of the optical detection. The digitally

fabrication method was developed by casting PDMS on the 3D printed mold/frame. The fabrication of a simple core/clad structure of titanium dioxide (TiO_2) rutile particle dispersed in PDMS as optical core and carbon black doped PDMS as a cladding of was demonstrated. This proposed SOT-FIA module was used in a flow injection analysis system with compact LED detection system for iron determination by colorimetric assay in drinkable tap water samples as chemical application of the newly proposed optical system that is potential of on-demand and on-site measurement.

References

[1] D.A. Skoog, D.M. West, F.J. Holler, S. R. Crouch, Fundamentals of Analytical Chemistry. Belmont: Brooks/Cole, Cengage Learning. 9 (2014) 1.

[2] "Analytical Chemistry - American Chemical Society". American Chemical Society. (retrieved 26 May 2017).

[3] "Dynamic range", Electropedia, IEC, (accessed 26 January 2020)

[4] F.J. Amore, G. V Cox, J. Lai, R.R. Langner, D.G. Crosby, F.L. Estes, N.I. Mcclelland, W.F. Phillips, D.H. Freeman, W.E. Gibbs, G.E. Gordon, L.H. Keith, D.H. Freeman, R. Libby, J.K. Taylor, D. Macdougall, Guidelines for Data Acquisition and Data Quality Evaluation in Environmental Chemistry, Anal. Chem. 52 (1980) 2242–2249.

[5] M. Walker, J.G. Kublin, J.R. Zunt, Accuracy, Precision, and Reliability of Chemical Measurements in Natural Products Research, Fitoterapia. 42 (2009) 115–125.

[6] M.C. Yebra-Biurrun, Flow injection analysis of marine samples. New York: Nova Science Publishers. (2009).

[7] J. Ruzicka, E.H. Hansen, Peer Reviewed: Flow Injection Analysis: From Beaker to Microfluidics, Anal. Chem. 72 (5) 212A–217A.

[8] MindTouch of department of Education Open Textbook Pilot Project of California State University, Flow injection analysis, https://chem.libretexts.org/Courses/Northeastern_University/13%3A_Kinetic_Methods/13.4%3A_Flow_Injection_Analysis, May 2017 (accessed 21 January 2020).

[9] A. Cerdà, V. Cerdà, an introduction to flow analysis, https://wikimili.com/en/Flow_injection_analysis#cite_note-:0-6, Mallorca: Sciware, 2019 (accessed 25 January 2020).

[10] M. Trojanowicz, K. Kołacińska, Recent advances in flow injection analysis, analyst. 141 (2016) 2085–2139.

[11] R.N.M.J. Pascoa, I.V. Toth, A.O.S.S. Rangel, Review on recent applications of the liquid waveguide capillary cell in flow-based analysis techniques to enhance the sensitivity of spectroscopic detection methods, Anal. Chim. Acta. 739 (2012) 1–13.

[12] L.S.G. Teixeira, F. R. P. Rocha, A green analytical procedure for sensitive and selective determination of iron in water samples by flow-injection solid-phase spectrophotometry, Talanta. 71 (2007) 1507–1511.

[13] S.S.M.P. Vidigal, I.V. Toth, A.O.S.S. Rangel, Exploiting the bead injection LOV approach to carry out spectrophotometric assays in wine: Application to the determination of iron, Talanta. 84 (2011) 1298–1303.

[14] Y.L. Yu, Y. Jiang, R.-H. He, Development of a miniature analytical system in a lab-on-valve determination of trace copper by bead injection spectroscopy, Talanta. 88 (2012) 352–357.

[15] D.A. Bui, P.C. Hauser, Analytical devices based on light-emitting diodes – a review of the state-of-the-art, Anal. Chim. Acta. 853 (2015) 46–58.

[16] M. Trojanowicz, W. Augustyniak, A. Hulanicki, Photometric flow-injection measurements with flow-cell employing light emitting diodes, Microchim. Acta. 83 (1984) 17–25.

[17] P.K. Dasgupta, I.-Y. Eom, K.J. Morris, J. Li, Light emitting diode-based detectors. Absorbance, fluorescence and spectroelectrochemical measurements in a planar flow-through cell, Anal. Chim. Acta. 500 (2003) 337–364.

[18] T.R. Dias, M.A.S. Brasil, M.A. Feres, B.F. Reis, A flow cell with a new design to improve the utilization of the radiation emitted by LED and employed as a radiation source for photometric detection, Sens. Actuators, B. 198 (2014) 448–454.

[19] C.K. Pires, B.F. Reis, A. Morales-Rubio, M. de la Guardia, Speciation of chromium in natural waters by micropumping multicommutated light emitting diode photometry, Talanta. 144 (2015) 432–438.

[20] P. Chuntib, J. Jakmunee, Simple flow injection colorimetric system for determination of paraquat in natural waters, Talanta. 144 (2015) 432–438.

[21] K.T. Lau, S. Baldwin, R.L. Shephard, P.H. Dietz, W.S. Yerzunis, D. Diamond, Novel fused-LEDs devices as optical sensors for colorimetric analysis, Talanta. 63 (2004) 167–173.

[22] L. Tymecki, M. Pokrzywnicka, R. Koncki, Paired emitter detector diode (PEDD)-based photometry –an alternative approach, Analyst. 133 (2008) 1501–1504.

[23] M. Pokrzywnicka, R. Koncki, L. Tymecki, Towards optoelectronic urea biosensors, Anal. Bioanal. Chem. 407 (2015) 1807–1812.

[24] D. Cogan, J. Cleary, T. Phelan, E. McNamara, M. Bowkett, D. Diamond, Integrated flow analysis platform for the direct detection of nitrate in water using a simplified chromotropic acid method, Anal. Methods. 5 (2013) 4798–4804.

[25] D.A. Bui, P.C. Hauser, Absorbance measurements with light-emitting diodes as a sources: Silicon photodiodes or light-emitting diodes as detectors, Talanta. 116 (2013) 1073–1078.

[26] T. Duda, L.V. Raghavan, 3D metal printing technology. IFAC-PapersOnLine. 49 (2016) 103–110.

[27] H. Bikas, P. Stavropoulos, G. Chryssolouris, Additive manufacturing methods and modeling approaches: a critical review. Int. J. Adv. Manuf. Technol. 83 (2016) 389–405.

[28] S.C. Ligon, R. Liska, J. Stampfl, M. Gurr, R. Mülhaupt, Polymers for 3D printing and customized additive manufacturing. Chem. Rev. 117 (2017) 10212–10290.

[29] A. Busachi, J. Erkoyuncu, P. Colegrove, F. Martina, C. Watts, R. Drake, CIRP Journal of Manufacturing Science and Technology A review of Additive Manufacturing technology and Cost Estimation techniques for the defence sector, CIRP J. Manuf. Sci. Technol. 19 (2017) 117–128.

[30] Y. He, Y. Wu, J. Fu, Q. Gao, J. Qiu, Developments of 3D printing microfluidics and applications in chemistry and biology: a review. Electroanalysis 28 (2016) 1658–1678.

[31] M. Pohanka, Three- dimensional printing in analytical chemistry: principles and applications. Anal. Lett. 49 (2016) 2865–2882.

[32] A.J. Capel, R.P. Rimington, M.P. Lewis, S.D.R. Christie, 3D printing for chemical, pharmaceutical and biological applications, Nat. Rev. Chem. 2 (2018) 422–436.

[33] K.C. Dhankani, J.M. Pearce, Open source laboratory sample rotator mixer and shaker. Hardware X. 1 (2017) 1–12.

[34] B. Wijnen, E.J. Hunt, G.C. Anzalone, J.M. Pearce, Open- source syringe pump library. PLOS ONE. 9 (2014) 1–8.

[35] S. Balakrishnan, M.S. Suma, S.R. Raju, S.D.B. Bhargav, S. Arunima, A Scalable Perfusion Culture System with Miniature Peristaltic Pumps for Live-Cell Imaging Assays with Provision for Microfabricated Scaffolds, BioReseach. 4 (2015) 343–357.

[36] E.C. Sweet, R. R. Mehta, R. Lin, L. Lin, Finger-powered, 3D printed microfluidic pumps. Int. Solid State Sensor Actuators Microsyst. Conf. (2017).

[37] V. Gupta, S. Beirne, P.N. Nesterenko, B. Paull, Investigating the effect of column geometry on separation efficiency using 3D printed liquid chromatographic columns containing polymer monolithic phases. Anal. Chem. 90 (2018) 1186–1194.

[38] F. Cecil, M. Zhang, R.M. Guijt, A. Henderson, P.N. Nesterenko, B. Paull, M.C. Breadmore, M. Macka, Analytica Chimica Acta 3D printed LED based on-capillary detector housing with integrated slit, Anal. Chim. Acta. 965 (2017) 131–136.

[39] H.D. Whitehead, J.V. Waldman, D.M. Wirth, G. LeBlanc, 3D Printed UV-Visible Cuvette Adapter for Low-Cost and Versatile Spectroscopic Experiments, ACS Omega. 2 (2017) 6118–6122.

[40] G.C. Anzalone, A.G. Glover, J.M. Pearce, Open-source colorimeter, Sensors (Switzerland). 13 (2013) 5338–5346.

[41] J. Prikryl, F. Foret, Fluorescence detector for capillary separations fabricated by 3D printing. Anal. Chem. 86 (2014) 11951–11956.

[42] M. Michalec, Ł. Tymecki, 3D printed flow-through cuvette insert for UV–Vis spectrophotometric and fluorescence measurements, Talanta. 190 (2018) 423–428.

[43] Y. Liang, Q. Liu, S. Liu, X. Li, Y. Li, M. Zhang, One-step 3D printed flow cells using single transparent material for flow injection spectrophotometry, Talanta. 201 (2019) 460–464.

[44] E. Mattio, F. Robert-peillard, C. Branger, K. Puzio, A. Margaillan, Talanta 3D-printed flow system for determination of lead in natural waters, Talanta. 168 (2017) 298–302.

[45] V. Gupta, P. Mahbub, P.N. Nesterenko, B. Paull, Analytica Chimica Acta A new 3D printed radial flow-cell for chemiluminescence detection: Application in ion chromatographic determination of hydrogen peroxide in urine and coffee extracts, Anal. Chim. Acta. 1005 (2018) 81–92.

[46] C. Dixon, J. Lamanna, A.R. Wheeler, Printed microfluidics. Adv. Funct. Mater. 27 (2017) 1604824.

[47] V. Faustino, S.O. Catarino, R. Lima, G. Minas, Biomedical microfluidic devices by using low- cost fabrication techniques: a review. J. Biomech. 49 (2016) 2280–2292.

[48] P. Abgrall, A.M. Gué, Lab- on-chip technologies: making a microfluidic network and coupling it into a complete microsystem - a review. J. Micromechan. Microengineer. 17 (2007) R15–R49.

[49] R. Amin, S. Knowlton, A. Hart, B. Yenilmez, F. Ghaderinezhad, S. Katebifar, M. Messina, A. Khademhosseini, S. Tasoglu, 3D- printed microfluidic devices. Biofabrication 8 (2016) 22001.

[50] M.D. Symes, P.J. Kitson, J. Yan, C.J. Richmond, G.J.T. Cooper, R.W. Bowman, T. Vilbrandt, L. Cronin, Integrated 3D- printed reactionware for chemical synthesis and analysis, Nat. Chem. 4 (2012) 349–354.

[51] P.J. Kitson, S. Glatzel, W. Chen, C.G. Lin, Y.F. Song, L. Cronin, 3D printing of versatile reactionware for chemical synthesis, Nat. Protoc. 11 (2016) 920–936.

[52] P.J. Kitson, S. Glatzel, L. Cronin, The digital code driven autonomous synthesis of ibuprofen automated in a 3D- printer-based robot, Beilstein J. Org. Chem. 12 (2016) 2776–2783.

[53] P.J. Kitson, G. Marie, J.P. Francoia, S.S. Zalesskiy, R.C. Sigerson, J.S. Mathieson, L. Cronin, Digitization of multistep organic synthesis in reactionware for on-demand pharmaceuticals, Science. 359 (2018) 314–319.

[54] P.J. Kitson, M.H. Rosnes, V. Sans, V. Dragone, L. Cronin, Configurable 3D- printed millifluidic and microfluidic 'lab on a chip' reactionware devices, Lab. Chip 12 (2012) 3199–3522.

[55] V. Dragone, V. Sans, M.H. Rosnes, P.J. Kitson, L. Cronin, 3D-printed devices for continuous- flow organic chemistry, Beilstein J. Org. Chem. 9 (2013) 951–959.

[56] J.S. Mathieson, M.H. Rosnes, V. Sans, P.J. Kitson, L. Cronin, Continuous parallel ESI-MS analysis of reactions carried out in a bespoke 3D printed device, Beilstein J. Nanotechnol. 4 (2013) 285–291.

[57] A.J. Capel, S. Edmondson, S.D.R. Christie, R.D. Goodridge, R.J. Bibb, M. Thurstans, Design and additive manufacture for flow chemistry, Lab Chip. 13 (2013) 4583–4590.

[58] F. Li, N.P. Macdonald, R.M. Guijt, M.C. Breadmore, Using printing orientation for tuning fluidic behavior in microfluidic chips made by fused deposition modeling 3D printing, Anal. Chem. 89 (2017) 12805–12811.

[59] N.P. Macdonald, J.M. Cabot, P. Smejkal, R.M. Guijt, B. Paull, M.C. Breadmore, Comparing Microfluidic Performance of Three-Dimensional (3D) Printing Platforms, Anal. Chem. 89 (2017) 3858–3866.

[60] T. Monaghan, A.J. Capel, S.D. Christie, R.A. Harris, R.J. Friel, Solid- state additive manufacturing for metallized optical fiber integration, Compos. Part A 76 (2015) 181–193.

[61] T. Monaghan, M.J. Harding, R.A. Harris, R.J. Friel, S.D.R. Christie, Customisable 3D printed microfluidics for integrated analysis and optimisation, Lab Chip. 16 (2016) 3362–3373.

[62] A.J. Capel, A. Wright, M.J. Harding, G.W. Weaver, Y. Li, R.A. Harris, S. Edmondson, R.D. Goodridge, S.D.R. Christie, 3D printed fluidics with embedded analytic functionality for automated reaction optimisation, Beilstein J. Org. Chem. 13 (2017) 111–119.

[63] C.M.B. Ho, S.H. Ng, K.H.H. Li, Y.J. Yoon, 3D printed microfluidics for biological applications, Lab Chip. 15 (2015) 3627–3637.

[64] B.N. Johnson, K.Z. Lancaster, I.B. Hogue, F. Meng, Y.L. Kong, L.W. Enquist, M.C. McAlpine, 3D printed nervous system on a chip, Lab Chip. 16 (2016) 1393–1400.

[65] J. Liu, H.H. Hwang, P. Wang, G. Whang, S. Chen, Direct 3D- printing of cell- laden constructs in microfluidic architectures, Lab. Chip 16 (2016) 1430–1438.

[66] K.B. Anderson, S.Y. Lockwood, R.S. Martin, D.M. Spence, A 3D printed fluidic device that enables integrated features, Anal. Chem. 85 (2013) 5622–5626.

[67] J.L. Erkal, A. Selimovic, B.C. Gross, S.Y. Lockwood, E.L. Walton, S. McNamara, R.S. Martin, D.M. Spence, 3D printed microfluidic devices with integrated versatile and reusable electrodes, Lab Chip. 14 (2014) 2023–2032.

[68] G.J. LaBonia, S.Y. Lockwood, A.A. Heller, D.M. Spence, A.B. Hummon, Drug penetration and metabolism in 3D cell cultures treated in a 3D printed fluidic device: assessment of irinotecan via MALDI imaging mass spectrometry, Proteomics. 16 (2016) 1814–1821.

[69] A.I. Shallan, P. Smejkal, M. Corban, R.M. Guijt, M.C. Breadmore, Cost effective three-dimensional printing of visibly transparent microchips within minutes, Anal. Chem. 86, (2014) 3124–3130.

[70] J. Stone-Sundberg, W. Kaminsky, T. Snyder, P. Moeck, 3D printed models of small and large molecules, structures and morphologies of crystals, as well as their anisotropic physical properties, Cryst. Res. Technol. 50 (2015) 432–441.

[71] P.A. Wood, A.A. Sarjeant, I.J. Bruno, C.F. Macrae, H.E. Maynard-Casely, M. Towler, The next dimension of structural science communication: simple 3D printing directly from a crystal structure, CrystEngComm 19 (2017) 690–698.

[72] M.J. Robertson, W.L. Jorgensen, Illustrating concepts in physical organic chemistry with 3D printed orbitals, J. Chem. Educ. 92 (2015) 2113–2116.

[73] C.S. Higman, H. Situ, P. Blacklin, J.E. Hein, Hands- on data analysis: using 3D printing to visualize reaction progress surfaces, J. Chem. Educ. 94 (2017) 1367–1371.

[74] T. Tabassum, M. Iloska, D. Scuereb, N. Taira, C. Jin, V. Zaitsev, F. Afshar, T. Kim, Development and Application of 3D Printed Mesoreactors in Chemical Engineering Education, J. Chem. Educ. 95 (2018) 783–790.

[75] N.J. Herrick, Internal Reflection Spectroscopy, Wiely Intersc., NetWork,1967.

[76] N.J. Herrick, G.I. Loeb, Multiple internal reflection fluorescence spectrometry, Anal. Chem. 45 (1973) 687–691.

[77] E. Katz, Surface Plasmon resonance – a method to analyze interfacial optical properties and to develop biosensors, The Hebrew University of Jerusalem, (available on (⟨http://chem.ch.huji.ac.il/eugeniik/spr.htm⟩), last accessed Sep. 2019).

[78] U. Utzinger, R.R. Richards-Kortum, Fiber optic probes for biomedical optical spectroscopy, J. Biomed. Opt. 8 (2003)121–147.

[79] R.T. Chen, WDM and photonic switching devices for network applications, Soc. Photo Opt.2000/06, SPIEproceedingsseries, SPIE-International Society for Optical Engine (June2000), English, 284p. ISBN-10:081943566X; ISBN-13:978-0819435668.

[80] R.H. Byrne, W.S. Yao, E. Kaltenbacher, R.D. Waterbury, Construction of a compact spectrofluorometer/spectrophotometer system using a flexible liquid core waveguide, Talanta 50 (2000) 1307–1312.

[81] W. A. Murray, W. L. Barnes, Plasmonic Materials, Adv. Mater. 19 (2007) 3771-3782.

[82] W.L. Barnes, Metallic metamaterials and plasmonics, Philos. Trans. R. Soc. A Math. Phys. Eng. Sci. 369 (2011) 3431–3433.

[83] A. Sahota, Future Outlook, Sustain. How Cosmet. Ind. Is Green. Up. (2013) 301–314.

[84] H. Higuchi, H. Yoshioka, H. Nomada, Y. Oki, K. Morita, Carbon–polydimethylsiloxane-based integratable optical technology for spectroscopic analysis, Talanta. 166 (2015) 428–432.

[85] Spectrophotometric Determination of Iron, https://carleton.ca/chemistry/wp-content/uploads/speclab.pdf (accessed 30 March 2020).

[86] L.S. Clesceri, A.E. Greenberg, A.A. Eaton, Standard methods for the examination of water and wastewater, 20th ed. American Public Health Association, American Water Works Association, and Water Environment Federa- tion. 3500 Fe Iron; (1998) 3-76.

[87] R.N.M.J. Páscoa, I. V. Tóth, A.O.S.S. Rangel, Sequential injection trace determination of iron in natural waters using a long-pathlength liquid core waveguide and different spectrophotometric chemistries, Limnol. Oceanogr. Methods. 7 (2009) 795–802.

[88] P. Gupta, K. Hourigan, S. Jadhav, J. Bellare, P. Verma, Effect of lactate and pH on mouse pluripotent stem cells: Importance of media analysis, Biochem. Eng. J. 118 (2017) 25–33.

[89] M.A. Chaudhry, B.D. Bowen, J.M. Piret, Culture pH and osmolality influence proliferation and embryoid body yields of murine embryonic stem cells, Biochem. Eng. J. 45 (2009) 126–135.

[90] F.M. Harold, J. Van Brunt, Circulation of H+ and K+ across the plasma membrane is not obligatory for bacterial growth, Science. 197 (1977) 372–373.

[91] K. Masahiro, M. Manabu, Challenges for industrializing tissue factories, Iryou Kikigaku (Jpn. J. Med. Instrum.) 81(6) (2011) 434-438.

[92] M. Fujitani, N.S. Huddin, S. Kawai, K. Kanie, Y. Kiyota, K. Shimizu, H. Honda, R. Kato, Morphology-based non-invasive quantitative prediction of the differentiation status of neural stem cells, J. Biosci. Bioeng. 124 (2017) 351–358.

[93] A.M. Gonzalez-Suarez, J.G. Pena-Del Castillo, A. Hernández-Cruz, J.L. Garcia-Cordero, Dynamic generation of concentration and temporal-dependent chemical signals in an integrated microfluidic device for single-cell analysis, Anal. Chem. 90 (2018) 8331–8336.

[94] J. Song, H. Ryu, M. Chung, Y. Kim, Y. Blum, S. sik Lee, O. Pertz, N.L. Jeon, Microfluidic platform for single cell analysis under dynamic spatial and temporal stimulation, Biosens. Bioelectron. 104 (2018) 58–64.

[95] Y. Nakashima, Y. Yang, K. Minami, Development of a micro cell compression stimulator for evaluating real-time cellular responses, Rev. Sci. Instrum. 83 (2012).

[96] Details, Raffle, Patent Application Publication No. U.S. patent 2016/01 04348 A1 (14 April 2016), Sheet 1 of 43.

[97] F. Matsuoka, I. Takeuchi, H. Agata, H. Kagami, H. Shiono, Y. Kiyota, H. Honda, R. Kato, Morphology-Based Prediction of Osteogenic Differentiation Potential of Human Mesenchymal Stem Cells, PLoS One. 8 (2013).

[98] S. Sugimura, T. Akai, T. Somfai, M. Hirayama, Y. Aikawa, M. Ohtake, H. Hattori, S. Kobayashi, Y. Hashiyada, K. Konishi, K. Imai, Time-Lapse Cinematography-Compatible

Polystyrene-Based Microwell Culture System: A Novel Tool for Tracking the Development of Individual Bovine Embryos1, Biol. Reprod. 83 (2010) 970–978.

[99] L.G. Costa, Neurotoxicity of pesticides: a brief review, Front. Biosci. 13 (2007) 1240.

[100] C. Lu, K. Toepel, R. Irish, R.A. Fenske, D.B. Barr, R. Bravo, Organic diets significantly lower children's dietary exposure to organophosphorus pesticides, Environ. Health Perspect. 114 (2006) 260–263.

[101] J.M. Starr, R. Tornero-Velez, S.E. Graham, M.F. Hughes, M.J. DeVito, K.M. Crofton, M.J. Wolansky, E.J. Scollon, D.G. Ross, Environmentally relevant mixing ratios in cumulative assessments: A study of the kinetics of pyrethroids and their ester cleavage metabolites in blood and brain; and the effect of a pyrethroid mixture on the motor activity of rats, Toxicology. 320 (2014) 15–24.

[102] G. Shan, H. Huang, D.W. Stoutamire, S.J. Gee, G. Leng, B.D. Hammock, A sensitive class specific immunoassay for the detection of pyrethroid metabolites in human urine, Chem. Res. Toxicol. 17 (2004) 218–225.

[103] C.A. Ki, P. Lohstroh, S.J. Gee, N.A. Gee, B. Lasley, B.D. Hammock, High-throughput automated luminescent magnetic particle-based immunoassay to monitor human exposure to pyrethroid insecticides, Anal. Chem. 79 (2007) 8883–8890.

[104] H.J. Kim, K.C. Ahn, A. González-Techera, G.G. González-Sapienza, S.J. Gee, B.D. Hammock, Magnetic bead-based phage anti-immunocomplex assay (PHAIA) for the

detection of the urinary biomarker 3-phenoxybenzoic acid to assess human exposure to pyrethroid insecticides, Anal. Biochem. 386 (2009) 45–52.

[105] J.C. Chuang, J.M. Van Emon, R.M. Trejo, J. Durnford, Biological monitoring of 3-phenoxybenzoic acid in urine by an enzyme-linked immunosorbent assay, Talanta. 83 (2011) 1317–1323.

[106] K.C. Ahn, S.J. Gee, H.J. Kim, P.A. Aronov, H. Vega, R.I. Krieger, B.D. Hammock, Immunochemical analysis of 3-phenoxybenzoic acid, a biomarker of forestry worker exposure to pyrethroid insecticides, Anal. Bioanal. Chem. 401 (2011) 1285–1293.

[107] N. Vasylieva, J. Zhang, Z. Li, B.D. Hammock, J. Huo, M. Qi, D. Wan, D. Li, B. Barnych, Development of a highly sensitive direct competitive fluorescence enzyme immunoassay based on a nanobody–alkaline phosphatase fusion protein for detection of 3-phenoxybenzoic acid in urine, J. Agric. Food Chem. 66 (2018) 11284–11290.

Chapter 2

Methodology

2.1 Materials

For fabrication of the proposed optical device using in chemical and biological applications, the flexible material as polydimethylsiloxane (PDMS) was used as the main material to compose with other material for improving special optical properties of the desired optical device.

2.1.1 Polydimethylsiloxane (PDMS)

Polydimethylsiloxane (PDMS) or dimethylpolysiloxane or dimethicone is a group of polymeric organosilicon compounds that are commonly referred to as silicones [1]. PDMS has properties of flexible, optically clear, inert to chemical compounds, non-toxic, and non-flammable. PDMS has widely used in many applications range from additives of customer goods, surgery, cosmetics, commonly used devices and medical devices to elastomers. PDMS is hydrophobic and resist to water and stable in chemical compounds and organic solvent. Because the PDMS is adsorbed UV light region, but transparent in visible region, thus the PDMS can used as optical device instead of glass or mirror as the light guide. The PDMS is commonly fabricated an assistance of visual function for example contact lenses.

2.1.2 Carbon black (CB)

Carbon black (CB), a typical carbonaceous aerosol, is an important by-product of incomplete combustion of fossil fuel, biomass, biofuel, etc. [2-4] Black carbon particles can strongly absorb incoming solar radiation in visible region across a broad wavelength range. Black carbon (BC) particles are typically composed of multiple spherules with small size of average diameter 20 nm.

2.1.3 Titanium dioxide (TiO_2)

Titanium dioxide (TiO_2) is an important industrial material as a main component of paint, pigment, cosmetics, etc. [5]. Due to the rutile titanium dioxide particle with a high refractive index of ~2.8, the contrast between refractive index of the TiO_2 particles and the surrounding medium can provide the stronger of amplitude of the scattering events. The phenomena of multiple scattering occurred between the incident radiation and small particles of TiO2 dispersed in the polymer matrix induces the opacity of architectural white paint [6]. Thus, the rutile TiO_2 particle is popularly used as a white pigment in an industry and research. In the past few years, there were numerous studies of various parameters such as size, shape, and chemical nature of the pigment to increase the effectiveness of TiO_2 in paint manufacturers [7,8]. Also, extrinsic parameters included the filling fractions and the spatial dispersion state of the pigments in the polymer matrix were concerned. The major effect of decrease in light scattering is the packing of the pigments that unavoidably arises in high concentration of painted pigments. The filling fractions as the larger amount of TiO_2 pigments added to the formulation for reaching a nonnegligible enhancement of the overall paint opacity is important to optimize for use in the industrial and research application.

2.2 3D printing

In this research, the optical device or mold/frame of the optical device were printed by material jetting process using continuous inkjet printing (CIJ). The UV-curable inkjet 3D-printer (Agilista 3200, Keyence, Japan) with a UV-curable soft silicone ink (AR-G1L,

Keyence, Japan) was used for fabrication of the PDMS optical device. The silicone optical device was designed using the 3D CAD program. After that the STL file of the optical device was sent to the 3D inkjet printer. Then the printer was processed to print by UV-curing of the silicon gum ink and the 3D printed silicone optical device was observed. The 3D printed optical device could investigate the printing quality and if the 3D printed optical device did not meet the desired quality, the re-printing process can be easily produced to make the qualifiable optical device. The illustration of 3D printing process of 3D printed silicone optical device is presented in Figure 2.1.

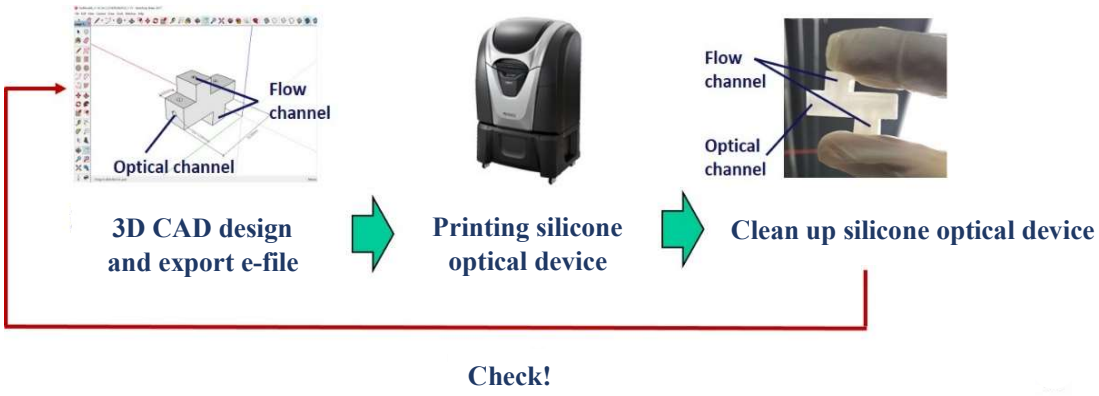

Fig. 2.1 Illustration of 3D printing process of 3D printed silicone optical device

Also, the inkjet 3D-printer was used to print the mold/frame of the optical device by a UV-curable urethane acrylate monomer ink (AR-M2, Keyence, Japan). The 3D printed mold/frame as the master pattern will further use for fabrication of the special designed PDMS optical device as shown in Figure 2.2. The step of 3D printing is similar to the 3D printed silicone optical device. However, after printing, the 3D printed molds/frames were

mounted in form of the optical design and filled with PDMS. Then, after the PDMS is casted, the 3D printed molds/frames were removed, and the optical device was observed.

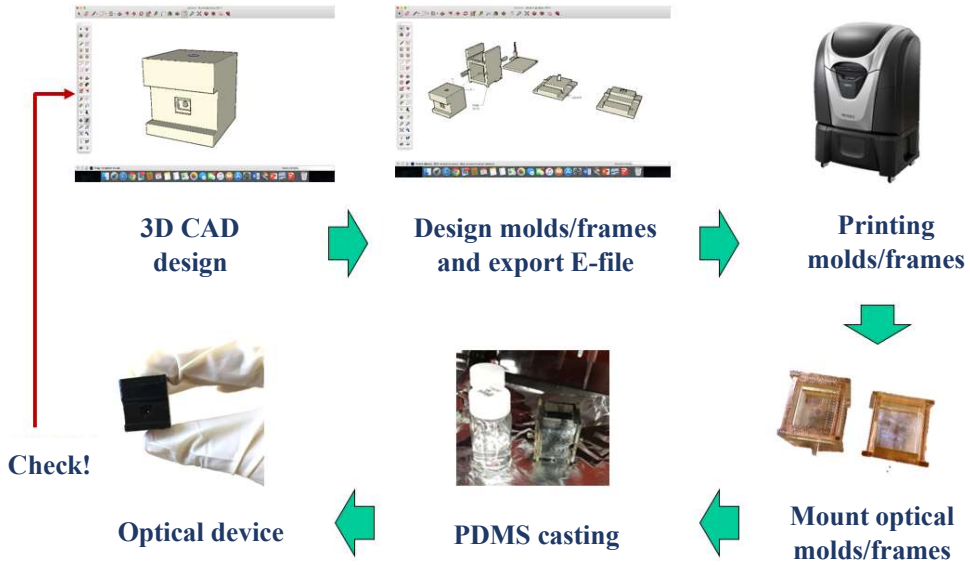

Fig. 2.2 Illustration of 3D printing process of 3D printed mold/frame of the optical device

2.3 Optical detector

2.3.1 Compact microplate reader

Figure 2.3 shows the compact microplate reader which there is dimensions of B6-sized (128 x 182 x 80 mm) like those of a cell culture microwell plate. This device consists of light sources of 24 light emitting diodes (LED), the 24 color sensors, and a SOT spatial filter for reducing noise effect. The power supply of the 24c-CMPL is alternating current (AC) 100 voltages. The color sensor (S11059-02DT/-03DS, Hamamatsu Photonics K.K.) that is responsive to red (615 nm), green (530 nm), blue (460 nm), and infrared (855 nm)

light was used for detection in the microplate reader collecting 16-bit digital data as results for each color. An Arduino microcomputer (Arduino Nano, Arduino) was connected to color sensors as the measurement unit carried out the 0–65535 data of 16 bits through the Arduino connected to a PC.

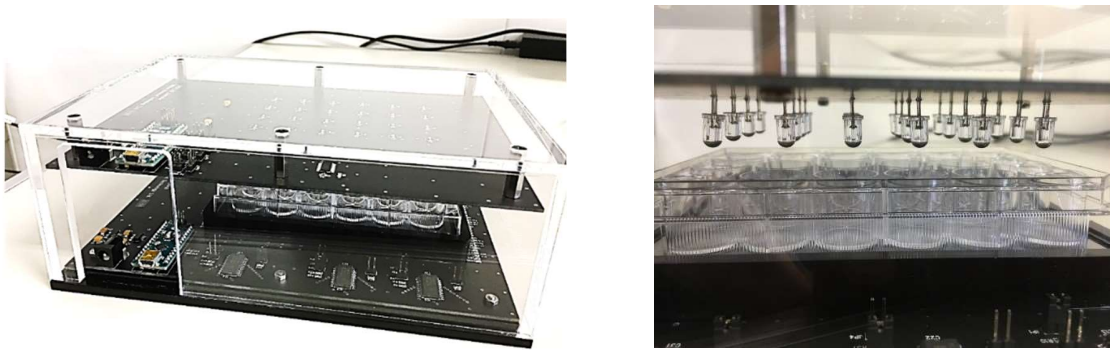

Fig. 2.3 Images of fabricated compact microplate reader

2.3.2 Ushio picoexplorer™ model PAS-110 absorbance sensor

The Ushio picoexplorer absorbance sensor is a compact laboratory research device in size of 70 x 150 x 30 mm and weight of 200 grams (Fig. 2.4), which is easily controlled by a smartphone or tablet mobile device. A quick concentration of chemical and biological compounds by colorimetric assays or reagents can be observed via this analytical tool. The sensor unit is white LED sensor which is sensitive to red (615 nm), green (530 nm), blue (460 nm) light. The readout data is 16-bit digital data for each color. The device uses 4.5 voltages if direct current (DC) using 3 AAA-type batteries or 5V DC (micro-USB connector). The operation of the Ushio picoexplorer is conveniently connected Bluetooth via a smartphone or tablet. Measurements obtained in 16-bit digital data can be saved in the

application and/or uploaded to a computer. Thus, using this device can safe the analysis time and the labors required for measurements.

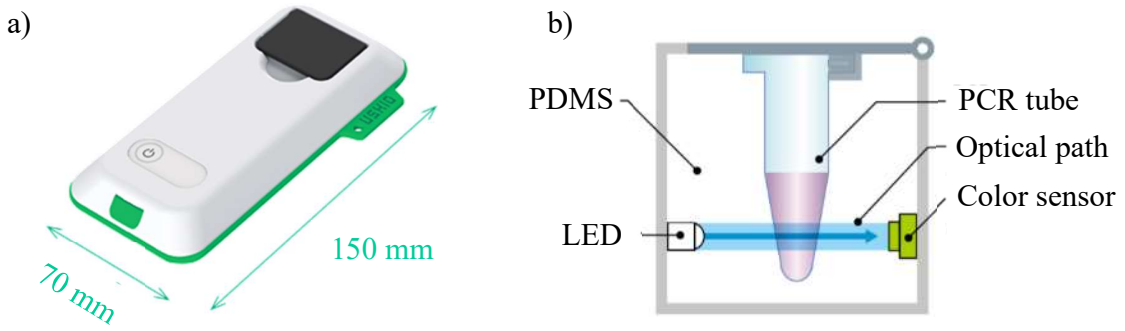

Fig. 2.4 a) Appearance of Ushio picoexplorer™ model PAS-110 absorbance sensor b) Schematic of detector of the Ushio picoexplorer [9].

References

[1] Linear Polydimethylsiloxanes, Joint Assessment of Commodity Chemicals, September 1994 (Report No. 26) ISSN 0773-6339-26.

[2] T.C. Bond, S.J. Doherty, D.W. Fahey, P.M. Forster, T. Berntsen, B.J. Deangelo, M.G. Flanner, S. Ghan, B. Kärcher, D. Koch, S. Kinne, Y. Kondo, P.K. Quinn, M.C. Sarofim, M.G. Schultz, M. Schulz, C. Venkataraman, H. Zhang, S. Zhang, N. Bellouin, S.K. Guttikunda, P.K. Hopke, M.Z. Jacobson, J.W. Kaiser, Z. Klimont, U. Lohmann, J.P. Schwarz, D. Shindell, T. Storelvmo, S.G. Warren, C.S. Zender, Bounding the role of black carbon in the climate system: A scientific assessment, J. Geophys. Res. Atmos. 118 (2013) 5380–5552.

[3] M. Shiraiwa, Y. Kondo, T. Iwamoto, K. Kita, Amplification of light absorption of black carbon by organic coating, Aerosol Sci. Technol. 44 (2010) 46–54.

[4] G. Shrestha, S.J. Traina, C.W. Swanston, Black carbon's properties and role in the environment: A comprehensive review, Sustainability. 2 (2010) 294–320.

[5] A.M. Fox, M.T. Dulay, Heterogeneous photocatalysis, Chem. Rev. 93 (1993) 341.

[6] J.C. Auger, V.A. Martinez, B. Stout, Theoretical study of the scattering efficiency of rutile titanium dioxide pigments as a function of their spatial dispersion, J. Coatings Technol. Res. 6 (2009) 89–97.

[7] M.P. Diebold, Technical Challenges for the TiO_2 Industry, JCT Coatings Tech. 1 (1) (2004) 36–44.

[8] D.J. Rutherford, Influence of TiO_2 Flocculation on the Optical Properties of Alkyd Emulsion Paints, Euro. Coat. J., 6 (1) (2001) 18–27.

[9] Ushio America, Inc, Picoexplorer PAS-110, https://www.ushio.com/files/specifications/picoexplorer-pas110.pdf (accessed 30 March 2020).

Chapter 3

Continuous cell culture monitoring using a compact microplate reader with a silicone optical technology-based spatial filter

3.1 Introduction

The development of industry of cell culture and regeneration of medicine relates to monitor the cell continuously. The management of the cell culture environment involved monitoring of the culture medium as temperature, humidity, and pH is very important. The monitoring conditions of culture medium traditionally investigated the pH values which effects to the cell condition. However, the method required skillful workers. Therefore, the microdevices were developed to use for continuous monitoring of cell states and quantitative analysis of culture medium [1-3]. These devices benefits control and measure single cells but the devices could not observe the cell state of cell population. Other methods were determining the cell state via the recovery of medium and the evaluation of the production of oxygen proteins, and amino acids [4]. However, the drawbacks of these methods were requirement of removing the culture dish from the incubator and contamination from the process of opening the lid to recover of the culture medium. An alternative approach is measurement of cell morphology using imaging data [5,6], but the instrument for investigation of cell morphology is expensive and complicated usage.

In previous research, a silicone optical technology (SOT) was developed the optical detection that has an excellent noise reduction effect [7]. The SOT concept was successfully applied to fabricate small, portable optical detection devices. The optical structure based on SOT concept consists of optical core using transparent polydimethylsiloxane (PDMS) and optical trapping layer as cladding using PDMS containing carbon black pigment. This structure provided optical properties that scattering light is adsorbed on the optical trapping

layer by carbon black pigment and allows only straight light to pass via optical core path acting as a spatial filter. It is realized that larger signal to noise (S/N) ratio compared with traditional optical systems. In this study, a compact microplate reader which can continuously and quantitatively monitor the cell state without altering environment of cell culture environment in a 24-well plate was proposed. The SOT spatial filter was embedded into the compact microplate reader to provide the ability of low noise detection. The fundamental characteristics, the optical properties for reducing noise, and biological application for cell activity of the newly developed device were evaluated.

3.2 Materials and methods

3.2.1 Device design and optical properties evaluation

An illustration of the compact microplate reader is presented in Figure 3.1. The compact device in dimensions of cell culture microwell plate was fabricated consisting of 24 LED light sources, 24 color sensors, and a SOT spatial filter. In this work, the color sensor that is sensitive to red, green, blue, and infrared light (mention in Chapter 2) was used for detection. The diameter of the optical channel was 1 mm and the length of the light guide are designed for 10 mm. The light guide using SOT spatial filter was developed to be thin and long shape for minimizing the noise signal such as scattering light and reflected light. Each LEDs has distance between them for 18 mm. The arrangement of LED light and color sensor were set in the same line for effective detection. The structure of the fabricated device which is B6-sized (182 mm x 128 mm x 80 mm) is showed in Figure 3.2. Due to using the SOT

spatial filter, the displacing of the culture plate cover does not affect to the absorption measurement, because only straight light can be detected. The tilted incidence light was trapped providing the reducing noise level of the SOT spatial filter embedded on the proposed compact reader with benefit of open space adsorption measurement. A power supply of this device was AC voltage of 100 V. All the sensors are connected by an Arduino microcomputer executed for readout data analysis. The Arduino connected to a PC was used to obtain the 0–65535 data of 16 bits as results of the fabricated device.

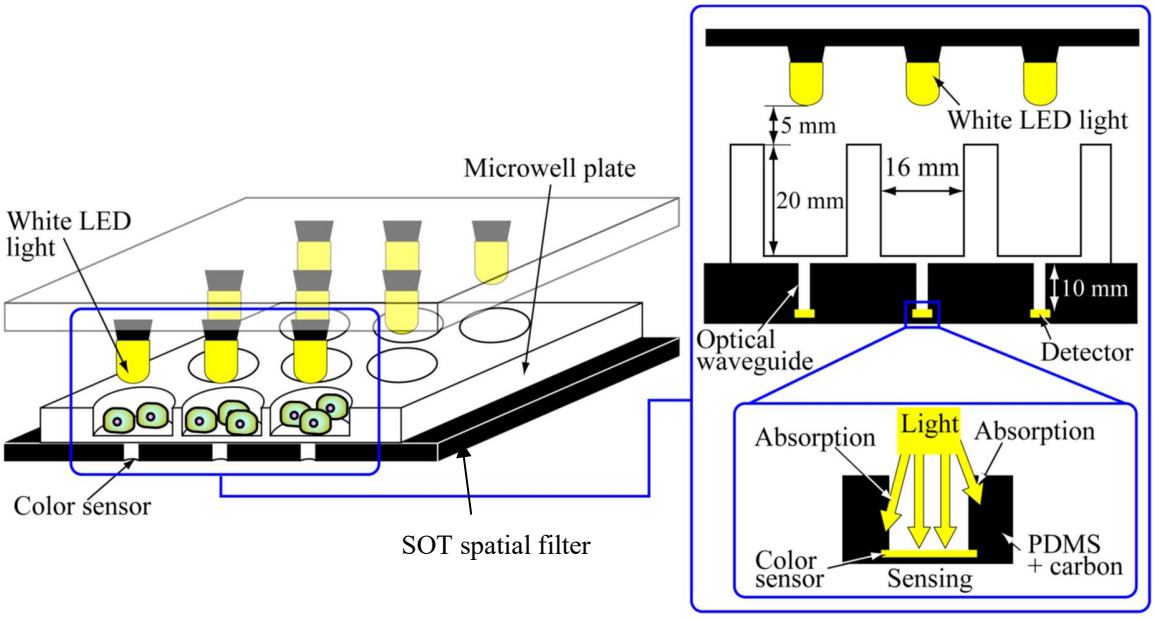

Fig. 3.1 Illustration of the compact microplate reader. The SOT spatial filter was set on the bottom of the device. The SOT spatial filter as an optical path provides excellent noise reduction efficiency.

The trapping efficiency of the SOT spatial filter was demonstrated to confirm the properties of trapping the stray light. The incident light passed through the spatial filter was measured in function of the incident angle. The compact microplate reader was tested the crosstalk as the noise effected from the near LED according to the design of microplate and from the outside light while measuring. The Red-Green-Blue-Infrared (RGB-IR) signal obtained from the LED sensor was compared the intensity between switch on and off the near LED and the intensity between light room and dark room.

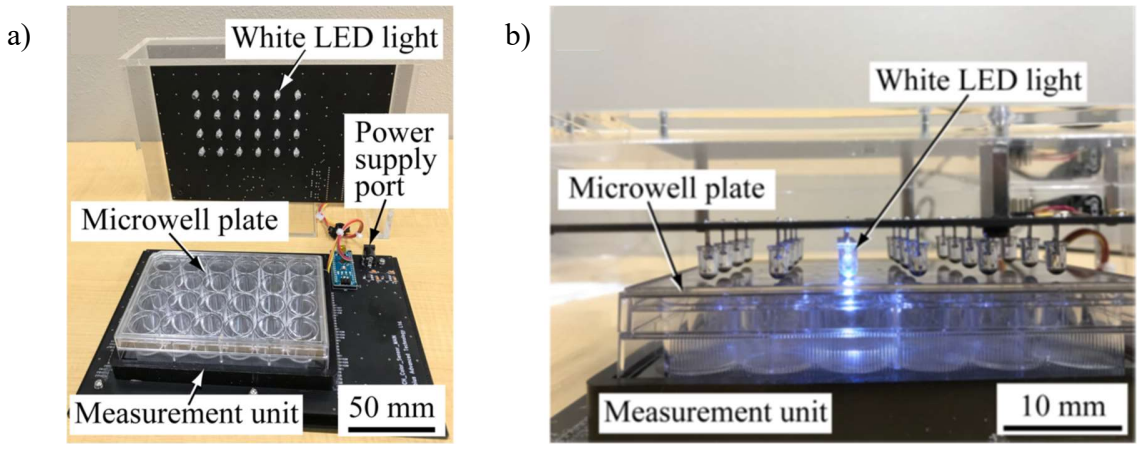

Fig. 3.2 Fabricated compact reader device a) Real image of the proposed device which the 24-well culture plate was directly set on the SOT spatial filter including the color sensors set below b) The image of side view of the proposed device showing that each LED light is aligned on each well of the 24-well culture plate.

3.2.2 Measurement of the concentration of the solution

A colorimetric assay of methylene blue (MB) solution (company mentioned in [8]) was performed to investigate ability of quantitative analysis of the proposed device. The concentration of 1.9, 3.8, 7.5, 15, and 30 μM of MB solution were prepared. 1 ml of the MB solution and blank using ultrapure water were added into each well of a 24-well plate of the fabricated microplate reader. The light intensity resulting at 16-bit resolution. The light intensity was then calculated to absorbance (Abs) using beer-lambert's law equation as $Abs = \log_{10}(I_0/ I)$, where I_0 is the intensity of initial light and I is the intensity of transmitted light and Abs were plotted versus the concentrations of MB solution.

3.2.3 Measurement of the pH in the culture medium

Continuously monitoring of change in pH of the culture medium can be evaluated by adsorption detection of color changes in the culture medium using the proposed optical device. The culture medium was prepared by MEM-α (company mentioned in [8]) supplemented with 10% fetal bovine serum, FBS (company mentioned in [8]) and 1% penicillin-streptomycin, PS (company mentioned in [8]). 1.0 ml of the prepared culture medium was added to each well of the 24-well plate and then, the plate was fixed on the proposed device. The fabricated device was incubated to monitor the change in pH of the culture medium by measuring the light adsorption. The results from the proposed device were validated with a traditional pH/mV meter (company mentioned in [8]). The measurement time of both methods were 24 hrs. which the measurement results was observed every 2 hrs.

The results from two methods were comparison to confirm the reliability of the fabricated compact device.

3.2.4 Evaluation of cell activity

The fabricated compact microplate reader was used for investigating cell activity during cultivation to examine the benefit of monitoring cell behavior in real time. A WST-1 assay using Osteoblastic cells/ MC3T3-E1 (company mentioned in [8]) was demonstrated to measure cell activity. Osteoblastic cells cultured in the medium of MEM-α supplemented with 10% FBS and 1% PS were added in concentration of 5.0×10^4 cells/ml to all wells. Then, the fabricated compact device was controlled the temperature using incubator and the cell activity was continuously observed by measuring the absorbance every 24 h for 168 h.

3.3 Results and discussion

3.3.1 Light absorption characteristics of the SOT spatial filter

3.3.1.1 Trapping efficiency of the SOT spatial filter

Figure 3.3 presents the trapping efficiency graph which related to the effect of the SOT spatial filter on the absorption of incident light. This data was updated from previous published result [8]. The intensity of light passing through the SOT spatial filter embedded on the fabricated device was dramatically decreased when the incident angle was 0 to 20 degrees. The intensity was still decreased as the function of incident angle. The transmitted light was lower than 10% compared to the initial transmitted intensity at 0 degree when the incident angle was over 10 degrees. This indicated that the indirectly incident light was

effectively scattered or absorbed by the black PDMS optical trapping layer. Thus, in the fabricated device that the detector of color sensor is attached in the SOT spatial filter at a deeper position (1 mm diameter of optical hole of the spatial filter and 10 mm of detection length), incident light from the near LED was trapped by the SOT spatial filter before reaching the bottom of the microwell plate. Therefore, the noise effect from the adjacent LED was reduced by the spatial filter. The stray light was trapped on the spatial filter providing a 99.5% trapping performance which confirmed the special optical properties of SOT spatial filter for reduction of the noise signal. A larger S/N ratio is observed due to trapping of light reflection at the optical path interface and passing of only straight light transmitted by the special SOT filter.

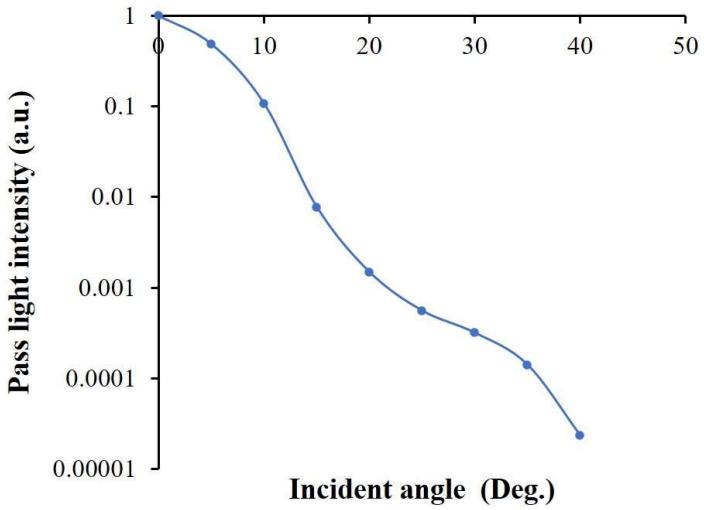

Fig. 3.3 Trapping efficiency graph evaluated by the SOT spatial filter. The pass light intensity was decreased in the function of incidence angle. The pass light intensity was less than 10% at 10 degrees.

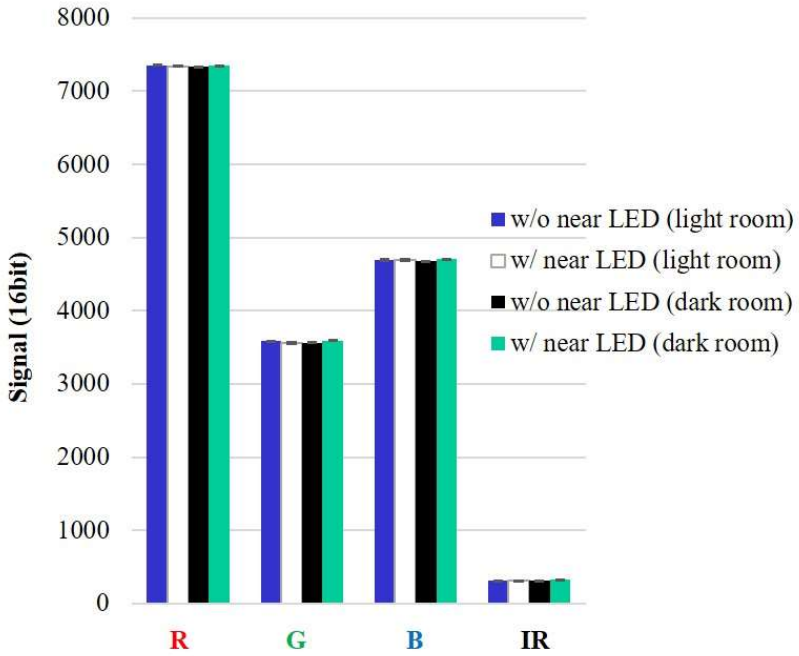

Fig. 3.4 Bar graph of the Red-Green-Blue-Infrared signal when comparison of the free air sample under condition of light room vs dark room and switch on vs switch off the near LED.

3.3.1.2 Crosstalk testing and noise reduction effect

The crosstalk was evaluated by measuring RGB-IR signal of the free air in microwell plate in light room and dark room 3 times repeatedly. In addition, the near LED (9 LEDs around the observed LED) was switched on and off to measure the effect of noise from the near LED light in both light room and dark room. The percentage difference of the signal from the light room and the dark room and the percentage difference of the signal from switch On and off of near LED were calculated from the average of RGB-IR signal at each condition. The results are presented in Table 3.1 and Fig. 3.4 which %RSD for each condition of intra-day experiment was lower than 1.5%. These results show that effects of outer light and inner LED light were insignificantly different as lower than 1% of % crosstalk except the IR signal.

It was more affect to IR signal from inner and outer light compared to Red-Green-Blue signal. However, the % crosstalk still was lower than 3% in all cases. This shows that the SOT spatial filter performed excellent ability to absorb the tiled incident light as interfered light form outside and the near LED light.

Table 3.1 Cross talk testing and reduction of noise signals results from the proposed compact device. The RGB-IR signal of the blank air sample was evaluated in light room versus dark room and switch on vs switch off the near LED.

Condition	**%Different**			
	R	G	B	IR
Switch on & off near LED (light room)	0.15	0.52	0.20	0.53
Switch on & off near LED (dark room)	0.22	0.80	0.73	2.19
Light room Vs dark room	0.25	0.65	0.50	2.98

3.3.2 Measurement of solution concentration

The methylene blue (MB) solution at different concentrations were evaluated the transmitted light signal using the fabricated compact device. The results of the signal from the proposed device are presented in Fig. 3.5 showing that decrease in overall signal when increase in the MB concentration. Because the blue color of MB solution can be adsorbed the transmitted light of the proposed compact device, the observed signal after passing through the blue solution of MB solution was decreased. However, there were wide variation of 24 wells microplate in the measurement results due to deviations of position between sensors and the LED light sources, the sensors and the 24 wells, and the LED light sources.

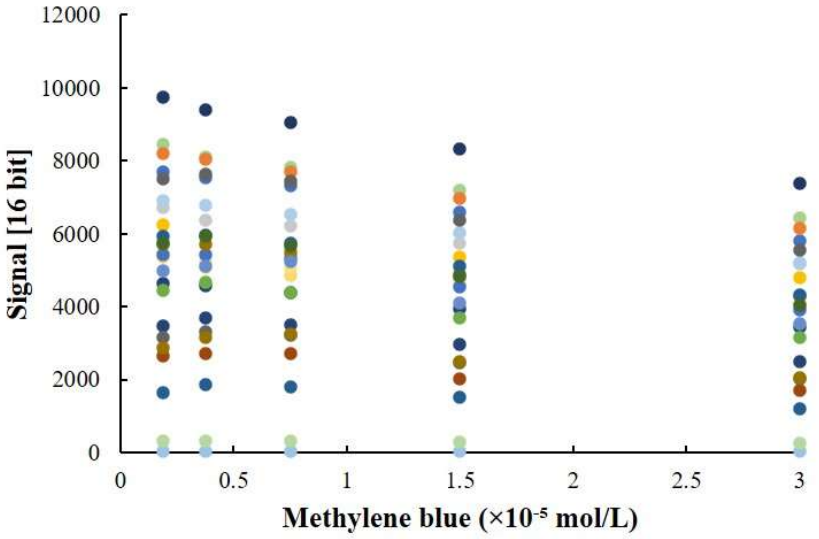

Fig. 3.5 Optical signals for all wells in the 24-well plate investigated by the fabricated compact device

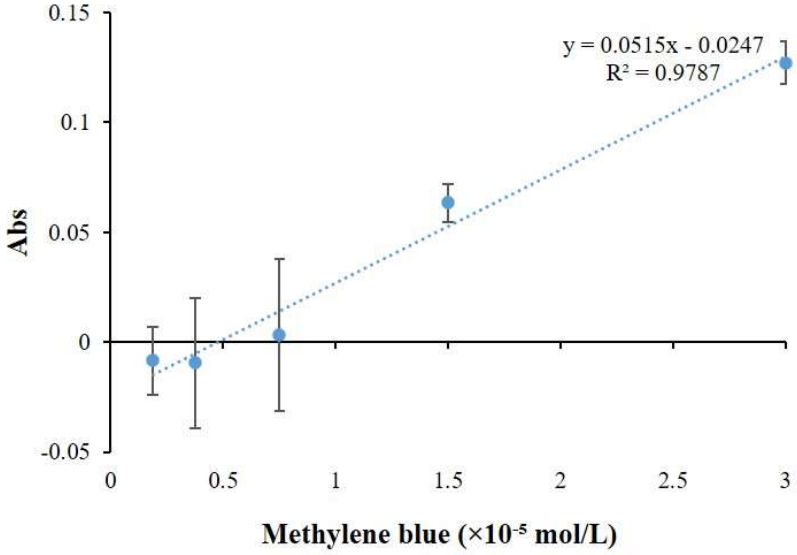

Fig. 3.6 Calibration curve of methylene blue measuring by the compact microplate reader

The methylene blue concentration was plotted in a function of absorbance of fabricated compact device at 615 nm referred as the calibration curve of methylene blue. The absorbances were calculated from the measured signals based on the beer-lambert's law equation. Figure 3.6 presents the calibration curve of the MB solution which was observed that the absorbance of the MB solution increased when the concentration of the MB solution also increased. The results showed that the detection limit of the MB solution of this fabricated device was 10 μM and the quantitation limit which provided the accurate measurement of the fabricated compact device was 15 μM. These results confirmed that the proposed microplate reader was successfully detected color changes of the culture medium with high accuracy in each well.

3.3.3 Change in pH of the culture medium

The results of changes in the pH of the culture medium over time using a pH/mV meter (n=3) are shown in Figure 3.7a). It indicated that the pH value in the culture medium increased over time. However, after 8 h, the pH value was constant at pH 9.0. Comparison to the results obtained the fabricated compact device as shown in Figure 3.7b), the absorbances (n=5) were plotted versus the cultivation time presenting a similar trend to the traditional pH meter. Thus, the proposed device attained continuous monitoring of pH values by measuring absorbance of the culture medium over time. The proposed method based on the absorbance of the culture medium can be the quantitative measurement of the cell state without requirement of recovery the medium during the cell culture.

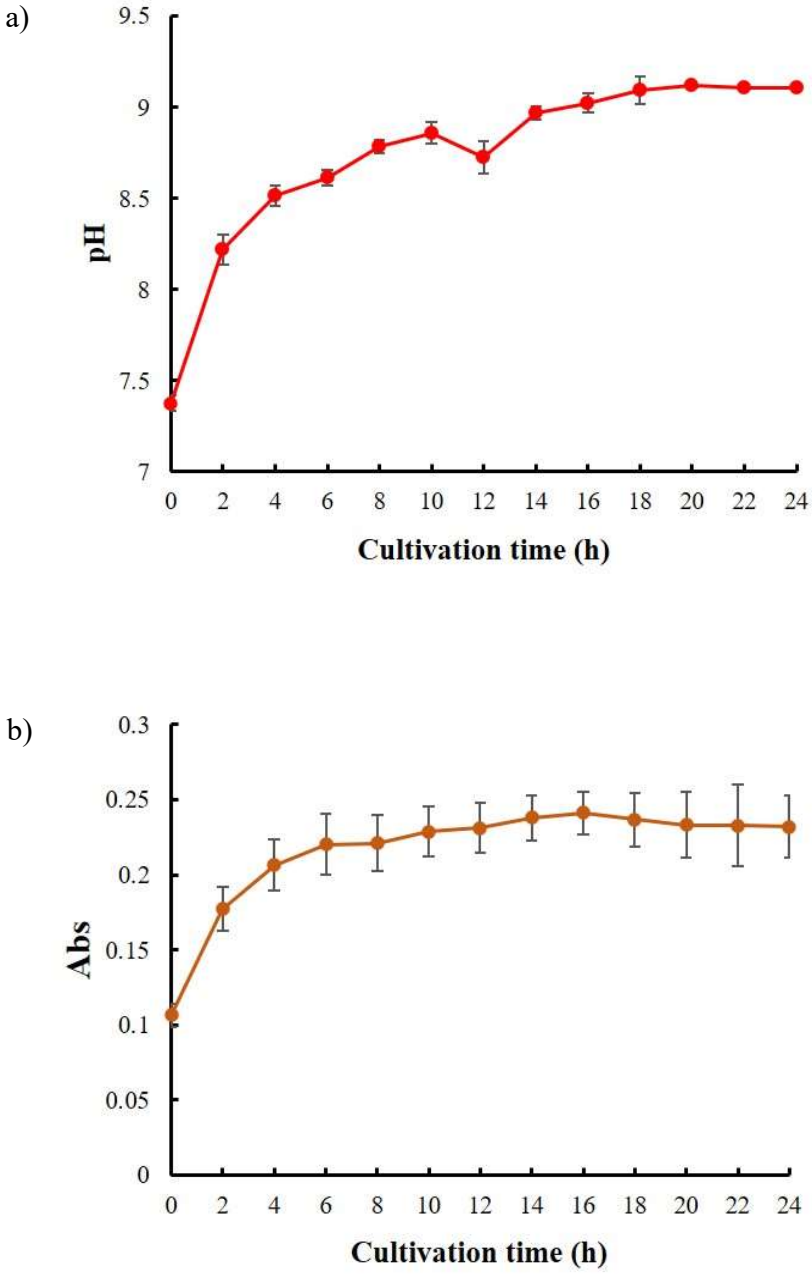

Fig. 3.7 a) Changes in the pH of the culture medium observed by a pH/mV meter over time. b) Changes in the absorbance of the culture medium in microwells observed by the developed compact device (λ = 530 nm).

3.3.4 Cell activity and ammonium concentration in the culture medium

The cell activity of Osteoblastic cells cultured in the medium was achieved over time. Results measured 5 times at each cultivation time show in Figure 3. From the cultivation time of 24 to 72 h, the cell activity increased as observed absorbance from the fabricated compact device increased. However, the absorbance values showed nearly unchanging after 72 h. These results indicate that cell generation was occurred to increase the number of cells during 24-72 h, but the culture cells were saturated that were no longer proliferation after 72 h. Thus, the constant absorbances were observed meaning that increase in culture cells were stopped after 72 h.

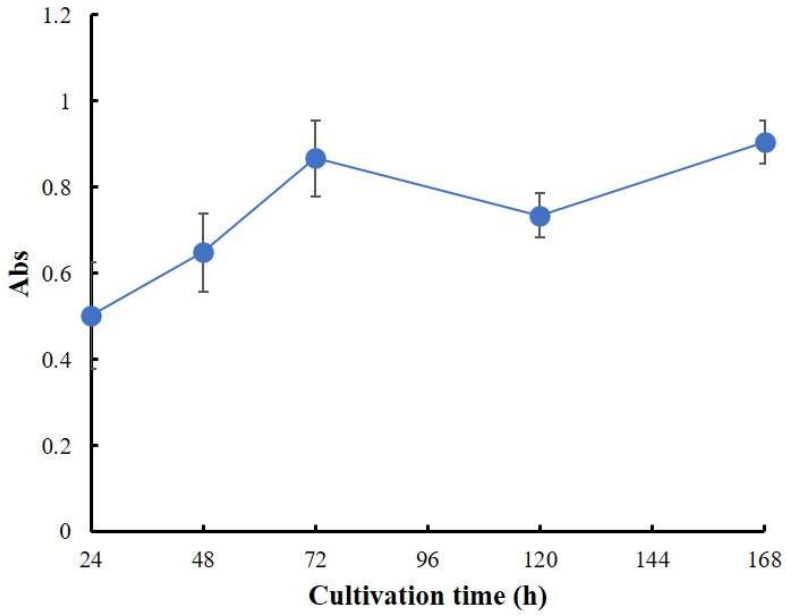

Fig. 3.8 Cell activity of Osteoblastic cells using the fabricated device (n=5). The measurement wavelength was 460 nm.

The calibration curve of ammonium plotted between absorbance and ammonium concentration shows in Figure 3.9. Changes in absorbance with respect to the ammonium concentration were measured 3 times (n=3) repeatedly. The results showed that calibration curved was linear from 0-1 mM of the ammonium concentrations with high accuracy and precision. The absorbance increased while the ammonium concentration in the culture medium also increased. The results confirmed that the fabricated compact device can continuously monitoring cell activity and evaluating any substance production during the cultivation time without the recovery of the culture medium. Thus, the proposed 24c-CMPL can be used to measure the state of cells with high accuracy and precision. Also, it can monitor the culture environment in real time without changing the cell culture environment.

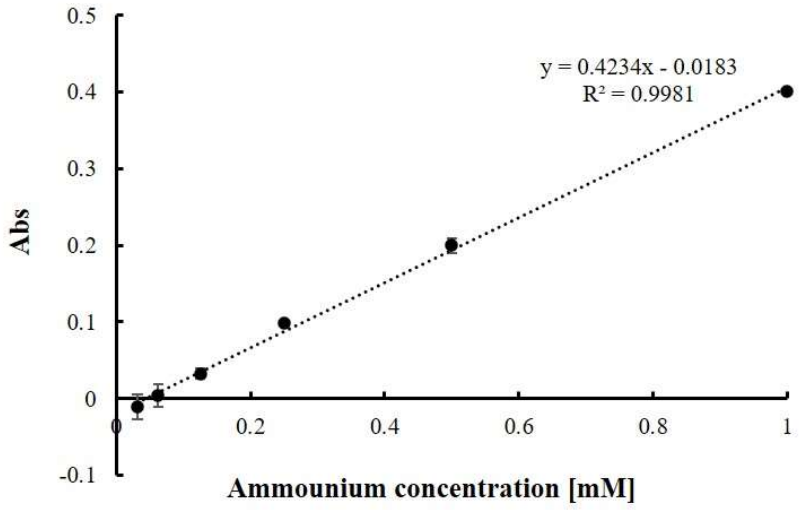

Fig. 3.9 Calibration curve of ammonium concentration (n=3). The measurement wavelength was 615 nm.

The potential of the proposed compact device overcomes the traditional method for managing system of cell culture. It can be effectively used for induced pluripotent stem cells. In the process of culture of cells derived from patients in vitro, the culture cells need to be safe for long time periods [9]. Moreover, this process is expensive, time-consuming, and labor-intensive [10]. Currently, the process recovery the cell culture medium was sued to approach quality control of cultivation of cells. However, the contamination can be risked occurring because of the opening of the cover during the recovery of the culture medium and contaminated equipment. Thus, the proposed small microplate reader that can be used to monitor cell culture continuously in real time without changing the culture environment enables to manage and control the culture of cells with high efficiency and evaluate the quantitative analysis of culture cells in the medium with high accuracy and precision.

3.4 Conclusion

The compact microplate reader was successfully fabricated using the SOT concept for reduction of noise effect. The real-time monitoring of the cell activity, substance production, and culture environment can be observed using this device. The methylene blue solution used to confirm the ability of optical detection for quantitative analysis based on absorbance with high accuracy using methylene blue. Moreover, the proposed device was validated the potential of measuring pH of the culture medium by the pH meter. The fabricated compact device was used to monitor changes in cell activity continuously over time and detect the ammonium substance during the cell culture in real time without altering the cell surroundings.

Reference

[1] A.M. Gonzalez-Suarez, J.G. Pena-Del Castillo, A. Hernández-Cruz, J.L. Garcia-Cordero, Dynamic generation of concentration and temporal-dependent chemical signals in an integrated microfluidic device for single-cell analysis, Anal. Chem. 90 (2018) 8331–8336.

[2] J. Song, H. Ryu, M. Chung, Y. Kim, Y. Blum, S. sik Lee, O. Pertz, N.L. Jeon, Microfluidic platform for single cell analysis under dynamic spatial and temporal stimulation, Biosens. Bioelectron. 104 (2018) 58–64.

[3] Y. Nakashima, Y. Yang, K. Minami, Development of a micro cell compression stimulator for evaluating real-time cellular responses, Rev. Sci. Instrum. 83 (2012).

[4] Details, Raffle. "Patent Application Publication." Patent Application Publication Apr. 14, 2016 Sheet 1 of 43 US 2016/0104348 A1.

[5] F. Matsuoka, I. Takeuchi, H. Agata, H. Kagami, H. Shiono, Y. Kiyota, H. Honda, R. Kato, Morphology-Based Prediction of Osteogenic Differentiation Potential of Human Mesenchymal Stem Cells, PLoS One. 8 (2013).

[6] S. Sugimura, T. Akai, T. Somfai, M. Hirayama, Y. Aikawa, M. Ohtake, H. Hattori, S. Kobayashi, Y. Hashiyada, K. Konishi, K. Imai, Time-Lapse Cinematography-Compatible Polystyrene-Based Microwell Culture System: A Novel Tool for Tracking the Development of Individual Bovine Embryos1, Biol. Reprod. 83 (2010) 970–978.

[7] H. Higuchi, H. Yoshioka, H. Nomada, Y. Oki, K. Morita, Carbon–polydimethylsiloxane-based integratable optical technology for spectroscopic analysis, Talanta. 166 (2015) 428–432.

[8] Y. Nakashima, M. Kounoura, C. Malasuk, K. Nakakubo, N. Watanabe, S. Iwata, K. Morita, Y. Oki, S. Kuhara, K. Tashiro, Y. Nakanishi, Continuous cell culture monitoring using a compact microplate reader with a silicone optical technology-based spatial filter, Rev. Sci. Instrum. 90 (2019).

[9] R. Nakajima, T. Kobayashi, N. Moriya, M. Mizutani, K. Kan, T. Nozaki, K. Saitoh, M. Yamato, T. Okano, S. Takeda, A novel closed cell culture device for fabrication of corneal epithelial cell sheets, J. Tissue Eng. Regen. Med. 9(11) (2015) 1259-1267.

[10] H. Kagami, H. Agata, R. Kato, F. Matsuoka, A. Tojo, Fundamental technological developments required for increased availability of tissue engineering. In Regenerative Medicine and Tissue Engineering - Cells and Biomaterials, InTechOpen. (2011).

Chapter 4

3D printing optical devices based on silicone optical technology (SOT) and its application on analytical chemistry

4.1 Introduction

Currently, trend of analytical system or device has become small, portable, and rapid-fabrication/prototyping to adapt and access for on-demand and on-site measurement. For example, micro-total analysis systems (μ-TAS) or lab-on-ship devices have been popular in this decade because of its advantages as small size, ease to fabricate, less-time production, increase in throughput, and effective chemicals or biologicals detection. Flow injection analysis (FIA) is one of the chemical analysis techniques which need to minimize the system for ease to use on-site measurement. Traditionally, the detection part in FIA system was spectrophotometer which was an optical system configured optical components in a space [1,2]. The light path of the traditional optical detection was bulky due to requirement of space for optical system. Moreover, it needs robust frames using the heavy material for precise mounts. These made traditional optical systems cumbersome and expensive. Thus, optical system which the light path was filled with transparent and solid-state medium called "filled path" optical system [3,4] was demonstrated to replace the blank space in transitional optical system. This replacement showed ability of reducing in fundamental base and increase in stability, but a tenability was decreased.

Recently, we proposed monolithic and compact optical system based on polydimethylsiloxane (PDMS) as common matrix, and termed silicone optical technology (SOT) [5]. Previous work, the optical channel with core of transparent PDMS optical channel and clad of the carbon dispersed PDMS worked as a simple and filled quasi spatial filter (SOT-QSF) that can trap the tilted incidence such as stray lights from the multiple scattering

due to the filled optical cavity, because of the refractive index matching on the core and clad boundary. The carbon black pigment adsorbed the tilted incident light, thus only the light propagating along the filled optical channel (PDMS core) can pass to the detector showed low noise level detection. Thus, the SOT-QSF could be successfully embedded by inserting PDMS core with black PDMS clad to avoid the noise lights of unexpected incident angle as tiny and light-weighted optical system for spectroscopy detection.

Novel 3D fabrication technology as 3D printing has widely used in many applications such as food design [6,7], innovative tool for math and geometry teaching [8], construction industry [9,10] and so on. 3D printing or an additive manufacturing (AM) process defined as 'the process of joining materials to make objects from 3D model data, usually layer upon layer, as opposed to subtractive manufacturing methodologies, such as traditional machining' [11,12]. Its benefits were provided as automation, lower costs, save times, reduction of waste materials and transcendence of limits of fabrication processes for developing products. Also, the 3D printing was high reducibility [13]. Owing to lots of its advantages, we were interested in using 3D printing technology for rapid and easy fabrication process of optical devices based on SOT concept. On the other hand, the surface quality and translucent of the 3D printable material seems insufficient to print the optical system directly.

In this study, an optical device which is flexible, small, and light weight was fabricated by combining 3D printing technique and SOT-QSF planting for using in flow injection analysis (FIA) system. The flexible frame was directly fabricated using silicone 3D printer, and simple injecting and blowing method was developed for embedding of SOT-QSF

by coating black PDMS (carbon dispersed PDMS) and injecting transparent PDMS. The appearance and microscopic image were investigated the properties of coated surface. Furthermore, trapping performance of the planted SOT-QSF was performed to show its ability for suppressing the noise level of the detection. This simple and versatile embedding method can realize rapid and flexible fabrication of SOT based FIA optical system by combining the 3D-printing technologies.

4.2 Materials and methods

As main matrix, polydimethylsiloxane-SIM360 or PDMS-SIM360 and its catalyst or CAT 360 (company mentioned in [16]) were adapted. Carbon black ((company mentioned in [16])) with 5 wt.% was mixed by mixing rotator ((company mentioned in [16])) at auto-rotating 1,108 rpm for 200 seconds, 4-5 times. 3D silicone optical frame was printed using an inkjet and UV-curable 3D-printer (mentioned in Chapter 2) with ink material UV-curable soft silicone (mentioned in Chapter 2). Therefore, this silicone optical device was soft, flexible and proper for many applications. The 3D CAD (Computer aid design) model for fabricating silicone 3D printing optical module was designed in dimension 20 x 30 x 20 mm using Sketch up make 2017 program (Fig. 4.1a). In this work, 2 types of channel/hole were designed to cross each other as flow channel and optical channel. The diameter of flow channel was 2.0 mm for PTFE tube of flow injection analysis system and optical channel was 2.0 mm diameter.

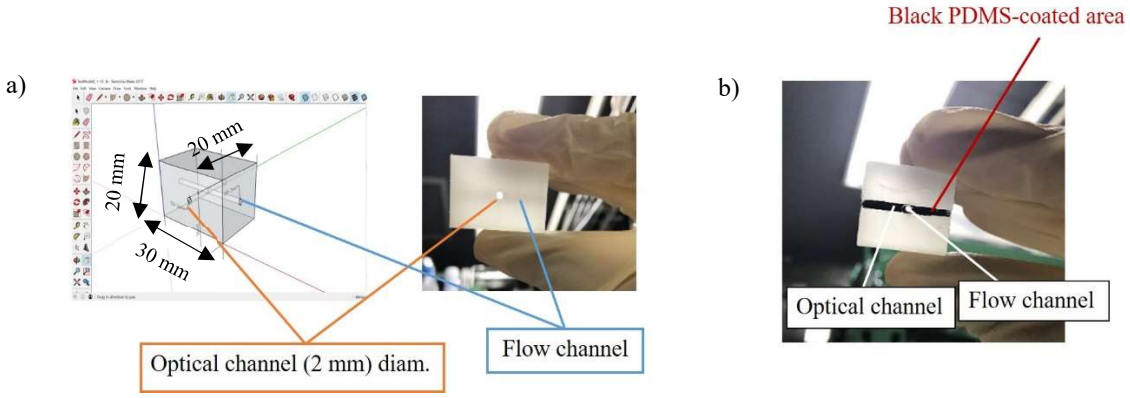

Fig. 4.1 a) 3D CAD design (20 x 30 x 20 mm, OD = 2.0 mm) and image of 3D printed silicone optical device b) Cross section cut of SOT device after coating process

The addition of the embedded SOT-QSFs into modules was as followings: after silicone frame printed, the black PDMS was coated with injection and air-blowing. Firstly, the black PDMS was mixed with catalyst and injected with using pneumatic syringe dispenser ((company mentioned in [16])) into the hole for optical apertures. After that, controlled air from the dispenser was pursed for making black PDMS coated inside the holes. Since the air exhausted from the opposite side's aperture and crossed holes (for flow channels), This process was done from the opposite side. The pressure of 0.05 to 0.125 mPa was used for injection of the black PDMS and pressure of 0.03 to was used to blow the black PDMS for coating around the channel. Then, the heated air ((company mentioned in [16])) was blown to cure the black PDMS on the optical channel for 1 minutes (Fig. 4.1b). Finally, the clear PDMS was filled into the optical channel for making the filled optical path of the SOT optical modules.

4.3 Results and discussion

4.3.1 Properties of coated black PDMS surface

The inside-coating of black PDMS in the 2 mmφ holes were investigated in term of surface appearance investigated by naked-eyes, microscopic surface character investigated by microscope, surface thickness investigated by microscope, and surface roughness investigated by AFM microscope.

Figure 4.2 presented the visible and microscopic images (company mentioned in [16]) of coated black PDMS surface varied condition of coating. The pressure of the PDMS injection was varied from 0.050 mPa to 0.125 mPa, and air-blowing pressure of 0.030 and 0.060 mPa were investigated. When the viscosity of the PDMS was 7000 mPa · s, more than 0.100 mPa was needed to fill the cylinder of 2 mmφ x 10 mm, and the air pressure of more than 0.040 mPa was required for eject the filled PDMS and then apply coating. The injection pressure of 0.050-0.075 mPa provided incomplete coated area, and pressure of 0.125 mPa remained debris at the cross-section part after the blowing. On the other hand, the air pressure of 0.040 and 0.050 mPa could eject the filled PDMS and showed acceptable coating condition as shown in Figure 4.2. Since the higher pressure provided no coating but remove the black PDMS from the optical holes, the best coating condition was obtained at blowing pressure of 0.050 mPa.

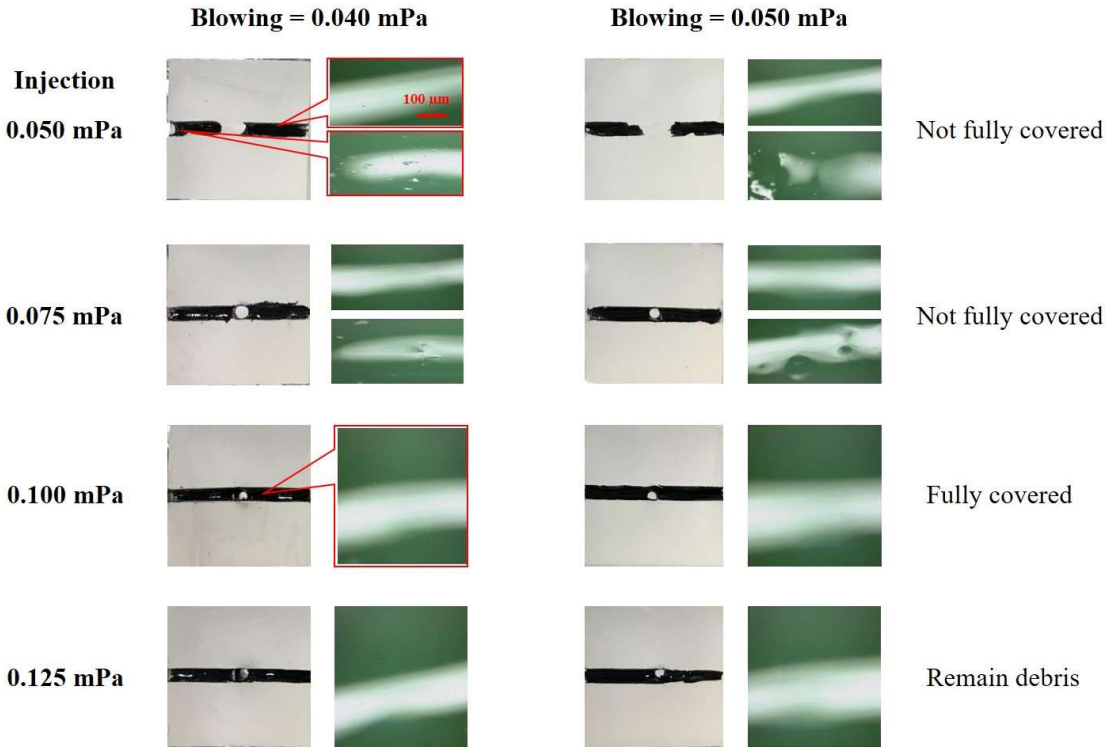

Fig. 4.2 The visible images and microscopic images (x250) of coated black PDMS surface on 3D printed silicone optical device varied by injection and blowing pressure of syringe dispenser. The green area was non-black PDMS coated area and the white transparent area was the coated area of optical channel.

Subsequently, the black PDMS layer's pealed from the hole's inside wall was observed using microscope measurement ((company mentioned in [16])), and the cross-section was shown in Figure 4.3a. The coating condition was 0.100 mPa of injection pressure and 0.050 mPa of blowing pressure. The thickness about 500-600 µm was confirmed. In comparison with rough outer-side (right in the picture, boundary with 3D printed silicone), the inner-side showed smooth curvature surface.

Figure 4.3b represented microscopic profile of the inner side surface with nanoscale hybrid AFM (company mentioned in [16]). The left image is x250 magnification, and right image is AFM profile of 20 x 20 µm area. The average RMS of coated surface was 30 to 100 nm, which showed that the coated surface was smooth, uniform and proper for using as optical channel.

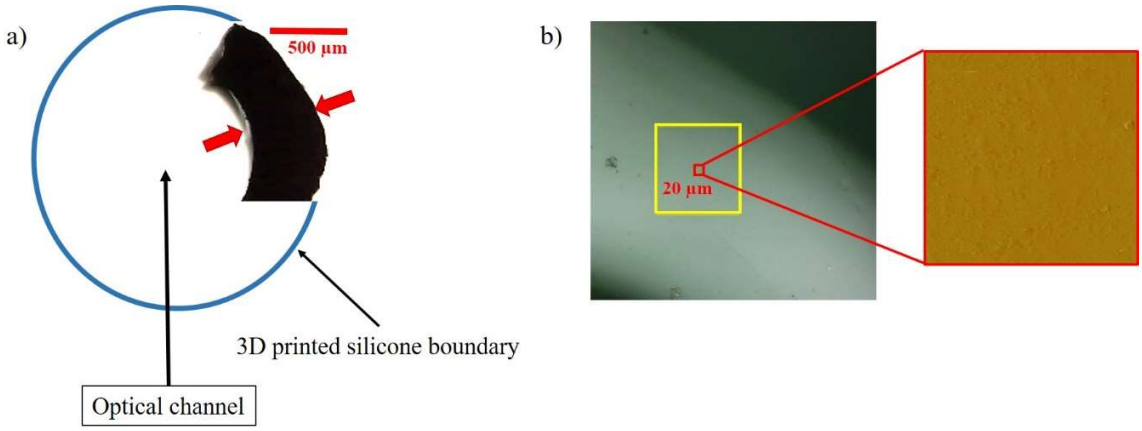

Fig. 4.3 a) The microscopic images (40x) of coated black PDMS surface (cross section cut) b) The AFM microscopic image (250x, 20x20 µm) of coated black PDMS surface

4.3.2 Trapping efficiency of SOT-QSF optical module

The efficiency of the planted SOT-QSF can be evaluated by checking transmittance of the tilted light against the optical axis. In previous work, similar structure (core: PDMS/clad: carbon mixed PDMS) of SOT-QSF (1 x 2 mm2 width and 10 mm Long) were evaluated. The result presented that first scattering suppress noise to 0.5% in boundary of PDMS/black PDMS and 2~3 Scattering is sufficient trapping performance such as OD > 4 [5].

In this work, to evaluate trapping performance of modules with SOT-QSF with injection coating was tested as first step. Since the whole module was translucent, the supporting holes for optical baffle was also introduced. As shown in figure 4.4, 2 types of module such as, without filling black PDMS in the baffles hole, and with filled as baffles. Center schematic shows an experimental setup for evaluation of trapping efficiency, the laser beam at 532 nm was aligned with an Al mirror and was increased by concave lens to cover the entrance of the SOT-QSF. The detector collected the light intensity in every 5 degrees of torsion angle until 30 degrees and then was converted to normalized intensity by dividing the obtained intensity with the intensity at 0 degree (highest intensity). The trapping performance was evaluated 3 times repeatedly to obtain the average normalized intensity. Then the transmitted laser light intensity was plotted as versus the torsion angle.

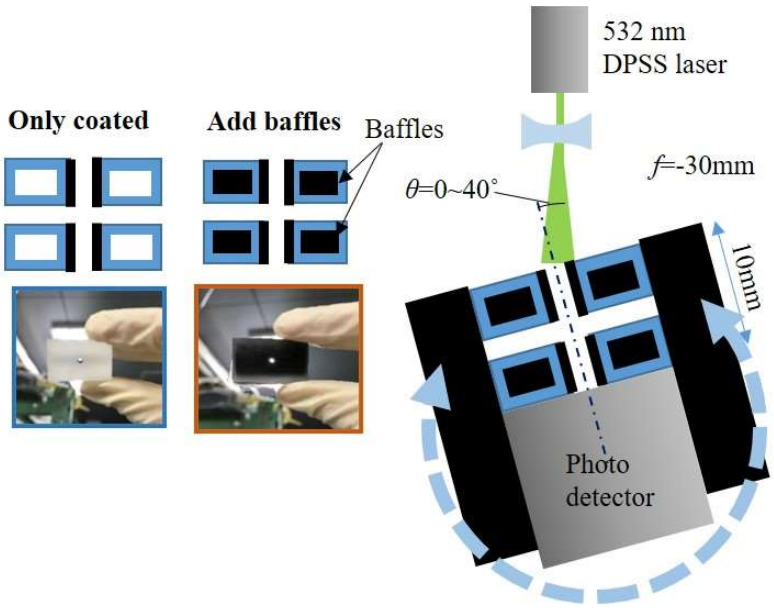

Fig. 4.4 Experimental setup of in-house instrument for trapping performance

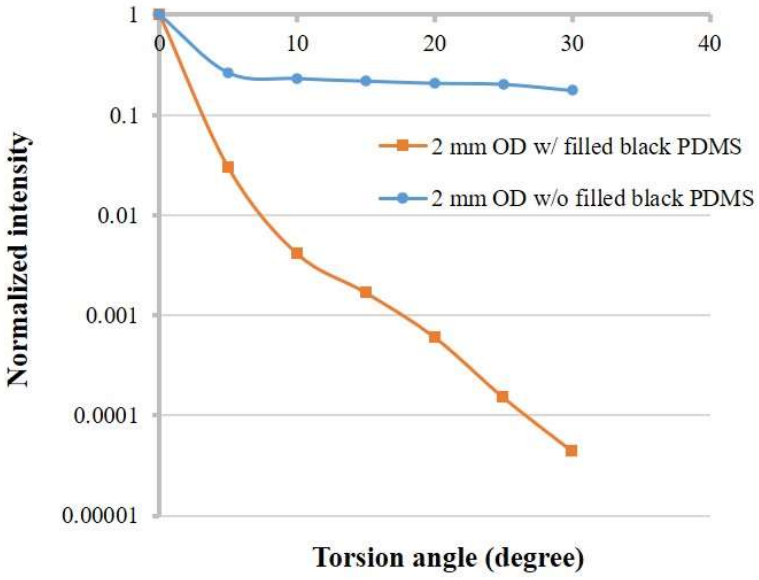

Fig. 4.5 Experimental trapping efficiency which normalized intensity of the SOT-QSF optical module for analytical chemistry application plotted versus the torsion angle. Blue line in the graph indicated non-filled black PDMS SOT-QSF optical module and orange line indicated filled black PDMS SOT-QSF optical module.

The result in Figure 4.5 showed that the SOT optical module with planted SOF-QSF and internal bulks of black PDMS obtained a good trapping efficiency which can reduce the pass light down to 10^4 times at 30 degrees of torsion angle even though there was some 3D printed silicone material that is translucent. On the other hand, the light can be trapped only 83% at 30 degrees of torsion angle (0.17 of normalized intensity as shown in Fig. 4.4) due to the PDMS/coated black PDMS boundary without internal bulks. This could be investigated that there is some tilted incident light pass to the detector and cannot be trapped in case of non-filled SOT-QSF optical module. 99.9% of trapping efficiency was observed with SOT-QSF and internal balks, the 3D printing method can be possible to create the

channel for adding the blank PDMS internal bulks. This means on-demand and on-site, and rapid fabrication of SOT based FIA system-modules with planted SOT-QSF can be achieved with 3D printed silicone frame.

4.4 Conclusion

The proposed rapid and digital fabrication of silicone optical module was demonstrated by using 3D printable UV-cured-PDMS frame and injection coating of optical trapping layer. The facile coating method was demonstrated using syringe dispenser and the results of physical properties of coated surface showed proper and acceptable properties which able to use as the surface of optical channel. A simply fabricated SOT optical modules from 3D printed frame and coated quasi special filter showed 99.9% trapping performance on tilted light incidence, by introducing internal baffles. In future, this proposed SOT optical device will be developed to gather with flow analysis system as simple, low cost, flexibility, portability and high sensitivity device utilized for on-site and on-demand measurement.

References

[1] A.R.H. Cole, A.A. Green, G.A. Osborne, G.D. Reece, Vacuum grating spectrometer for the mid and far infrared, Appl. Opt. 9 (1970) 23–29.

[2] F.J. Fortes, J.J. Laserna, The development of fieldable laser-induced breakdown spectrometer: no limits on the horizon, Spectro chim. Acta Part B. 65 (2010) 975-990.

[3] N.J. Herrick, K.H. Beckmann, Internal Reflection Spectroscopy, Wiely Intersc., Net Work. (1967) 215-245.

[4] N.J. Herrick, G.I. Loeb, Multiple internal reflection fluorescence spectrometry, Anal. Chem. 45 (1973) 687–691.

[5] H. Higuchi, H. Yoshioka, H. Nomada, Y. Oki, K. Morita, Carbon–polydimethylsiloxane-based integratable optical technology for spectroscopic analysis, Talanta. 166 (2015) 428–432.

[6] J. Sun, Z. Peng, W. Zhou, J.Y.H. Fuh, G.S. Hong, A. Chiu, A Review on 3D Printing for Customized Food Fabrication, Procedia Manuf. 1 (2015) 308–319.

[7] F.C. Godoi, S. Prakash, B.R. Bhandari, 3d printing technologies applied for food design: Status and prospects, J. Food Eng. 179 (2016) 44–54.

[8] M. Huleihil, 3D printing technology as innovative tool for math and geometry teaching applications, 2017 IOP Conf. Ser.: Mater. Sci. Eng. 164 (2017) 1-7.

[9] I. Perkins, M. Skitmore, Three-dimensional printing in the construction industry: A review, Int. J. Constr. Manag. 15 (2015) 1–9.

[10] F. Bos, R. Wolfs, Z. Ahmed, T. Salet, Additive manufacturing of concrete in construction: potentials and challenges of 3D concrete printing, Virtual Phys. Prototyp. 11 (2016) 209–225.

[11] T. Duda, L.V. Raghavan, 3D Metal Printing Technology, IFAC-PapersOnLine. 49 (2016) 103–110.

[12] H. Bikas, P. Stavropoulos, G. Chryssolouris, Additive manufacturing methods and modeling approaches: A critical review, Int. J. Adv. Manuf. Technol. 83 (2016) 389–405.

[13] B. Satyanarayana, K.J. Prakash, Component Replication Using 3D Printing Technology, Procedia Mater. Sci. 10 (2015) 263–269.

[14] G.M. Whitesides, J.L. Wilbur, E.L. Cheung, L.K. Lee, M.G. Prentiss, R.J. Jackman, Elastomeric Optics, Chem. Mater. 8 (2002) 1380–1385.

[15] P. Liebetraut, S. Petsch, J. Liebeskind, H. Zappe, Elastomeric lenses with tunable astigmatism, Light Sci. Appl. 2 (2013).

[16] C. Malasuk, K. Nakakubo, H. Yoshioka, K. Morita, and Y. Oki, 3D printing optical devices based on silicone optical technology (SOT) and its application on analytical chemistry, Proc. of SPIE OPTO 2018, 10914.

Chapter 5

Compact and on-demand 3D-printed optical device based on silicone optical technology (SOT) for on-site measurement: Application to flow injection analysis

5.1 Introduction

The purposes of development of analytical devices are to miniaturize, make portable, and easy fabricated because trend of the device need to achieve function of adaptability and accessibility for on-site analysis. Previously, real time, portable and diagnostic reader devices were presented as micro total analysis systems (μTASs) or lab-on-chip devices [1-3]. These were the first ideal devices for on-site measurement analysis and many of analytical chemistry techniques required to develop the devices that are small size, convenience use, and portability for on-site analysis. The contemporary analytical technique called flow injection analysis (FIA) which is the automated method for chemical and biological analysis was also developed to miniaturize using in various applications [4]. The miniaturize FIA system provided benefits that can reduce the amount of sample and reagent, highly reproduce, expand the sample into the reagent stream, and easily use for on-site analysis. Focusing on detection part of FIA system, traditional instrument for detection in the FIA system was spectrophotometer, which is robust, tunable, and precise. However, the traditional optical system is hard to integrate, large, expensive, and not suitable for on-site analysis function. Thus, the development of analytical instruments for detection in FIA system have been newly designed based on the function of simple and compact devices [5,6]. The use of optoelectronic components as light-emitting diodes (LEDs) were demonstrated to use as light sources in miniaturized flow-through FIA systems. Previous researches were applied the LED light source for determination of transition metal [7,8], organic compound as the pesticide paraquat [9], and enzymatic reaction [10] in the FIA system. These presented that

the LED-based flow cells using as optical detection were successfully utilized for chemical analysis using miniaturized FIA system.

Previous research of the developed compact optical system was demonstrated in 2017 [11]. It was termed silicone optical technology (SOT) which using polydimethylsiloxane (PDMS) as a conventional material for fabrication of a small, lightweight optical system for spectroscopic detection. The properties as spatial filter was performed by construction of simple coaxial structure using transparent PDMS as optical core channel and carbon dispersed PDMS as cladding of the optical channel. This optical filter named the quasi-spatial filter (SOT-QSF) could reduce the effect of inclined light. It can cut off and block stray light scattered from interfered light because there is counterpart of refractive index at the core and cladding border of PDMS/carbon dispersed PDMS. The SOT-QSFs were confirmed the special properties of trapping the undesired light which the inclined incident light is adsorbed and scattered by the carbon black mixed PDMS layer, only the straight light can propagate along the PDMS core [12,13]. This attained the advantage of high sensitivity with low noise effect. Thus, the SOT-QSF was used to embed in the miniaturized optical system for on-site detection of spectroscopic analysis. However, the simple coaxial SOT structures need to develop the fabrication method to be simpler without complex fabrication processes.

Currently, a novel 3D fabrication technology of three-dimensional (3D) printing has been widely used in many analytical chemistry applications [14]. The 3D printing technique is the process that materials are combined to form the 3D objects by the computer control [15]. Many researchers used this technique for fabrication of microfluidic devices [16,17],

ultraviolet (UV)-visible cuvette adapter [18], and open-source colorimeter [19] related to chemical analysis. Because of advantages in automation processes, saving times, inexpensive process, and waste reduction, the 3D printing method have been gained in attention for chemists to use for simple fabrication of instruments. In addition, the 3D printing process is able to reproduce with high precision and various design for suitable use. Thus, in this work, we proposed to use the 3D printing technique for development of fabrication process of optical device based on SOT concept. However, the quality of 3D printing device and the translucent of the 3D printing material is the main issue in this research. Hence, the surface modification of 3D printing device is required in case of fabrication of the optical device.

In this work, we proposed new fabrication method using a combination of 3D printing and a SOT-QSF planting process for making a small, flexible, and lightweight optical device. A 3D printer using silicone gum as the printing material was used to fabricate a compact and flexible optical module that has simple optical/flow channel for coupling with the FIA system. An injection coating method was demonstrated to modify the 3D printed surface to be proper for using as the optical device. The simple injection and blowing method were used to embed SOT-QSF that has the core/clad structure with coating black PDMS (carbon dispersed PDMS) as cladding of optical trapping layer before injecting of transparent PDMS as the optical window core. The physical properties including coated surface appearance, thickness and the roughness were studied. The optical properties of embedded SOT-QSF were investigated trapping efficiency and reduction noise testing to guarantee the benefit of the optical device that can suppress the noise effect during detection. The developed SOT optical device was used with FIA system and simple and compact LED detection system for

determination of the iron content in real samples to ensure the chemical analysis applications of the device. The analytical characteristics, % recovery and validation using conventional spectrophotometer was achieved to guarantee its ability for on-demand and on-site chemical analysis.

5.2 Materials and methods

5.2.1 Reagents and standards

The transparent optical path was fabricated using polydimethylsiloxane-SIM360 and its catalyst (from the same company as in Chapter 4) mixed at a ratio of 10:1. The cladding of the SOT optical device was fabricated using 5 wt.% of carbon black mixed with PDMS. The planetary mixer (from the same company as in Chapter 4) was used to mix the black PDMS under condition of autorotation at 1108 rpm for 200 seconds and repeated the process of mixing for four to five times.

5.2.2 SOT-FIA optical module design

In this work, the Sketch-up Make 2017 program was used to design the model of 3D computer-aided design (CAD) to fabricate 3D-printed silicone optical module for FIA system. We created the optical module in dimensions of 10 x 30 x 8 mm, entire length = 20 mm shown in Figure 5.1. The optical channel and flow channel were perpendicular to each other. The inlet and outlet of the flow channel were in opposite direction as two separable vertical channels and the optical channel were set as long plane channel. The diameter of the flow channel was 1.8 mm that was compatible to the size of polytetrafluoroethylene (PTFE) tube

of the FIA system. The optical channel was 2.0 mm diameter. The length of the detection zone which is in both sides of optical channel was 10 mm in length and the sample zone which is in the center of optical channel as sample flow-through path was also 10 mm in length.

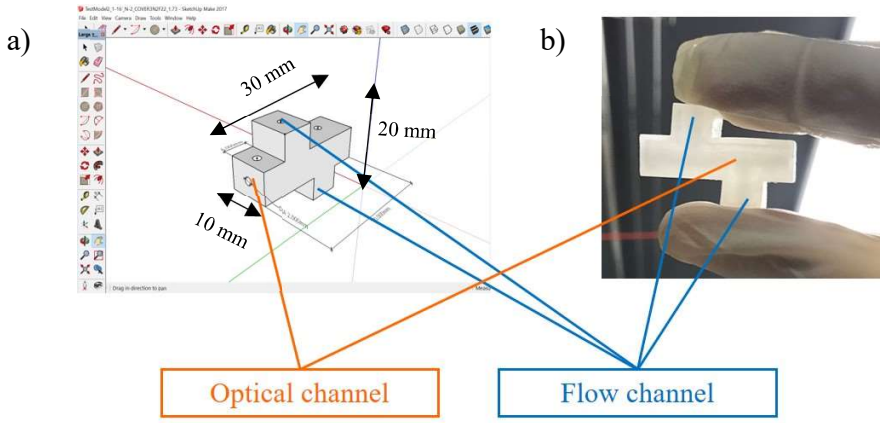

Fig. 5.1 a) 3D CAD design (10 mm×30 mm×20 mm, diameter = 2.0 mm) b) Real image of the silicone 3D printed optical module.

5.2.3 Fabrication method for the SOT-FIA module

An illustration of the fabrication process of SOT-FIA module was presented in Figure 5.2. A UV-curable inkjet 3D-printer (from the same company as in Chapter 4) was used with a UV-curable soft silicone polymer (from the same company as in Chapter 4) for making of the silicone optical module by printing directly. The properties of 3D printed optical device was flexible, soft and appropriate for various applications. Because the surface roughness of the 3D printed module is approximately from 20 to 100 μm, it cannot properly use for the optical channel in the detection system. Thus, the process of smoothing surface is needed. Also, the process of coating black PDMS as the optical trapping layer is needed due to the

translucent of AR-G1L silicone gum ink of 3D printer (Fig. 5.1 b)). The embedding method of the SOT-QSFs into the 3D printed silicone module was attained by a simple coating method.

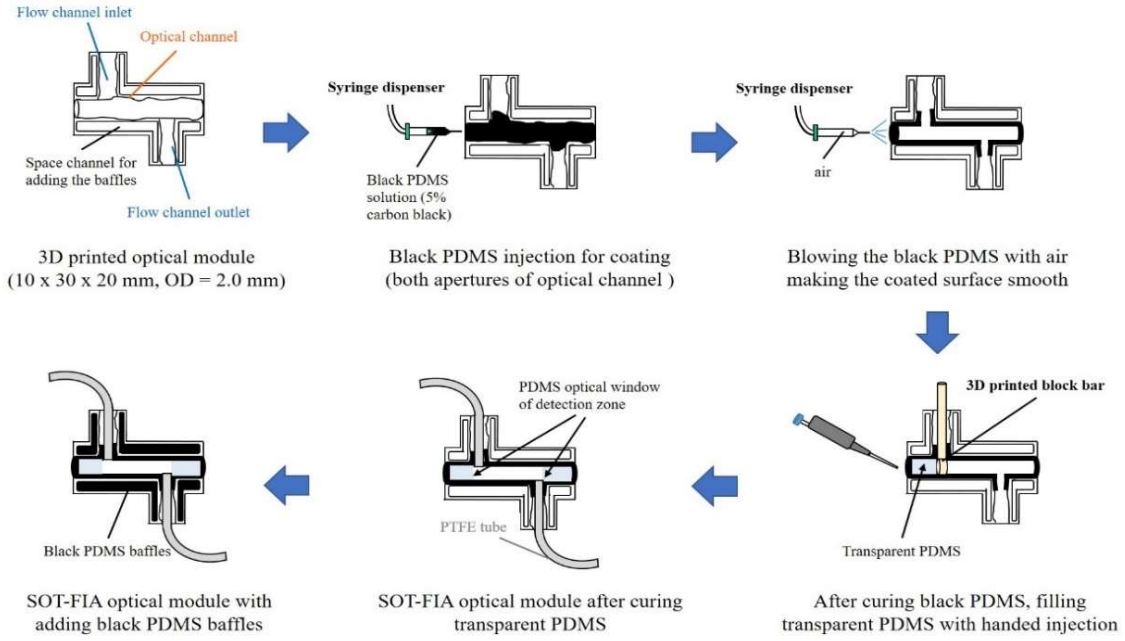

Fig. 5.2 Illustration of the fabrication process of SOT-FIA optical module using injection coating method for embedding the SOT-QSF.

First step, after mixing the PDMS with 5 wt.% carbon black as the black PDMS, the solution was injected into the holes of the optical channel by using a pneumatic syringe dispenser (from the same company as in Chapter 4). The injection pressure was varied from 0.050 to 0.150 mPa. After that, the free air was blown into the optical channel aperture to coat the black PDMS around the interior of the optical channel with varying the controlled air pressure of syringe dispenser from 0.050 to 0.070 mPa. The blowing of free air was needed to process for both opposite sides of the optical channel because the uniform coating

was required, and the air was for one side. The optimized conditions for the coating method were investigated and then heated air was blown for 90 seconds to cure the black PDMS coated on the inner of optical channel by using a hot dryer (from the same company as in Chapter 4). Form the coating process of the optical trapping layer, the inner surface of the optical channel was modified to be smoother than normal 3D printed surface boundary which could confirm by a microscopic study.

Next step, the transparent PDMS was injected in the optical channel via a hand injection process to form the optical core structure based on SOT concept. The transparent PDMS acted as the optical window of the detection zone of the proposed optical module. The 3D printer with acylated monomer ink (from the same company as in Chapter 2) was used to a 3D printed plastic block bar. It was used for preventing the PDMS to enter the sample zone. The sample zone length was varied from 5.0 to 10.0 mm to optimize the highest sensitivity of the optical device. Before use of the block bar, the polishing process was needed to adjust the smoothness of the 3D printed block bar surface using the SiC abrasive paper (company mentioned in [23]) and polishing cloth (company mentioned in [23]). The plastic block bar as mold for fabrication of the optical window was placed into the flow channels to separate the detection part and the sample part when the filled optical window was formed. After injection of the PDMS into the detection zone, the face side of the optical channels was placed on an acrylic place to form the flat and smooth optical window. Then, the PDMS window was cured at ambient condition for 24 h to complete making the filled optical window and the plastic block bar was removed. The process of fabrication of the optical window was repeated for another side of optical channels. After that, the black PDMS bulks were added

into the SOT optical module and compared its trapping effect for the inclined light with another module without black PDMS internal bulks. Finally, the PTFE tube sized outer diameter of 1/16" × inner diameter of 0.040" (company mentioned in [23]) was entered into the flow channels and then the clear PDMS was injected into the flow channel for joining the tube.

5.2.4 SOT-FIA module optical properties evaluation

The optical properties of the proposed optical module were evaluated by trapping efficiency and noise reduction effect. The trapping performance that measured the transmitted light passing through the SOT spatial fitter against the optical axis was evaluated to confirm the capability of trapping the stray light. An in-house instrument setup was used for trapping performance experiment. The testing of noise interference was performed by integration of the proposed optical device with an LED detection system (from the same company as in Chapter 2) as the SOT-FIA optical system. The red-green-blue (RGB) signals of the blank air were observed between light room and dark room to confirm there is no different results of the signal between both conditions.

5.2.5 Application of the SOT-FIA optical system

The FIA system (company mentioned in [23]) was connected with the proposed SOT-FIA optical system that gathered with the LED detection system. The flow rate of the FIA system was varied from 0.5 to 10 ml/min to check the robustness of the SOT-FIA optical system. Also, the chemical resistance to acid, base, and organic solution of the proposed optical system was tested. The chemicals used in this work were analytical grade. A Direct-

Q system (Merck Millipore) was used for production of deionized water using in this work. 10 mM of HCl (company mentioned in [23]) at pH = 2.0, 10 mM of NaOH (company mentioned in [23]) at pH = 12.0, and 50% v/v of ethanol solution (company mentioned in [23]) were prepared to confirm endurance properties of the SOT-FIA optical module.

The proposed optical system was demonstrated chemical application for determination of the iron content in natural water. The colorimetric assay of the iron with o-phenanthroline was demonstrated to ensure beneficial in chemical application of the proposed optical system. 1 mg of iron(II) chloride tetrahydrate (company mentioned in [23]) was dissolved in 100 ml of 10 mM HCl solution to prepare the stock solution of 10 mg L^{-1} of Fe(II). Then, the stock solution was then diluted into a series of concentrations from 0.01 to 0.1 mg L^{-1}. 0.05% w/v o-phenanthroline (company mentioned in [23]) in phosphate buffer solution, pH 4.0 (company mentioned in [23]) was mixed with 2% ascorbic acid (company mentioned in [23]) to prepared the mixture reagent. The ascorbic acid was used to reduce Fe(III) to Fe(II) in the natural water sample because the colorimetric assay is specific to Fe(II). The flow condition was 1.0 ml/min at ambient condition. The Blue signal of RGB sensor related to the Fe(II) concentration were obtained by Ushio Picoexplorer LED detection system (λ_{range} = 400–540 nm). The measuring of the signal was repeated three times for each Fe(II) concentration and the average B signal was calculated. The absorbance of Fe(II) solution was obtained by calculation based on the Beer-Lambert's law that equation is presented in [23]. The natural water samples were collected from the local river water, seawater, and potable water supply. To prepare the samples, these samples were filtered using a 0.5 μm PTFE membrane (company mentioned in [23]). Then, the total iron content in

samples was mixed with the same reagent that used with the Fe(II) standard. The accuracy of the proposed optical system was confirmed by spiked recovery and the results from the proposed method were validated by transitional spectrophotometry (company mentioned in [23]) at 510 nm (λ_{max}) under the same conditions.

5.3 Results and discussion

5.3.1 Properties of surface coated using the injection-blowing method

The surface properties of coated black PDMS surface were evaluated to ensure good surface properties for optical detection applications. The surface appearance of coated black PDMS in the optical channel was investigated by the naked eye and a microscope. The other surface characteristics as surface thickness and surface roughness were confirmed by the microscope and atomic force microscopy (AFM). The process of coating black PDMS surface was repeatable that showed 90% of satisfied reproducibility confirmed by microscopic study.

The condition of coating process was varied at 0.050, 0.075, 0.100, 0.125, and 0.150 mPa of the PDMS injection pressures and at 0.050, 0.060, and 0.070 mPa of air-blowing pressures to observe the optimum condition for the fabrication. Figure 5.3 presents the apparent and microscopic images (from the same company as in Chapter 4) of the black PDMS coated surface in each condition. The results shows that the PDMS solution which its viscosity was 7,000 mPa needed <0.100 mPa of injection pressure to fill the optical channel

of 2 mm diameter with 15 mm of length and <0.050 mPa of blowing air pressure to eject the filled PDMS solution and achieve a coating of optical channel.

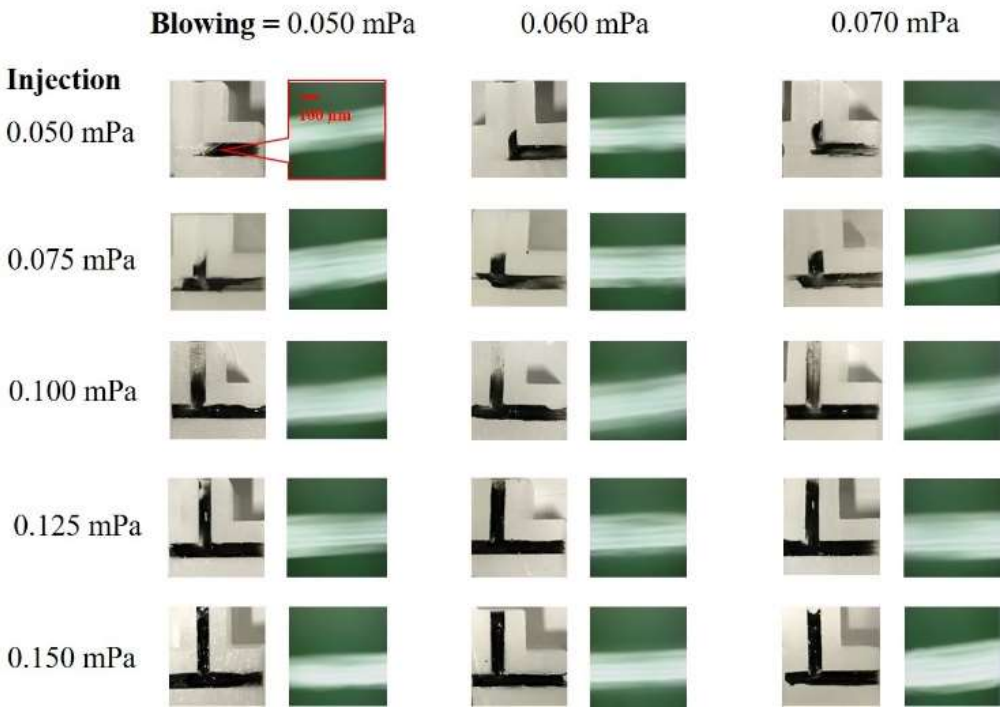

Fig. 5.3 Visible images and microscopic images (×250) of black PDMS-coated surface on the proposed 3D printed optical device under different conditions of injecting and blowing method. Non-black PDMS coated areas show in green areas and the coated areas of the optical channels show in white transparent areas.

Under condition of injection pressure ranged from 0.050 to 0.075 mPa, incomplete coated surface of the black PDMS was observed. The whole coated surface of black PDMS on the optical channel was presented when using the injection pressure of 100 mPa and 125 mPa provided the uniform coating. However, using higher injection pressure of 150 mPa, it

caused blocking of the black PDMS to the flow channel after blowing of air because overabundant solution of black PDMS was injected. The most uniformly and smoothest coted surface which is proper for use of the optical device was observed when using injection pressure of 0.125 mPa with air pressures of 0.05 to 0.07 mPa. The condition of blowing pressure from 0.050 to 0.070 mPa showed no significant effect of coating process that could enough remove the black PDMS from the optical channel and provide good coating. Thus, the 0.125 mPa of injection pressure with 0.060 mPa of blowing pressure was the optimum condition of coating process.

The coated surface under the optimum coating conditions of 0.125 mPa and 0.060 mPa of injection pressure and blowing pressure, respectively was measured the thickness using a microscope (from the same company as in Chapter 4). The black PDMS coating layer was cut from the optical channel in cross section and the microscopic image is presented in Figure 5.4 a). This showed the thickness of the coated layer was approximately 500–600 μm. The coated surface with black PDMS was smoother than the other side of the 3D printed surface that guaranteed the success of surface modification by coating process.

The roughness of the black PDMS coated surface was observed using nanoscale hybrid AFM (from the same company as in Chapter 4) to confirm the quality of the coating method. The results of surface roughness are showed in Figure 5.4 b). which the AFM profile image observed area of 50 × 50 μm^2 shows as big green image and a 2D virtual surface image (×250 magnification) shows in brown image. 30-100 nm of the average root mean square (rms) roughness of the coated surface was obtained. This indicated that the coated surface

using simple injecting and blowing method provided suitable surface properties of optical channel.

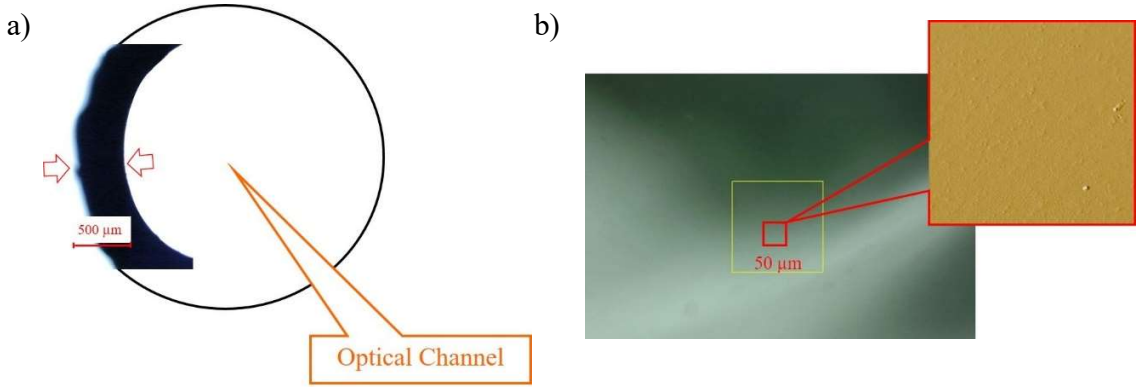

Fig. 5.4 a) Microscopic images of black PDMS coated surface (40×) and b) AFM microscopic image of black PDMS-coated surface (250× magnification, 50 × 50 µm^2)

5.3.2 Evaluation of optical properties of SOT-FIA module

5.3.2.1. Optical trapping efficiency

In previous work, the trapping efficiency of a similarly structured SOT-QSF which has dimensions of 1 x 2 mm^2 with 20 mm length was investigated by measuring the transmitted light intensity with respect to the optical axis. A single scattering was observed to suppress noise to 0.02% in the black PDMS optical trapping layer, also 2-3 scattering attained sufficient trapping efficiency [20].

In this work, two types of SOT-FIA optical module which one was filled with black PDMS baffles and another one was not added the black PDMS baffles were investigated the trapping performance. The in-house instrument setup was used in this work. A laser beam

(532 nm) was used as the light source. An Al mirrors and a concave lens (focal length f = −30 mm) was aligned to magnify the laser beam to cover the optical window of the optical module. The detector was a photomultiplier tube. The light intensity transmitted through the optical channel was collected at every 5 degrees of torsion angle until up to 60 degrees. The measurement of transmitted light at each torsion angle was repeated three times to obtain an average intensity. The average light intensities at different torsion degrees were calculated the normalized intensities, which is the ratio of the evaluated intensity to the initial intensity at 0 degree and were then plotted versus torsion angle.

Figure 5.5 shows the results of the trapping efficiency graph. The SOT-FIA optical module with adding the black PDMS bulks was performed an excellent trapping efficiency which can reduce the passing light down to the 10^4 times at 15 degrees of torsion angle. On the other hand, in case of only embedding of SOT-QSF of the optical module, the tilted incident light could be reduced down 7 times at the same torsion angles and could be further trapped down to 20 time at 60 degree. These results indicated that there is still tilted light passing to the detector because only SOT-QSF was not enough for adsorption of scattering without internal baffles of black PDMS. Thus, the trapping efficiency of 99.8% was obtained when using the proposed optical module with black PDMS bulks. Even though the SOT-FIA optical module remained some translucent part from the 3D printer ink. However, the 3d printing can provide availability of design of the 3D-printed silicone module that was able to introduce internal baffles of black PDMS. Thus, the proposed optical module with on-demand and rapid fabrication based on SOT theory was succeed to obtain an optical

properties of low noise level detection using 3D printed silicone module and coating method with adding the internal baffles of black PDMS.

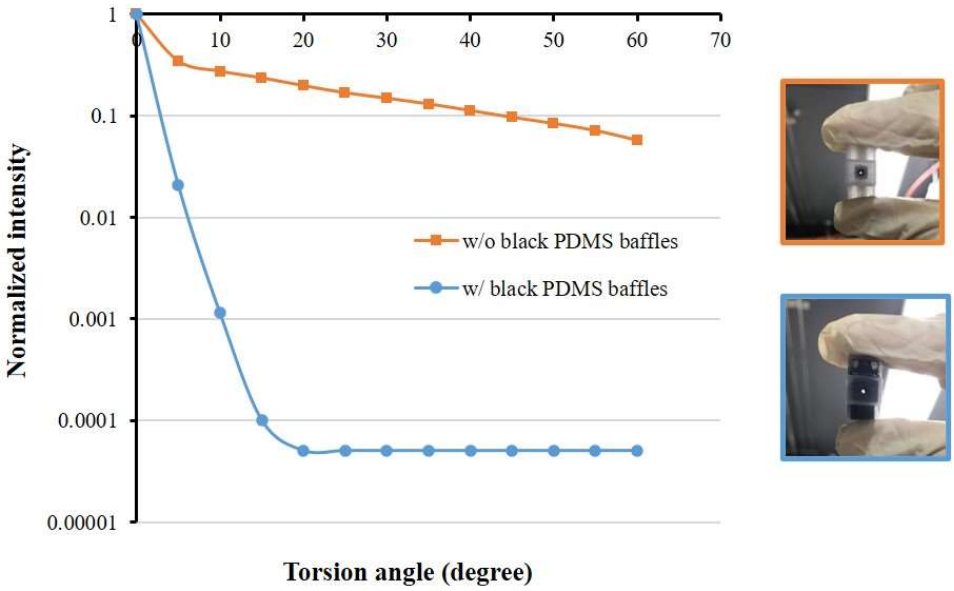

Fig. 5.5 Trapping efficiency graph of SOT-FIA module. The proposed optical module with black PDMS bulks shows as the blue line and the orange line shows the trapping efficiency of the optical module without the black PDMS bulks.

5.3.2.2. Noise reduction effect with LED detection system

The noise reduction effect was evaluated by measuring the RGB signals of the PAS110 Picoexplorer as LED detection system that integrated with the proposed SOT-FIA optical module between light room and dark room. The reducing noise background of the proposed optical module was confirmed by percentage difference in LED intensity (16-bit resolution) of the free air sample of the proposed optical device for 2 min between turn on and off the light.

Table 5.1 Noise effect results of the proposed optical module using compact LED detection system. The blank air sample was measured light intensity of RGB sensor at light room and dark room.

Sample zone[a] (mm)	Color	Intensity 16 bit (light room)	Intensity 16 bit (dark room)	% Difference ±RSD
5.0	R	2758.30 ± 14.23	2749.41 ± 4.05	0.32 ± 0.66
	G	4285.62 ± 20.04	4272.66 ±7.52	0.30 ± 0.64
	B	3255.58 ± 14.97	3249.40 ± 3.95	0.19 ± 0.58
7.5	R	3182.65 ± 12.46	3175.56 ± 3.13	0.22 ± 0.49
	G	4560.73 ± 22.59	4545.18 ± 6.98	0.34 ± 0.65
	B	3566.81 ± 15.20	3558.32 ± 4.01	0.24 ± 0.54
10.0	R	3497.38 ± 16.83	3482.25 ± 3.93	0.43 ± 0.59
	G	4780.63 ± 24.77	4762.79 ± 7.93	0.37 ± 0.68
	B	3896.43 ± 16.28	3889.28 ± 4.08	0.18 ± 0.52

[a] Measured three times repeatedly for each module *(n=3)*.

Table 5.1 presents the effect of noise reduction if the SOT-FIA optical module. The less difference of percentage in LED signal between the light and the dark room was observed to lower than 0.5% in all cases of sample zone. This results indicated that there was no significant effect from the external light form the light room because the visible interfered light was blocked by the black PDMS optical trapping layer and the internal baffles of our

proposed SOT-FIA optical module. Thus, the proposed optical device is guaranteed the ability of on-site miniaturized FIA system and an open-space measurement. The length of sample zone effected to the RGB intensity as results shown in Table 5.1. The 10 mm length of sample zone provide the highest RGB intensity that can relate to volume of the sample detected using the proposed optical device. This mean that the sensitivity of the optical system was affected by the sample volume. Hence, 10 mm of the sample zone of the SOT-FIA optical module was chosen for further study in chemical analysis applications.

5.3.3 Application of the SOT-FIA optical system

5.3.3.1. Robustness and chemical endurance of SOT-FIA optical module

The developed optical module with handheld LED detection system was coupled with simple FIA system to test the robustness of the proposed optical system. The flow rates of FIA system were varied from 0.5 to 10 ml/min to test the endurance of the optical module. The water was flowed continuously into the SOT-FIA optical module for 30 min to confirm there is no damage on the optical module. The results showed that there were no leakages of the optical module even if using high pressure of flowing solution. The acid solution of HCl 10 mm, pH = 2.0, base solution of NaOH 10 mm, pH = 12, and organic solution of ethanol 50% v/v were used to confirm the chemical endurance of the SOT-FIA optical module. The solutions were flowed three times repeatedly for 10 min per day and were observed for over 10 consecutive days. The AFM images (observed using mentioned equipment in Chapter 4) were used to evaluate the results of coated black PDMS surface after testing of flow of the acid, base, and organic solutions.

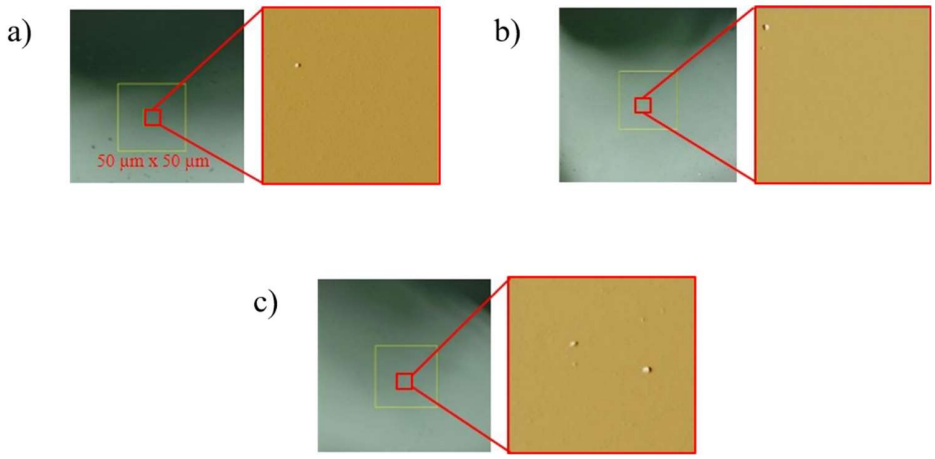

Fig. 5.6 AFM images and 2D virtual surface images of the coated surfaces after chemical resistance test: a) under acid conditions b) under base conditions and c) under organic conditions.

The results in Figure 5.6 shows that the black PDMS coated surfaces were still 30-100 nm of a rms roughness which means that the optical properties of the proposed optical module were the same as before flowing of the chemical solutions. Thus, the acid, base, and organic solutions were not affected to the measurement of the proposed optical device. These results confirmed that the SOT-FIA module has good chemical endurance under acid, base, and organic conditions.

5.3.3.2 Colorimetric determination of Fe(II) in real sample

Figure 5.7 shows the real image of compact handheld SOT-FIA optical system. The optical system composed of flow inlet and flow outlet for flowing solution into detection zone and passing to the waste tank, the LED light source, the SOT-FIA optical module, and color sensors for LED. This system was applied to determine the iron content in natural water.

The reagent using mixture of o-phenanthroline (0.05% w/v) with ascorbic acid (2%) in a phosphate buffer (pH 4.0). of was flowed at 1.0 ml/min at room temperature as reagent stream and then the standard solution of iron (0.01 to 0.1 mg l^{-1}) was injected 150 µl into the reagent stream. The color development was occurred orange color adsorbed at blue intensity of RGB signal which λrange was from 400 to 540 nm. Thus, the transmitted light intensity of B signal was observed 3 times at each concentration of Fe(II) to calculate the average B intensity corresponded to the iron concentration.

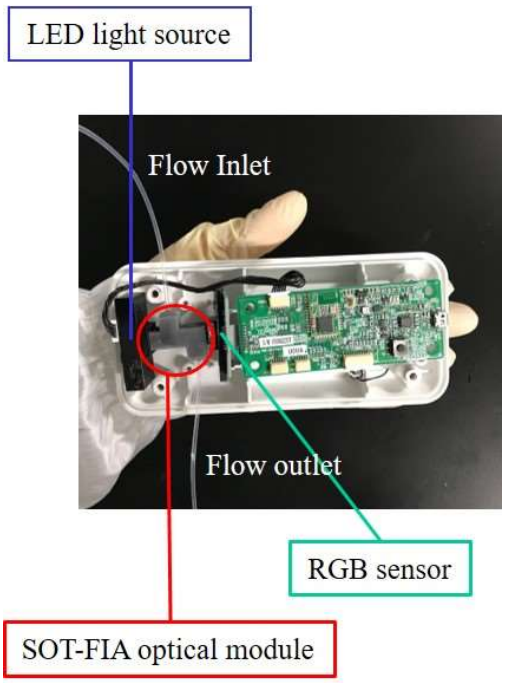

Fig. 5.7 Image of SOT-FIA system coupled with handheld LED detection system

Figure 5.8 a) presents the flow profiles of the iron determination using SOT-FIA optical system for 90 seconds. The B intensity reached highest absorption at 15 seconds.

Then, the absorbance of iron solution related to the concentration was calculated using the Beer-Lambert's law equation which is mentioned in [23]. The obtained absorbances were then plotted versus the Fe(II) concentrations as the calibration curve of iron. The calibration curve was linear from 0.01 to 0.1 mg l^{-1} of iron concentrations with the linear regression equation of y = 0.7642x+ 0.0018, the $R^2 \geq 0.99$ which was close to 1 showing high linearity with wide range of chemical analysis of the proposed measurement method.

a)

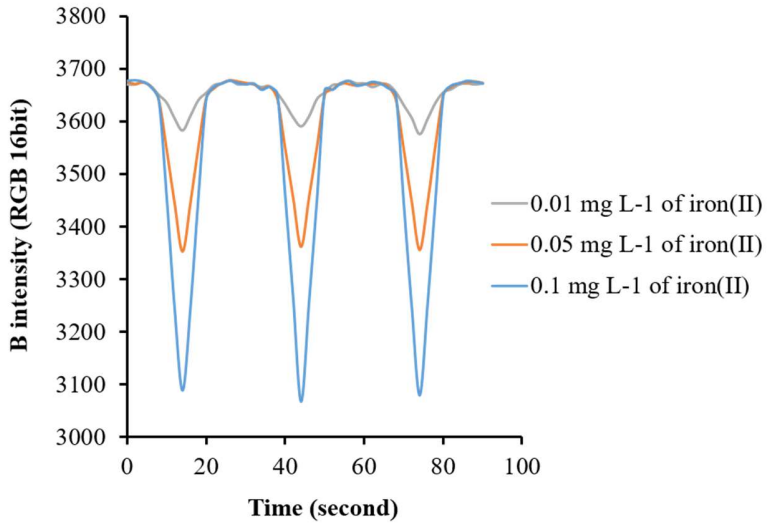

b)

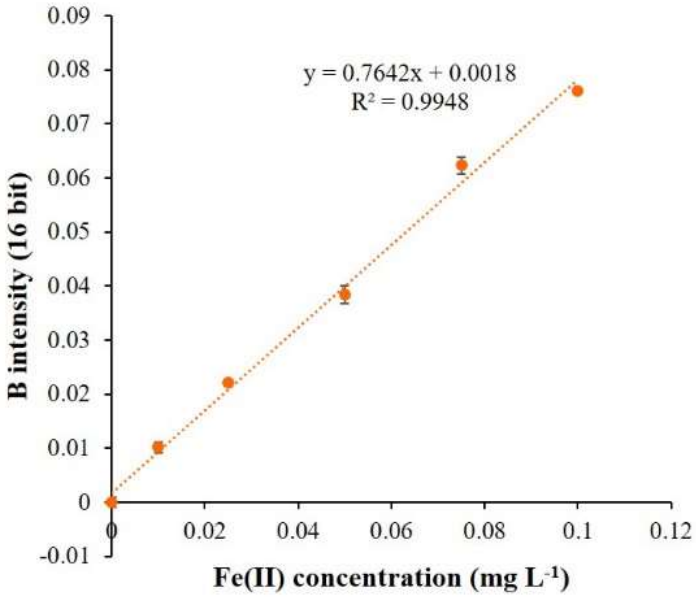

Fig. 5.8 Colorimetric determination of iron using the proposed optical system a) Examples of signal profiles of standard iron solution b) Calibration curve for iron colorimetric determination using the developed optical system.

The analytical characteristics of the proposed SOT-FIA optical system were compared with the previous research of iron determination with o-phenanthroline in natural water samples using FIA with spectrophotometric method (Table 5.2). The results show that the proposed optical system provided lower of the detection limit (LOD) as 3 μg l^{-1} and lower of the quantification limit (LOQ) as 10 μg l^{-1} than the previous reports [21,22].

Table 5.2 Comparison of analytical characteristics of flow methods for the determination of iron in natural water.

System	Detection mode	Range, (µg L^{-1})	LOD, (µg L^{-1})	LOQ, (µg L^{-1})	Additional Reagent	Reagent consumption/assay (mmol)	Sample rate h^{-1}	Reference
FIA	UV-Vis	100-3,000	20	70	Ascorbic acid	14	140-180	21
FIA	UV-Vis	200-1,000	10	35	Hydroxylamine	2.8	120	22
FIA	SOT-FIA with LED detection	10-100	3	10	Ascorbic acid	2.8	120	This chapter

The accuracy of the proposed method was guaranteed by applying to the real samples of various natural water samples. The samples of river, seawater, and potable water was investigated the percentage recovery of iron in the samples by adding 0.010, 0.025, and 0.050 mg l^{-1} of standard iron solution. The recovered iron concentrations from the samples was calculated comparison between before and after adding the standard iron. Good percentage recovery resulted in the range of 80% to 112% were observed to ensure the high accuracy of the proposed optical system (Table 5.3).

Table 5.3 Percentage recovery of iron from natural water samples.

Sample[a]	% Recovery		
	Fe(II) spiked concentration (μg L^{-1})		
	10	25	50
Potable	87.8 ± 0.1	99.5 ± 0.1	97.7 ± 0.1
Seawater	80.0 ± 0.1	98.5 ± 0.0	108.2 ± 0.1
River 1	90.0 ± 0.1	86.3 ± 0.1	85.9 ± 0.1
River 2	102.3 ± 0.1	111.0 ± 0.1	104.6 ± 0.2

[a] Measured five times repeatedly for each sample (n=5).

The iron contents in the natural water samples were investigated under the same conditions used for the standard iron solution. The results of iron concentrations in the natural water samples were repeated 5 times to obtain the average iron concentrations. The results present in Table 5.4 which the results obtained via the proposed method were compared with the traditional spectrophotometry (λ_{max} = 510 nm). % Deviations calculated by % difference of the concentration of the samples between results from the proposed optical device and the traditional measurement method were lower than 3.5% that means the proposed method agrees well with the traditional spectrophotometric method. Thus, this developed method is reliable and utilizes for using in real chemical analysis.

Table 5.4 Validated results of iron determination in natural water sample using the proposed optical system compared to the traditional detection of spectrophotometer.

Sample[a]	Fe(II) concentration ($\mu g\ L^{-1}$)		% Deviation
	UV-Vis spectrophotometer	FIA-SOT optical system	
Potable	15.88 ± 0.29	16.12 ± 0.30	2.30
Seawater	11.73 ± 0.13	12.10 ± 0.24	2.80
River 1	44.40 ± 0.19	44.87 ± 0.60	1.08
River 2	58.04 ± 0.20	60.08 ± 0.74	3.39

[a] Measured five times repeatedly for each sample (n=5).

5.4 Conclusion

The novel fabrication technique of the optical device using rapid digital fabrication of 3D printing with simple coating process was successfully demonstrated based on SOT concept. The SOT optical module printed from UV-curable silicone polymer was modified the 3D printed surface via injection coating method of the optical trapping layer using black PDMS solution. The syringe dispenser was used to perform cladding of black PDMS by simple injecting and blowing method. The transparent PDMS core was also simple fabricated by simply handed injection to create the SOT coaxial structure of PDMS core with black PDMS cladding. The coating process of black PDMS provided the benefit of adjustment of

the roughness of the 3D printed module and it is suitable for optical channel. The physical properties of coated black PDMS surface were evaluated and the results showed acceptable and proper coated surface using for optical detection. The optical properties of the developed optical module were confirmed the capability of trapping the stray light via trapping efficiency and reduction of noise background via noise reduction effect of different environment of the measurement between light room and dark room. The trapping performance of the proposed optical module showed 99.8% of trapping the inclined incidence light by introduction of black PDMS bulks into the optical module. The noise background was less than 0.5% indicating the special property of reducing noise background of the developed FIA module. The proposed optical device was integrated with the FIA system and LED detection system to ensure its ability of use for chemical analysis. The high robustness against high flowing pressure and high chemical endurance including acid, base, and organic solution of the fabricated optical module were confirmed. The real application for iron determination in the natural water samples was demonstrated to examine the utility of the proposed optical system. An excellent linearity, broad chemical analysis range, low detection limit, and good percentage recovery were achieved. Also, the results of iron contents in the natural water samples from the developed optical system agreed well with the traditional spectrophotometric method. This optical device developed to simple fabrication, low-cost, adjustability, movability, and highly sensitivity was utilized for fast on-site chemical analysis application.

References

[1] A.M. Streets, Y. Huang, Chip in a lab: Microfluidics for next generation life science research, Biomicrofluidics. 7 (2013) 1–23.

[2] P. Lisowski, P.K. Zarzycki, Microfluidic paper-based analytical devices (μPADs) and micro total analysis systems (μTAS): Development, applications and future trends, Chromatographia. 76 (2013) 1201–1214.

[3] E. Samiei, M. Tabrizian, M. Hoorfar, A review of digital microfluidics as portable platforms for lab-on a-chip applications, Lab Chip. 16 (2016) 2376–2396.

[4] M. Trojanowicz, K. Kołacińska, Recent advances in flow injection analysis, Analyst. 141 (2016) 2085–2139.

[5] M. Trojanowicz, W. Augustyniak, A. Hulanicki, Photometric flow-injection measurements with flow-cell employing light emitting diodes, Mikrochim. Acta. 83 (1984) 17–25.

[6] D.A. Bui, P.C. Hauser, Analytical devices based on light-emitting diodes - A review of the state-of-the-art, Anal. Chim. Acta. 853 (2015) 46–58.

[7] C.K. Pires, B.F. Reis, A. Morales-Rubio, M. de la Guardia, Speciation of chromium in natural waters by micropumping multicommutated light emitting diode photometry, Talanta. 72 (2007) 1370–1377.

[8] T.R. Dias, M.A.S. Brasil, M.A. Feres, B.F. Reis, A flow cell with a new design to improve the utilization of the radiation emitted by LED and employed as a radiation source for photometric detection, Sensors Actuators, B Chem. 198 (2014) 448–454.

[9] P. Chuntib, J. Jakmunee, Simple flow injection colorimetric system for determination of paraquat in natural water, Talanta. 144 (2015) 432–438.

[10] M. Pokrzywnicka, R. Koncki, Ł. Tymecki, Towards optoelectronic urea biosensors, Anal. Bioanal. Chem. 407 (2015) 1807–1812.

[11] H. Higuchi, H. Yoshioka, H. Nomada, Y. Oki, K. Morita, Carbon–polydimethylsiloxane-based integratable optical technology for spectroscopic analysis, Talanta. 166 (2015) 428–432.

[12] C. Malasuk, K. Nakakubo, S. Tsuru, H. Yoshioka, K. Morita, Y. Nakashima, Y. Oki, Silicone Optical Technology: Quasi Spatial Filter and Its Application for Multichannel Absorption Analysis, in: CLEO Pacific Rim Conf. 2018, Optical Society of America, Hong Kong, 2018: p. W3A.79.

[13] Y. Nakashima, M. Kounoura, C. Malasuk, K. Nakakubo, N. Watanabe, S. Iwata, K. Morita, Y. Oki, S. Kuhara, K. Tashiro, Y. Nakanishi, Continuous cell culture monitoring using a compact microplate reader with a silicone optical technology-based spatial filter, Rev. Sci. Instrum. 90 (2019).

[14] A.J. Capel, R.P. Rimington, M.P. Lewis, S.D.R. Christie, 3D printing for chemical, pharmaceutical and biological applications, Nat. Rev. Chem. 2 (2018) 422–436.

[15] H. Bikas, P. Stavropoulos, G. Chryssolouris, Additive manufacturing methods and modeling approaches: A critical review, Int. J. Adv. Manuf. Technol. 83 (2016) 389–405.

[16] T. Monaghan, M. J. Harding, R. A. Harris, R. J. Friel, and S. D. R. Christie, Lab Chip 16, 3362 (2016).

[17] A.J. Capel, A. Wright, M.J. Harding, G.W. Weaver, Y. Li, R.A. Harris, S. Edmondson, R.D. Goodridge, S.D.R. Christie, 3D printed fluidics with embedded analytic functionality for automated reaction optimisation, Beilstein J. Org. Chem. 13 (2017) 111–119.

[18] H.D. Whitehead, J. V. Waldman, D.M. Wirth, G. LeBlanc, 3D Printed UV-Visible Cuvette Adapter for Low-Cost and Versatile Spectroscopic Experiments, ACS Omega. 2 (2017) 6118–6122.

[19] G.C. Anzalone, A.G. Glover, J.M. Pearce, Open-source colorimeter, Sensors (Switzerland). 13 (2013) 5338–5346.

[20] C. Malasuk, K. Nakakubo, H. Yoshioka, K. Morita, Y. Oki, 3D printing optical devices based on silicone optical technology (SOT) and its application on analytical chemistry, (2019) 66.

[21] J. Mortatti, F.J. Krug, L.C.R. Pessenda, E.A.G. Zagatto, Determination of iron in natural waters and plant material with 1,10-phenanthroline by flow injection analysis, Analyst. 107 (1982) 659-663.

[22] A.U. Rehman, A. Waseem, M. Yaqoob, A. Nabi, Flow injection spectrophotometric determination of total iron in fresh waters, using 1,10-Phenanthroline Reagent, J. Chem. Soc. Pak. 30 (2008) 836-839.

[23] C. Malasuk, K. Nakakubo, R. Ishimatsu, Y. Nakashima, H. Yoshioka, K. Morita, Y. Oki, Compact and on-demand 3D-printed optical device based on silicone optical technology (SOT) for on-site measurement: Application to flow injection analysis, Rev. Sci. Instrum. 90 (2019).

Chapter 6

Enzyme-linked immunosorbent assay based on light absorption of enzymatically generated polyaniline: flow injection analysis for 3-phenoxybenzoic acid with anti-3-phenoxybenzoic acid monoclonal antibody

6.1 Introduction

Enzyme-linked immunosorbent assay (ELISA) is the process for biological analysis that combines the antigen-antibody interaction and enzymatic reaction by a chemically modified enzyme to the antibody or antigen [1]. The ELISA is one of a famous analytical technique for various kinds of analyte. Recently, the ELISA methods were demonstrated using nanoparticles [2-5] and enzyme for color development [6-7]. The ELISA is very selective because the interaction of antigen and antibody is specific reaction. The enzymatic reaction relates to the analysis time of ELISA because the process of enzymatic reaction depends on the increasing of concentration of products. Thus, the fast enzymatic rection provided the benefit of fast analysis time.

Flow injection analysis (FIA) is an automated analysis method that can perform continuous measurements. Currently, the FIA systems were proposed to apply in chemical and biological analysis. Frequently, the detection part of FIA was fluorescence detection [8], chemiluminescence detection [9,10], and light absorption detection [11–17] which are popular use in analytical chemistry applications. The detection part of FIA has been developed along with the development of the flow chips to provide the benefit of on demanded and convenience use in many applications. Recently, the 3D printing technique was used to fabricate the flow detection systems in various designs [18–20].

The combination of ELISA and FIA system can provide the advantages of automation, and continuous measurement of multi-samples and simplicity of some complex process in ELISA such as addition of chemicals, adsorption of antibody and antigen, and washing. The

in-situ and on-site analysis of flow ELISA can be achieved on a microchip device. The portable flow ELISA devices were developed using organic light-emitting diodes (OLED) and organic thin film photodiodes [21–23] as a compact detection. Many kinds of flow ELISA were successfully used for automated determination [24,25].

One of the enzymes and substates that usually use in ELISA were Horseradish peroxidase (HRP) and hydrogen peroxide (H_2O_2), respectively. For example, they were used as initiators for enzymatic oxidation with 3,3',5,5'-tetramethylbenzidine (TMB) and o-phenylenediamine (OPD) for color development in ELISA. However, the sensitivity must be improved by a long reaction time (~30 min) which is the drawback of enzymatic reaction using for color development in FIA-ELISA [1].

In case of aniline substate, it can be generated polyaniline using HRP and H_2O_2 [26–29]. Aniline has advantages of stability in light and heat, inexpensive, also fast analysis time over the other chemicals using in ELISA, because the enzymatic reaction of polyaniline is radical reaction that is shorten time due to quick production of polyaniline. In this work, we demonstrated a competitive FIA-ELISA method using the enzymatic reaction of generation of polyaniline presented via optical measurement in Figure 6.1. This competitive ELISA is used for determination of 3-phenoxybenzoic acid (3PBA) using a monoclonal antibody (mAb) as antigen-antibody interaction in ELISA. The fast reaction of polyaniline reaction is advantageous for FIA-ELISA. The detection of enzymatic rection of polyaniline has been reported using electrochemical detection of ELISA based on the redox current of radical

rection [30]. However, there is no report of use light absorption for detection of enzymatically generated polyaniline in ELISA.

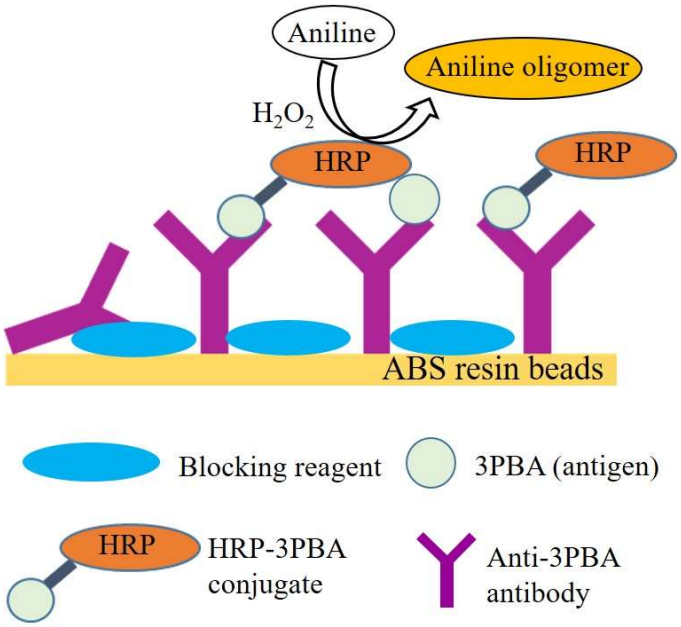

Fig. 6.1 Illustration of competitive ELISA of enzymatic reaction of polyaniline with 3PBA antigen-antibody interaction.

3-phenoxybenzoic acid (3PBA) is a major metabolite of synthetic pyrethroid insecticides that are a neurotoxin, and highly toxic to aquatic life [31]. After intake of pyrethroids form crops or diet products, the serum and enzyme in the liver as esterase enzymes adsorb and hydrolyze the pyrethroid compounds to 3-phenoxybenzaldehyde or 3-phenoxybenzyl alcohol which their half-lives are from 2.5 and 12 h. After that, 3PBA is produced by conversion of these compounds [32]. Thus, it can use as chemical label of synthetic pyrethroid insecticide exposure in human. The determination of 3PBA have been reported using anti-3PBA antibodies [33–37] and nanobodies [38]. In this work, a

monoclonal antibody (mAb) which is selective to 3PBA was produced and used as antibody reagent in ELISA for determination of 3PBA using enzymatically generated polyaniline.

We proposed FIA-ELISA for the determination of 3PBA with enzymatic reaction of polyaniline. The ELISA was performed on a Y-shaped channel acrylic chip with light absorption detection of blue light-emitting diode (LED). The Y-shaped channel was designed to adding ABS resin beads sized 1 mm that were immobilized by anti-3PBA mAb. The immobilized antibody beads were aimed to enhance the sensitivity and shorten the enzymatic reaction time. The optical device using concept of silicone optical technology (SOT) that has benefits of trapping the stray light and reduction of noise effect [39] was coupled with blue LED and photomultiplier tube (PMT) detector. The SOT optical device is in compact size, simply fabricated using 3D printer, and flexible using common material of polydimethylsiloxane (PDMS) was confirmed its potential using for on-site biological analysis.

6.2 Materials and methods

6.2.1 Fabrication of 3D printed SOT-FIA optical device

Figure 6.2 shows the design and real image of SOT-FIA optical device. This optical device was fabricated using rapid and digital fabrication of 3D printing method with simple injection coating method described in detail elsewhere [39,40]. UV-curable inkjet 3D-printer (company mentioned in [41]) was used to directly print a compact and flexible silicone optical device by using UV-curable soft silicone ink (company mentioned in [41]). 5 wt.%

of carbon black doped PDMS was used as the optical trapping layer to provide the trapping of stray light and noise reduction. 10 mm of detection length with 1.5 mm diameter was designed for using in FIA system. The optical channel was designed in perpendicular with the flow inlet and outlet that were connected to PTFE tube of FIA system. The optical channel was connected with the blue LED light source and PMT detector.

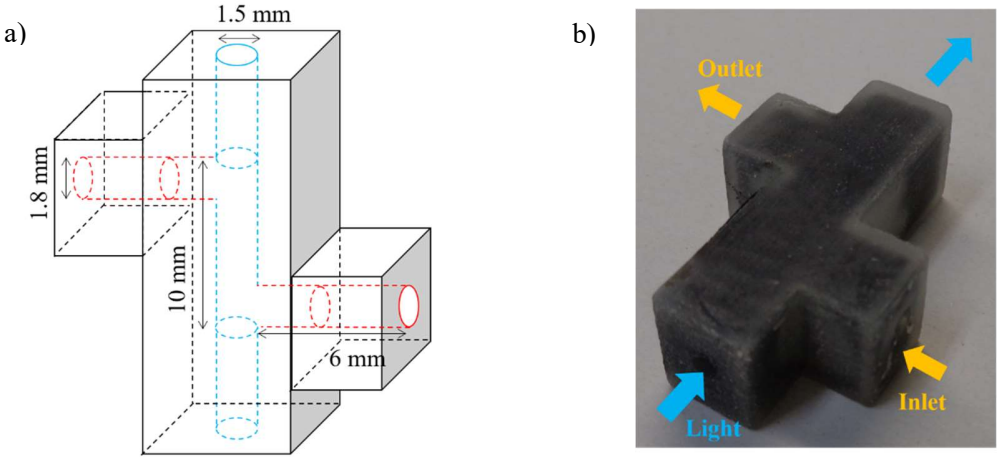

Fig. 6.2 a) An illustration of proposed optical module b) Real image of the proposed optical device

6.2.2 Characterization of enzymatic reaction of polyaniline

A UV-Vis spectrophotometer (company mentioned in [41]) was used to observe the absorption spectra and time-dependent absorbance of enzymatic reaction of polyaniline by HRP and H_2O_2. The absorption spectra were attained after 30 min of the enzymatic reaction. The time-dependent absorbance was investigated by adding the H_2O_2 into the mixture of aniline and HRP in the phosphate buffer solution at pH = 6.6 (optimum pH of HRP is 6.5).

The kinetics of the reaction was observed while the reaction solution was continuously stirred by a magnetic stirrer for ensuring the stability of the measurement.

6.2.3 Competitive FIA-ELISA

The FIA competitive ELISA was performed on an acrylic Y-shaped flow cell. Figure 6.3 presents the schematic of the FIA competitive ELISA system composed of the FIA injection part, the acrylic chip, and the detection part of the developed optical device for light absorption measurement.

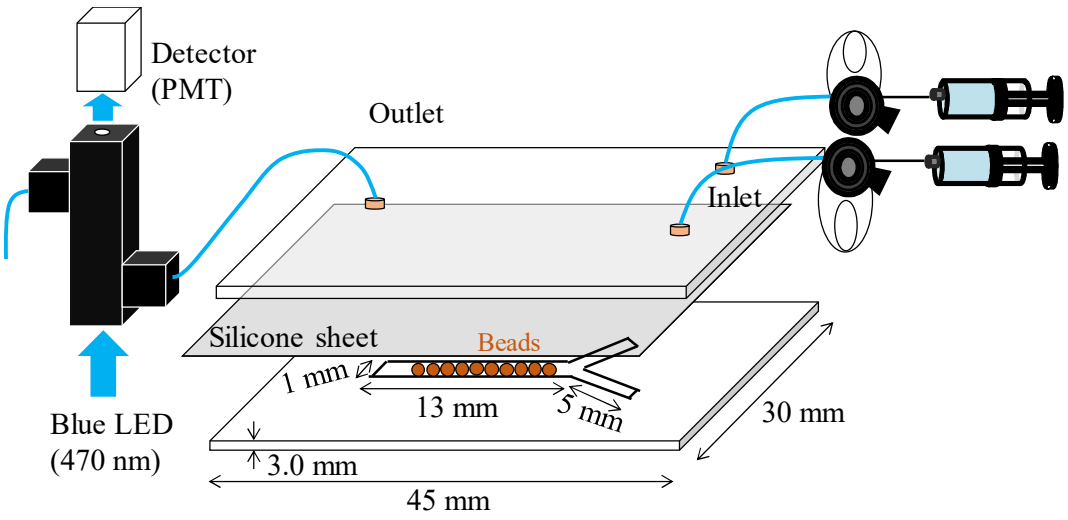

Fig. 6.3 A schematic of an acrylic Y-shaped flow cell for flow competitive ELISA

A Y-shaped channel with a depth of 1 mm was fabricated on the acrylic plate in dimension of 45×30×3 mm with holes for screws by grooving process. The silicone sheet, thickness of 100 µm was placed on top of the Y-shaped acrylic plate and was the covered with the acrylic plate on top before fixing with screws. The ABS bead resins 10 beads that were put in the Y-shaped channel were immobilized by the anti-3PBA mAb. The resin beads

were immersed into 1,000 ppm of the mAb in the phosphate buffer for 1 h at ambient condition. The washing step of the beads with ethanol and water was needed before the mAb immobilization. The flowing solution in the FIA competitive ELISA was controlled by two syringe pumps (company mentioned in [41]). Firstly, 100 µL of blocking solution 10,000 ppm (company mentioned in [41]) was flowed at 100 µL/min for 3 times repeatedly. It used to confirm that nonspecific adsorption of 3PBA-HRP conjugate was removed from the FIA-ELISA system. Next, one of the flow inlet was injected by 500 ppm of mixture of 3PA-HRP conjugate and 100 µL of 3PBA solution varied from 0.01 ppm to 10 ppm to perform the antigen-antibody reaction competitively on the beads with flow rate of 10 µL/min. Thereafter, another flow inlet was introduced by 500 µL of mixture of 10 mM aniline and 1 mM H_2O_2 at 100 µL/min to generate the enzymatic reaction of polyaniline on the bead surface. The flow outlet was coupled with the SOT-FIA optical module that one side of detection zone was connected to a light source of blue LED at λ=470 nm and another side was integrated with the detector of photomultiplier tube (PMT). The light signals obtained from the detector were converted to absorbance. 500 µL of 40 µM bromothymol blue solution (BTB) was injected to ensure the response of FIA when the solution do not react with the ABS beads. An artificial urine was prepared following reference recipe [41]. The artificial urine contained of 0.04 g of citric acid, 2.1 g of $NaHCO_3$, 5.2 g of NaCl, 0.37 g of $CaCl_2 \cdot 2H_2O$, 1.3 g of NH_4Cl, 0.49 g of $MgSO_4 \cdot 4H_2O$, 0.95 g of KH_2PO_4, 1.2 g of K_2HPO_4, 0.8 g of creatinine, 0.07 g of uric acid and 10 g of urea in 1 L of aqueous solution at pH =6.65 was used as a urine sample. A solution containing 3PBA-HRP conjugate and 3PBA was added 10 or 50 vol.% of aliquot artificial urine for evaluation of accuracy of the method. The flow condition

of FIA-ELISA was performed as same those described above for determination of 3PBA in artificial urine sample.

6.3 Results and discussion

6.3.1 Enzymatic reaction of polyaniline

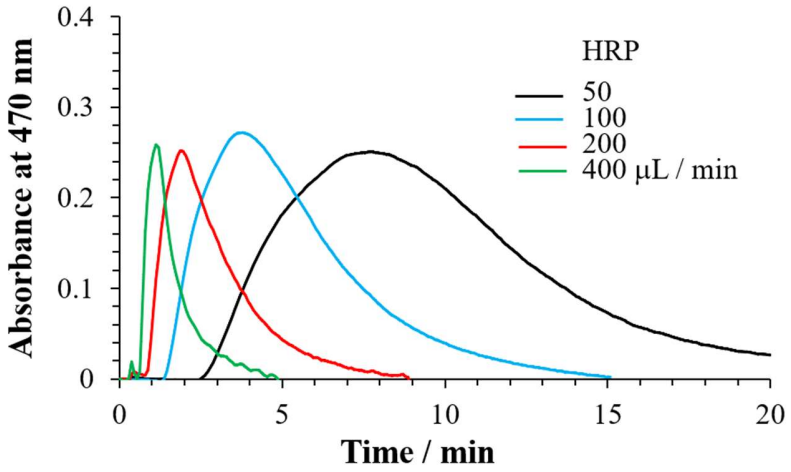

Fig. 6.4 Absorption spectra of enzymatic reaction of polyaniline in the function of HRP concentration, reaction condition was 10 mM aniline and 1 mM H_2O_2 in a phosphate buffer solution (pH = 6.6) for 30 min.

The absorption spectra of enzymatic reaction of polyaniline in the visible region was investigated shown in Figure 6.4. The maximum absorbance was presented at λ in range of 400 to 470 nm of each HRP concentration. The λ=470 nm was used for measuring the absorbance in the function of HRP concentration and the results showed that the absorbance increase when the HRP concentration also increased. The pH effects to the light absorption

in case that the pH was lower than 5, the absorbance can be observed in near infrared region, however the pH higher than 7 could not be observe the maximum absorption [26]. Because the main product of enzymatically generated polyaniline was oligomers of aniline that had various of molecular weight, the absorption spectra was broaden due to producing of various molecular weight of aniline oligomers.

The time-dependent absorbance of enzymatic reaction of polyaniline are presented in Figure 6.5 a). The H_2O_2 was added into mixture of aniline and HRP and the absorbance was monitored at λ=400 nm. The results showed that rapid increase of the absorbance was observed at the time of addition of H_2O_2 and then was gradually increased within 3 min. Thus, it can be occurred of two kinetic enzyme reaction. The faster rate constant of enzymatic reaction can relate to the generation of small oligomers of aniline like dimer and trimer. The slower kinetic enzyme reaction can probably response to polymerization of larger oligomers of polyaniline. Figure 6.5 b) shows the linear relation between the absorbance change that immediately occurred after the addition of H_2O_2 (initial velocity) and the concentration of HRP. This indicated that the HRP concentration increased provided the linear increase in initial velocity of the enzymatic reaction of polyaniline.

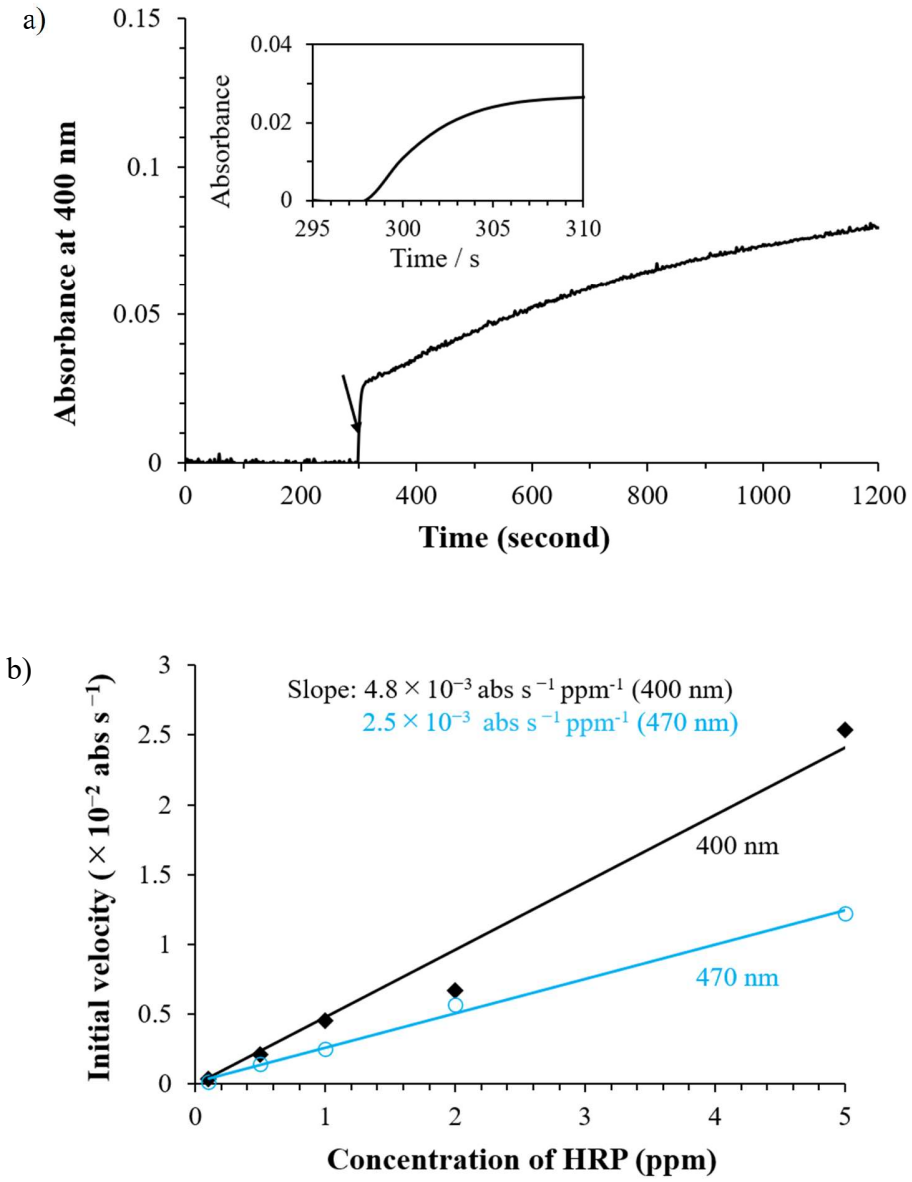

Fig. 6.5 a) Time dependent absorbance of enzymatic reaction of polyaniline under condition of 10 mM aniline, 1 ppm HRP and 1 mM H_2O_2 in a phosphate buffer solution (pH = 6.6). The addition time of H_2O_2 was indicated by the arrow b) Initial velocities against concentrations of HRP.

6.3.2 Flow competitive ELISA

The BTB solution was measured using the proposed FIA-ELISA system shown in Figure 6.3 to test the flow responses of non-reacted solution to the bead-filled region. The BTB was chosen as a reference solution to test the flow competitive ELISA because it was absorbed light at blue region. The BTB solution was injected at 100 μL/min as same as the proposed flow rate of antigen injection and the flow response was observed at around 4 min provided the maximum absorbance. At 4.5 min, the full width at half maximum (FWHM) of the flow response of BTB solution was investigated.

The flow responses of enzymatic reaction of polyaniline in the FIA competitive ELISA are presented in Figure 6.6 a). The absorbance changes were due to the polymerization of aniline and the absorbance responses was opposite to the 3PBA concentrations. The increase in 3PBA concentrations occurred the decrease in absorbance changes. From results of the flow responses, the maximum absorption was occurred around 5 to 6 min after the injection. The larger FWHMs than the BTB solution were observed such as 8.5 min for solution of 1 mg/L because there is enzymatic reaction of polyaniline on the immobilized mAb beads. The length of channel that was put the beads was 10 mm and the size of the beads was fitted to the depth of the channel, thus there is no effect of movement of the beads. From the using of flow rate was 100 μL/min, the retention time of the enzymatic reaction in the region filled with the beads was estimated to 3 seconds. The reaction time of enzymatic reaction was 1 to 2 min calculating by comparison of the peak position between polyaniline and BTB solutions.

A noise background of absorbance (N) in FIA competitive ELISA was 0.0015 (Fig.6.6 a)). Thus, the detection limit of the proposed method as 3N was 0.005 of absorbance changes Figure 6.6 presents the relationship between the changes in absorbance and the logarithm of the concentration of 3PBA. The decrease in amount of generation of polyaniline resulted in the decreased in the changes of absorbance. A reverse sigmoidal response was plotted shown in Figure 6.6 b). The linear decreasing response was observed from 0.2 to 2 ppm of 3PBA concentration which is able to apply for quantitative analysis of 3PBA.

The determination of 3PBA in urine is important because 3PBA is a chemical label to evaluate the exposure of synthetic pyrethroids. Thus, the developed FIA-ELISA was applied to determine 3PBA in the artificial urine to confirm the accuracy of the proposed FIA competitive ELISA. The matrix effect that related to the interference of the sample was evaluated in artificial urine to confirm the reliability of the proposed measurement method. 10 and 50 vol% of artificial urine were tested to measure the 3PBA concentrations at different concentrations of 0, 0.2, and 10 ppm under condition of 500 ppm of 3PBA-HRP conjugate in phosphate buffer solution, pH 7.2. The results show in Table 6.1 that there were no different results of 3PBA concentrations in both 10 and 50 vol% of artificial urine. Thus, there was no significant effect of the artificial urine to the antigen-antibody interaction and enzymatic reaction of FIA-ELISA. This can confirm that the proposed FIA competitive ELISA was accurate with no matrix effect form the sample.

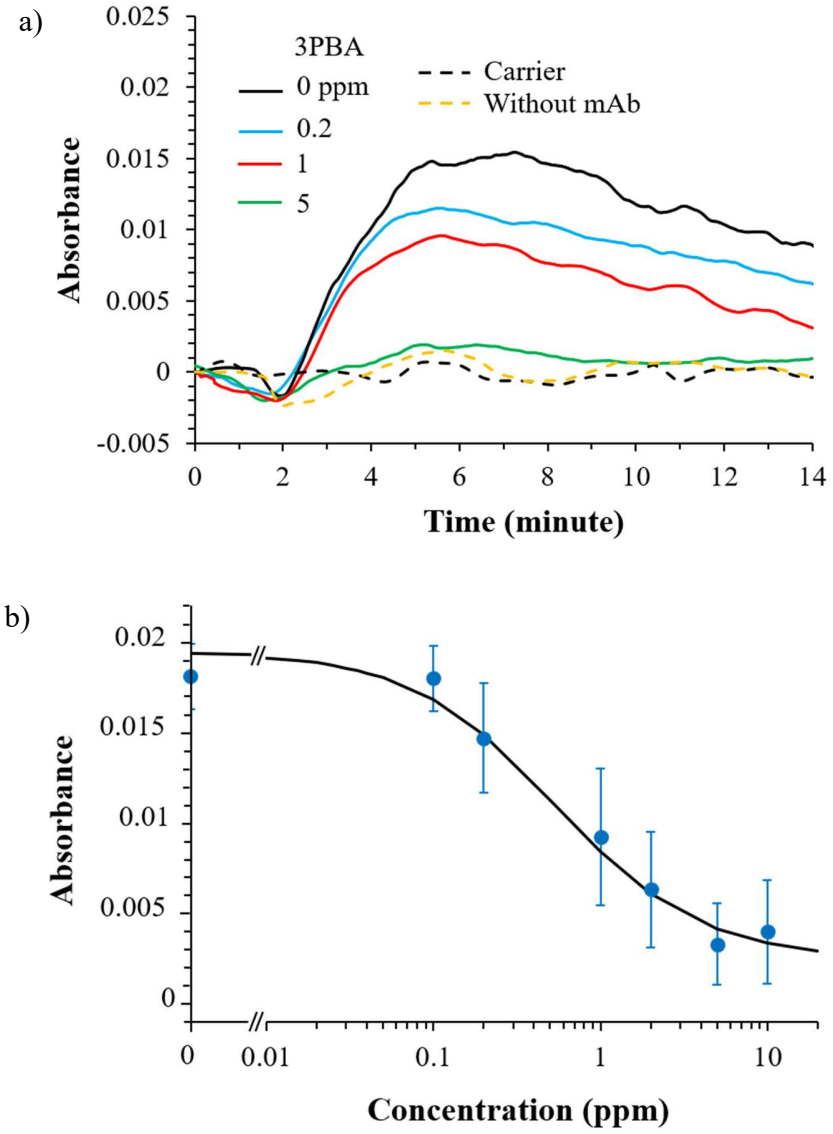

Fig. 6.6 a) Flow response of the enzymatic reaction of polyaniline observed by FIA competitive ELISA as illustrated in Fig. 6.3 b) The flow response of FIA-ELISA related to concentration of 3PBA antigen.

Table 6.1 Matrix effect of the artificial urine observed by the proposed FIA-ELISA.

Concentration of 3PBA / ppm	Absorbance × 10^2 Artificial urine / vol%		
	0	10	50
0	1.81±0.18	1.84±0.24	1.93±0.20
0.2	1.47±0.38	1.57±0.34	1.47±0.20
10	0.40±0.14	0.52±0.06	0.48±0.15

*Average and standard deviation for three measurements.

6.4 Conclusion

A flow competitive ELISA using the enzymatic reaction of polyaniline using H_2O_2 and HRP was successfully demonstrated based on light absorption for determination of 3PBA by mAb antibody. The enzymatically generated aniline provided the benefit of fast analysis time of the proposed ELISA due to the radical polymerization. The acrylic Y-shaped chip was used with placing of the immersed mAb antibody on the ABS resin beads that can enhance the enzymatic reaction of FIA-ELISA method. The flow response of enzymatic reaction of polyaniline at different concentrations of 3PBA was investigated that the absorbance changes was related to the enzymatic reaction and was competed with the concentration of 3PBA antigen. The determination of 3PBA in artificial urine was performed and it can confirm the accuracy of the proposed FIA competitive ELISA which showed no matrix effect of the sample to the ELISA.

References

[1] S. Aydin, A short history, principles, and types of ELISA, and our laboratory experience with peptide/protein analyses using ELISA, Peptides. 72 (2015) 4–15.

[2] Q. Kou, J. Li, Y. Li, C. Dong, J. Yan, L. Zhang, W. Wang, Ultrasensitive ELISA for the detection of hCG based on assembled gold nanoparticles induced by functional polyamidoamine dendrimers, Anal. Chim. Acta. 1042 (2018) 116–124.

[3] Y. Zou, Z. Zhao, Z. Zhang, G. Liang, H. Meng, N. Zhu, X. Wu, Z. Han, A novel and sensitive chemiluminescence immunoassay based on AuNCs@pepsin@luminol for simultaneous detection of tetrabromobisphenol A bis(2-hydroxyethyl) ether and tetrabromobisphenol A mono(hydroxyethyl) ether, Anal. Chim. Acta. 1035 (2018) 168–174.

[4] S. Dong, S. Wang, E. Gyimah, N. Zhu, K. Wang, X. Wu, Z. Zhang, A novel electrochemical immunosensor based on catalase functionalized AuNPs-loaded self-assembled polymer nanospheres for ultrasensitive detection of tetrabromobisphenol A bis(2-hydroxyethyl) ether, Anal. Chim. Acta. 1048 (2019) 50–57.

[5] Z. Yu, Y. Tang, G. Cai, R. Ren, D. Tang, Paper electrode-based flexible pressure sensor for point-of-care immunoassay with digital multimeter, Anal. Chem. 91 (2019) 1222–1226.

[6] Z. Chen, H. Wang, Z. Zhang, L. Chen, Chemical redox-cycling for improving the sensitivity of colorimetric enzyme-linked immunosorbent assay, Anal. Chem. 91 (2019) 1254–1259.

[7] D. Zhao, J. Sun, X. Yang, J. Li, C. Peng, S. Zhu, Fluorescence immunoassay based on the alkaline phosphatase triggered in situ fluorogenic reaction of o-phenylenediamine and ascorbic acid, Anal. Chem. 91 (2019) 2978–2984.

[8] E.J. Llorent-Martínez, M.P. Fernández-Poyatos, A. Ruiz-Medina, Automated fluorimetric sensor for the determination of zearalenone mycotoxin in maize and cereals feedstuff, Talanta. 191 (2019) 89–93.

[9] N. Bibi, A. Nabi, Manzoor Ahmed, M. Yaqoob, M. Asghar, S. Ali, Determination of hyoscine butylbromide in pharmaceuticals using Ce(IV)–Na_2SO_3 chemiluminescent system in flow injection analysis, J. Anal. Chem. 73 (2018) 1098–1104.

[10] S. Ali, A. Waseem, M. Asghar, F. Khan, A. Nabi, S. Iqbal, M. Yaqoob, Surfactant enhanced flow injection chemiluminescence method for vitamin D3 determination in pharmaceutical formulations, Spectrochim. Acta Part A Mol. Biomol. Spectrosc. 208 (2018) 150–156.

[11] N. Chen, J. Ma, K. Lin, D. Yuan, S. Wang, Automated determination of nitrate plus nitrite in aqueous samples with flow injection analysis using vanadium (III) chloride as reductant, Talanta. 146 (2015) 744–748.

[12] N. Youngvises, K. Suwannasaroj, J. Jakmunee, A. AlSuhaimi, Multi-reverse flow injection analysis integrated with multi-optical sensor for simultaneous determination of Mn(II), Fe(II), Cu(II) and Fe(III) in natural waters, Talanta. 166 (2017) 369–374.

[13] K. Chaiyasing, B. Liawruangrath, S. Natakankitkul, S. Satienperakul, N. Rannurags, P. Norfun, S. Liawruangrath, Sequential injection analysis for the determination of fluoroquinolone antibacterial drug residues by using eosin Y as complexing agent, Spectrochim. Acta - Part A Mol. Biomol. Spectrosc. 202 (2018) 107–114.

[14] M.R. Yaftian, M.I.G.S. Almeida, R.W. Cattrall, S.D. Kolev, Flow injection spectrophotometric determination of V(V) involving on-line separation using a poly(vinylidene fluoride-co-hexafluoropropylene)-based polymer inclusion membrane, Talanta. 181 (2018) 385–391.

[15] S. Baghi Sefidan, H. Eskandari, A.N. Shamkhali, Rapid colorimetric flow injection sensing of hypochlorite by functionalized graphene quantum dots, Sensors Actuators, B Chem. 275 (2018) 339–349.

[16] L. Ganranoo, R. Chokchaisiri, K. Grudpan, Simple simultaneous determination of iron and manganese by sequential injection spectrophotometry using astilbin extracted from Smilax china L. root, Talanta. 191 (2019) 307–312.

[17] S. Feng, J. Wu, D. Yuan, Y. Huang, K. Lin, Y. Chen, Spectrophotometric flow injection determination of dissolved titanium in seawater exploiting in-line nitrilotriacetic acid resin preconcentration and a long path length liquid waveguide capillary cell, Anal. Chim. Acta. 1053 (2019) 54–61.

[18] M. Michalec, Ł. Tymecki, 3D printed flow-through cuvette insert for UV–Vis spectrophotometric and fluorescence measurements, Talanta. 190 (2018) 423–428.

[19] E. Nossol, R.A.A. Muñoz, D.M.H. Mendonça, E.M. Richter, W.P. Silva, R.M. Cardoso, M.N.T. Silva, R.A.B. da Silva, 3D printing for electroanalysis: From multiuse electrochemical cells to sensors, Anal. Chim. Acta. 1033 (2018) 49–57.

[20] C. Calderilla, F. Maya, V. Cerdà, L.O. Leal, 3D printed device for the automated preconcentration and determination of chromium (VI), Talanta. 184 (2018) 15–22.

[21] M. Miyake, H. Nakajima, A. Hemmi, M. Yahiro, C. Adachi, N. Soh, R. Ishimatsu, K. Nakano, K. Uchiyama, T. Imato, Performance of an organic photodiode as an optical detector and its application to fluorometric flow-immunoassay for IgA, Talanta. 96 (2012) 132–139.

[22] R. Liu, R. Ishimatsu, M. Yahiro, C. Adachi, K. Nakano, T. Imato, Fluorometric flow-immunoassay for alkylphenol polyethoxylates on a microchip containing a fluorescence detector comprised of an organic light emitting diode and an organic photodiode, Talanta. 134 (2015) 37–47.

[23] R. Ishimatsu, A. Naruse, R. Liu, K. Nakano, M. Yahiro, C. Adachi, T. Imato, An organic thin film photodiode as a portable photodetector for the detection of alkylphenol polyethoxylates by a flow fluorescence-immunoassay on magnetic microbeads in a microchannel, Talanta. 117 (2013) 139–145.

[24] M.J. Uddin, J.S. Shim, Microfluidic Adapter Converting a 96-Well Cartridge into an Autonomous Microfluidic Device, Anal. Chem. (2018).

[25] P. Preechakasedkit, W. Siangproh, N. Khongchareonporn, N. Ngamrojanavanich, O. Chailapakul, Development of an automated wax-printed paper-based lateral flow device for

alpha-fetoprotein enzyme-linked immunosorbent assay, Biosens. Bioelectron. 102 (2018) 27–32.

[26] W. Liu, J. Kumar, S. Tripathy, K.J. Senecal, L. Samuelson, Enzymatically synthesized conducting polyaniline, J. Am. Chem. Soc. 121 (1999) 71–78.

[27] J. Hernández-Ruiz, R.N.F. Thorneley, F. García-Cánovas, A.N.P. Hiner, D.J. Lowe, J.N. Rodríguez-López, Mechanism of reaction of hydrogen peroxide with horseradish peroxidase: identification of intermediates in the catalytic cycle, J. Am. Chem. Soc. 123 (2002) 11838–11847.

[28] L.A. Samuelson, R. Nagarajan, J. Kumar, A.L. Cholli, S.K. Sahoo, S. Roy, An enzymatically synthesized polyaniline: a solid-state NMR study, Macromolecules. 37 (2004) 4130–4138.

[29] E. Flores-Loyola, R. Cruz-Silva, J. Romero-García, J.L. Angulo-Sánchez, F.F. Castillon, M.H. Farías, Enzymatic polymerization of aniline in the presence of different inorganic substrates, Mater. Chem. Phys. 105 (2007) 136–141.

[30] G. Lai, H. Zhang, T. Tamanna, A. Yu, Ultrasensitive immunoassay based on electrochemical measurement of enzymatically produced polyaniline, Anal. Chem. 86 (2014) 1789–1793.

[31] L.G. Costa, Neurotoxicity of pesticides: a brief review, Front. Biosci. 13 (2007) 1240.

[32] J.M. Starr, R. Tornero-Velez, S.E. Graham, M.F. Hughes, M.J. DeVito, K.M. Crofton, M.J. Wolansky, E.J. Scollon, D.G. Ross, Environmentally relevant mixing ratios in

cumulative assessments: A study of the kinetics of pyrethroids and their ester cleavage metabolites in blood and brain; and the effect of a pyrethroid mixture on the motor activity of rats, Toxicology. 320 (2014) 15–24.

[33] G. Shan, H. Huang, D.W. Stoutamire, S.J. Gee, G. Leng, B.D. Hammock, A sensitive class specific immunoassay for the detection of pyrethroid metabolites in human urine, Chem. Res. Toxicol. 17 (2004) 218–225.

[34] C.A. Ki, P. Lohstroh, S.J. Gee, N.A. Gee, B. Lasley, B.D. Hammock, High-throughput automated luminescent magnetic particle-based immunoassay to monitor human exposure to pyrethroid insecticides, Anal. Chem. 79 (2007) 8883–8890.

[35] H.J. Kim, K.C. Ahn, A. González-Techera, G.G. González-Sapienza, S.J. Gee, B.D. Hammock, Magnetic bead-based phage anti-immunocomplex assay (PHAIA) for the detection of the urinary biomarker 3-phenoxybenzoic acid to assess human exposure to pyrethroid insecticides, Anal. Biochem. 386 (2009) 45–52.

[36] J.C. Chuang, J.M. Van Emon, R.M. Trejo, J. Durnford, Biological monitoring of 3-phenoxybenzoic acid in urine by an enzyme-linked immunosorbent assay, Talanta. 83 (2011) 1317–1323.

[37] K.C. Ahn, S.J. Gee, H.J. Kim, P.A. Aronov, H. Vega, R.I. Krieger, B.D. Hammock, Immunochemical analysis of 3-phenoxybenzoic acid, a biomarker of forestry worker exposure to pyrethroid insecticides, Anal. Bioanal. Chem. 401 (2011) 1285–1293.

[38] N. Vasylieva, J. Zhang, Z. Li, B.D. Hammock, J. Huo, M. Qi, D. Wan, D. Li, B. Barnych, Development of a highly sensitive direct competitive fluorescence enzyme immunoassay based on a nanobody–alkaline phosphatase fusion protein for detection of 3-phenoxybenzoic acid in urine, J. Agric. Food Chem. 66 (2018) 11284–11290.

[39] H. Higuchi, H. Yoshioka, H. Nomada, Y. Oki, K. Morita, Carbon–polydimethylsiloxane-based integratable optical technology for spectroscopic analysis, Talanta. 166 (2015) 428–432.

[40] C. Malasuk, K. Nakakubo, R. Ishimatsu, Y. Nakashima, H. Yoshioka, K. Morita, Y. Oki, Compact and on-demand 3D-printed optical device based on silicone optical technology (SOT) for on-site measurement: Application to flow injection analysis, Rev. Sci. Instrum. 90 (2019).

[41] R. Ishimatsu, S. Shimizu, S. Hongsibsong, K. Nakano, C. Malasuk, Y. Oki, K. Morita, Enzyme-Linked Immunosorbent Assay Based on Light Absorption of Enzymatically Generated Polyaniline: Flow Injection Analysis for 3-Phenoxybenzoic Acid with Anti-3-Phenoxybenzoic Acid Monoclonal Antibody, Talanta. 218 (2020) 121102.

Chapter 7

Flow-through optical device based on Silicone Optical Technology (SOT) for determination of iron in drinkable tap water

7.1 Introduction

In 2017, a novel fabrication technique of the optical device which is compact and light-weight module, low cost, and simple fabrication using polydimethylsiloxane (PDMS) as a main material termed silicone optical technology (SOT) was demonstrated. The simple structure of the optical core using transparent PDMS with cladding of the carbon dispersed PDMS (K-PDMS) was created to propose the special properties of the straightforward optical filter called a filled quasi-spatial filter (SOT-QSF) [1]. Owing to the matching of reflective index of the core and cladding structure of PDMS and K-PDMS, this structure can trap the multiple scatterings of tilted incidence. The carbon black pigment dispersed PDMS can absorbed the scattering of the tilted light, hence, the straight light along the transparent PDMS core can only pass to the detector. Thus, an interfered light as noise signal was reduce due to this optical property of SOT optical device. The SOT-QSF was successfully embedded to fabricate of a sensitive compact optical device for many applications in previous studies [2-4].

The SOT optical device with compact size, inexpensive, and high sensitivity was developed to use with analytical chemistry technique of a flow injection analysis (FIA) [5]. It was successfully determined the iron content in natural water. A digital and rapid fabrication of a three-dimensional (3D) printing technique was acquired in fabrication process of the proposed optical device with the simple coating method. Because the 3D printing technique is convenient use as automated process, high reproducibility, low cost, and various design of on-demand fabrication, many researches have been reported to use the

3D printing for fabrication of analytical chemistry equipment [6,7]. For example, the flow cells of FIA system using with UV–Vis spectrophotometric detection were successfully fabricated using 3D printing method [8,9]. Previously, the compact SOT optical device for FIA application also attained using 3D printing method and showed good analytical performance which was able to apply for iron analysis in real samples. However, there are still many processes of fabrication, and the alignment with the design of the developed device was not good enough for highly sensitive detection in level of trace chemical analysis.

In this work, we proposed new designed of SOT optical device using with a flow injection analysis system (SOT-FIA optical device). A new material of titanium dioxide (TiO_2) particles was used to fabricate the optical device according to SOT concept. The proposed optical device was fabricated by simple casting method of the PDMS from the plastic 3D printed mold and frame using the poly acrylate polymer ink of 3D printer. A good aligned and excellent design of the optical device was created using the 3D CAD (computer aid design) program. In this work, we added the scattering optical layer using white particles of TiO_2 dispersed in PDMS (W-PDMS) to cover the optical core of the transparent PDMS. This optical layer was proved to enhance the sensitive optical detection by multi-scattering light of a white pigment of TiO_2. Moreover, the carbon black dispersed PDMS or K-PDMS was fabricated as the outer layer of the proposed optical device as the optical trapping layer that can trap the external light to reduce the noise background signal of the optical detection. The effect of the W-PDMS and the detection length of developed optical module to the sensitivity of the optical detection was evaluated. The optical properties of reduction the noise background level based on SOT concept was also evaluated. We integrated the

developed optical device with the FIA system and a compact and simple LED detection system for chemical analysis applications. To confirm the ability of trace analysis of chemical compounds, the proposed method was performed to determine the iron contents in drinkable tap water. Penn State College of Agricultural Sciences reports that the tap water should not have more than 300 μg L^{-1} of iron concentration [10]. High level of iron content in the water can be indicated by yellow color and metallic taste that is not safe for human health. This proposed method can be ensured the feature of drinkable tap water samples. The analytical performances, including the detection limit, the quantitation limit, precision, and the accuracy were investigated. Furthermore, and the method was validated with a traditional spectrophotometric method which can guarantee its ability of chemical analysis for on-site and on-demand measuring.

7.2 Materials and methods

7.2.1 Fabrication method of the SOT-FIA optical device

The 3D CAD program of Autodesk 123Design (Autodesk, USA) was used to design the mold or frame of the fabricated optical device for 3D printing technique. The mold of inner part of the SOT-FIA optical module was designed in oval shape in dimension of 10 mm short diameter × 20 mm long diameter × 8 mm height (10 mm × 20 mm × 8 mm). Another 3D printed frame was also created in oval shape with the dimension that was larger than the inner part of 20 mm × 30 mm × 10 mm. The inner part and the outer part were connected to fabricate the proposed optical device. On the surface of the outer part and the inner part frame,

two holes sized 4 mm diameter was designed in opposite side for inserting LED light source and the color sensors of Ushio picoexplorer absorbance meter (Ushio, Japan). 1 mm diameter of the flow channel was aligned in the center of the SOT-FIA module for inserting the PTFE tube of the FIA system. The two separable optical channels which were dimension of 4 mm diameter × 3 mm length were designed at 45 degrees to the flow channel. The detection length which is the length between the two separable optical channels was varied from 3 mm to 7 mm to evaluate the effect to sensitivity of the detection.

The polydimethylsiloxane-SIM360 and its catalyst (from the same company as in Chapter 4) using in the ratio of 10 to 1 of PDMS and catalyst were used as the main material for fabrication of proposed optical device. The white material contained 50% of titanium oxide, TiO_2 (company mentioned in [15]) was used to mix with the SIM360 PDMS for preparation of W-PDMS that the weight percentage was varied from 0–5 wt.%. The optical trapping layer of K-PDMS contain 5 wt.% of carbon black dispersed in PDMS was prepared by using carbon black (from the same company as in Chapter 4) mixed with PDMS. A rotating mixer (from the same company as in Chapter 4) was used to mix the W-PDMS and K-PDMS homogenously. The rotation condition was 1,108 rpm for 200 seconds. The mixing process was repeated for 4–5 times.

The optical channel of the clear PDMS was fabricated by filling the transparent PDMS into the 3D printed cylindrical shell (4 mm diameter × 5 mm length). Then, the transparent PDMS was leave in the shell for 1 day at ambient condition for curing PDMS and the shell was removed. Two cured clear PDMS optical channels were cut to have one

face at 45 degrees to the cross-section. The cut optical channels and the 1 mm diameter metallic bar were placed into an inner part of a 3D printed frame by attaching them together in 45 degrees. The metallic was place in the center as the mold of flow channel. The two cured transparent PDMS cylindrical optical channels were placed separable for design of the detection zone of the developed optical device which a distance was varied 3, 5, and 7 mm. The small amount of clear PDMS was injected to attach the optical channels with the metallic bar mold and then it was cured using the heating dryer at 100 degree Celsius (from the same company as in Chapter 4) for 1 minute. After that, the W-PDMS was added into an inner part 3D printed frame to create the optical scattering layer. W-PDMS was solidified for 1 day at ambient condition and then removed the frame and metallic bar.

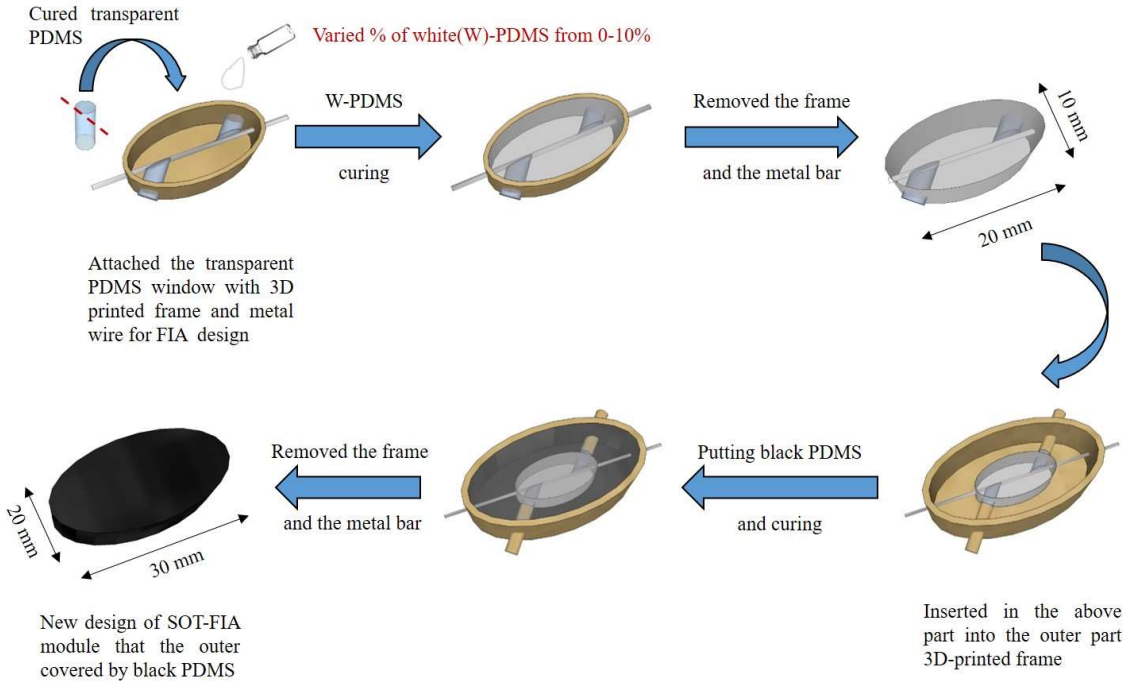

Fig. 7.1 Illustration of fabrication process of proposed device by a simple casting method.

Thereafter, the completed inner part of the proposed optical device was put into the outer frame of that proposed optical device for covering with K-PDMS optical trapping layer. The metallic bar with a 3D printed cylindrical mold (4 mm diameter × 10 mm length) were inserted to connect the inner part and the outer part 3D printed frame. Thus, the position of the flow channel and the optical channels were fixed at suitable position. The K-PDMS was added into the 3D printed outer frame to trap the stray light and block the external light. A curing condition of K-PDMS was 60 degree Celsius for 3 h in an oven, then, the 3D printed frame, 3D printed plastic bar, and the metallic bar were removed. Final step, the complete SOT-FIA device was fabricated using this simple casting method. The fabrication process of the proposed optical device was illustrated in Figure. 6.1.

This developed fabrication process overcomes the traditional prototyping of soft lithography for fabrication of traditional PDMS device. The soft lithography is the process used to make the PDMS device by casting the device form the master pattern. The master pattern of the soft lithography commonly uses the UV-exposure method or electron beam or laser light for fabrication called photo lithography and E-beam or laser lithography, respectively. The traditional method is very precise in nanometer unit, robust, and reproducible. However, the drawbacks are multi-step method, required skillful worker, time-consuming, and expensive. Thus, the proposed fabrication was able to fabricate the PDMS without the complex processing.

7.2.2 Optical properties evaluation of the SOT-FIA optical device

The proposed optical device coupled with the FIA system using 20 cm of reaction coil (from the same company as in Chapter 5) and the compact LED detection of Ushio absorbance meter was evaluated the optical properties of improvement of the sensitivity and reduction of noise effect. The improvement of the sensitivity was investigated by varying the weight percentages of W-PDMS from 0 to 5 wt.%. The transmittance of 100 μg L^{-1} of a standard iron(II)-phenanthroline solution (Fe(II)-phen complex) which the preparation of the solution was described in next part was obtained at different weight percentages of W-PDMS. Also, the 3 to 7 mm of detection length was investigated the transmittance of 100 μg L^{-1} of the standard Fe(II)-phen complex solution to observe the improvement of the sensitivity of detection. Moreover, the reduction of the noise background from the outside light which was the specific optical properties of the developed optical device were evaluated. The different percentages of the red-green-blue (RGB) signals of the LED detection between a light room and dark room were performed using blank air sample to confirm there is no effect of the noise signal from the measurement environment.

7.2.3 Application of the SOT-FIA optical system: colorimetric determination of iron(II)

The determination of iron content in drinkable tap water samples was performed through a colorimetric assay using proposed SOT-FIA optical system. In this work, the analytical grade chemicals and the deionized water from Direct-Q system (from the same company as in Chapter 5) were used to prepare the solution. 0.1 mg of iron(II) chloride

tetrahydrate (from the same company as in Chapter 5) was dissolved in 100 mL of 0.01 M HCl solution (from the same company as in Chapter 5) to prepare a stock solution of Fe(II) 1.0 mg L^{-1}. The series of Fe(II) concentration in the range of 10 to 150 µg L^{-1} were prepared for quantitative analysis of iron by diluting the stock solution. The reagent of colorimetric assay of iron was prepare by mixing of 0.025% w/v *o*-phenanthroline (from the same company as in Chapter 5) and 2% ascorbic acid (from the same company as in Chapter 5) in a phosphate buffer solution pH 4.0 (from the same company as in Chapter 5). The reagent solution was flowed in the FIA system at an optimum flow rate of 1.0 mL/min at ambient condition. The standard iron solution or the sample (100 µL) was injected into the reagent mixture stream. The orange color of Fe(II)-phen complex was formed using FIA system. The change in color of the solution was observed the change of the blue (B) signal of the simple and compact Ushio LED detection system which observed wavelength from 400 to 540 nm (the company mentioned in the Chapter 2). The recorded B signal was repeated 3 times and the average B signal correspond to the iron concentration was calculated. The tap water samples collected from the local tap water supply were investigated the iron contents in the samples. 0.5-µm PTFE membrane (from the same company as in Chapter 5) was used to prepared the sample by filtering the sample solution before injecting instead of the Fe(II) standard solution. The analytical performance including linearity, dynamic range, detection limit as LOD and quantification limit as LOQ, were evaluated. The precision of the proposed optical system was confirmed by the inter-day and intra-day variations of the iron analysis in the samples. the accuracy was also confirmed by the percentage of iron recovery. The validation method using traditional spectrophotometry at λ=510 nm (from the same company

as in Chapter 5) was performed to compare with the developed optical system under the same conditions.

7.3 Results and discussion

7.3.1 Optical properties evaluation of SOT-FIA module

7.3.1.1 Effect of W-PDMS on the optical intensity enhancement

Normally, the optical properties of titanium oxide (TiO_2) particle dominate in high refractive index and strong visible light scattering. The TiO_2 in size of micron range by the special rutile modification was used for fabrication of white pigment [11] which the light scattering can be occurred when the particle is larger size than the detected wavelength. Thus, to confirm the optical propertied of scattering light of the TiO_2 white pigment, the microscopic study of TiO_2 particle dispersed in PDMS (W-PDMS) was achieved using the scanning electron microscopy image (company mentioned in [15]). Figure 7.2 a) shows the microscopic image of 5 wt.% W-PDMS film (500 μm of thickness). The image could confirm that the size of white particles of TiO_2 pigment was range of 1 to 5 μm on the PDMS surface. Figure 7.2 b) shows a simulation of the light that propagated through the W-PDMS. The TiO_2 in the micron size can scatter the light which effected to the enhancement of the light intensity that propagated through the detector or LED sensor. While the inclined incident light and the outside light was absorbed by the K-PDMS optical trapping layer. Thus, the suppression of the noise signal from the optical tapping layer of K-PDMS can also help to enhance the sensitivity of the detection.

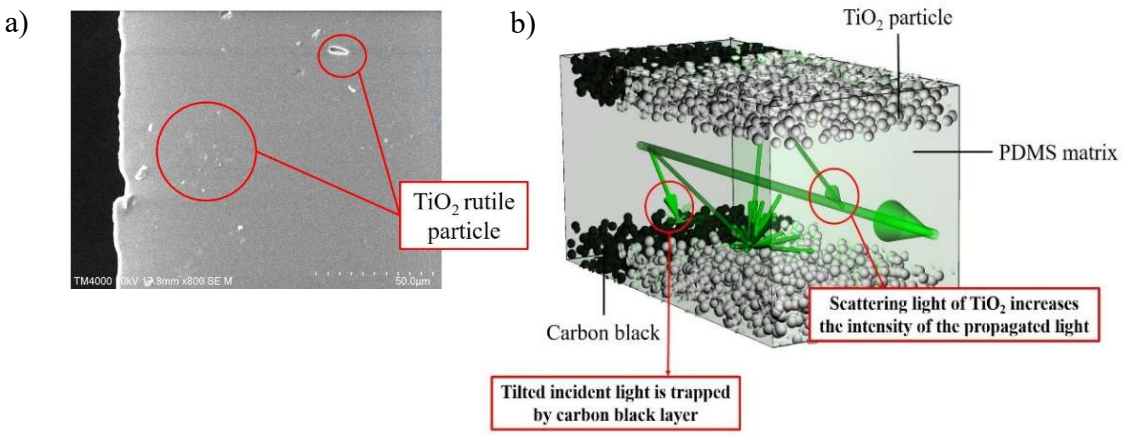

Fig. 7.2 a) SEM image (×50) of the surface of a W-PDMS film (500 µm thick). White spots indicate TiO_2 rutile particles. b) Illustration of the propagating light through the W-PDMS layer.

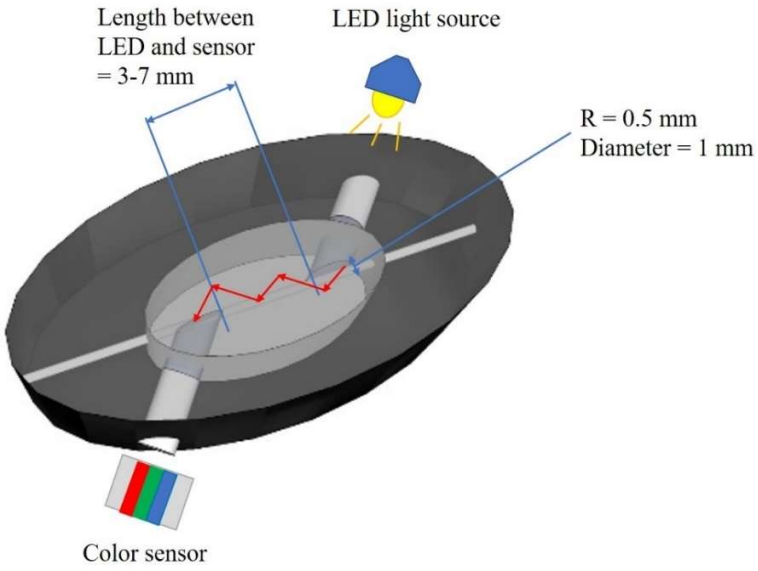

Fig. 7.3 Light propagation through W-PDMS

The propagation of light through W-PDMS was proposed showed in Figure 7.3. The multiple scattering was observed in case of TiO_2 particle dispersed in PDMS. The light intensity or the transmittance was supposed to increase in case of increase in TiO_2 particle contained in PDMS. Thus, there are 2 factors of W-PDMS that effected to the increase in light scattering. One is the weight percentages of W-PDMS and another one is the length of detection that can improve the light scattering of TiO_2 particle.

100 μg L^{-1} of the standard Fe(II)-phen complex solution were measured the blue intensity of RGB signal by using the 5 mm length of detection of the proposed optical module with different weight percentages of W-PDMS of 0, 0.25, 0.50, 1.0, 2.5, and 5.0 wt.%. The calculated transmittances (T) of the standard solution at different conditions of W-PDMS; according to the equation $T = I/I_0$, mentioned in [15] were showed in Table 7.1 Addition of white pigment of TiO_2 could obtained the higher B signal of the proposed optical device compared to no adding of the W-PDMS (0 wt.%). Moreover, increase in the percentages of TiO_2 pigment provided an increase in the transmittance of the standard solution which means that the sensitivity of the proposed optical device was increased, However, no difference of the observed transmittance was presented when the weight percentage of W-PDMS was higher than 1.0 %. This must be the results from the limitation of the LED light source energy. Thus, 1 wt.% of W-PDMS was selected for further study because high sensitivity of 34% transmittance of the Fe(II) solution and lowest substrate of TiO_2 white pigment provided the most beneficial over the other conditions.

Table 7.1 Transmittance test of the standard iron solution using the proposed optical device for different percentages of W-PDMS

SOT-FIA model (% of K color-W)	B intensity of blank solution (16 bit Intensity ± SD)	B intensity of iron(II) 0.1 ppm solution (16-bit Intensity ± SD)	Transmittance
0 %	10 ± 1	0.3 ± 0.6	0.03
0.25 %	30 ± 1	3 ± 1	0.10
0.50 %	70 ± 2	14 ± 1	0.20
1.0 %	130 ± 1	45 ± 1	0.34
2.5 %	132 ± 2	46 ± 1	0.34
5.0 %	137 ± 1	48 ± 1	0.35

7.3.1.2 Effect of detection length on the sensitivity of detection

100 µg L^{-1} of Fe(II) standard solution was tested at different detection lengths of 3 mm, 5 mm, and 7 mm that was the distance between both optical channels. The obtained B intensities of RGB signal were also calculated the transmittances via the previously mentioned equation and then plotted in the function of detection length shown in Figure 7.4 a). The transmittances were decreased when the length of detection increased. The absorbances (A) at different detection lengths of the proposed optical device were then calculated by using $-\log_{10}T$. The effective length (cm) as l in the Beer-Lambert's law equation; $A = \varepsilon cl$, mentioned in [15] was calculated using the observed absorbances of a 100 µg L^{-1} standard Fe(II)-phen complex solution with $\varepsilon = 1.1 \times 10^4$ $M^{-1}cm^{-1}$ of the Fe(II)-phen complex and iron concentration of the 1.8×10^{-6} M that equals to 100 µg L^{-1}.

Figure 7.4 b) shows the results of the effective lengths plotting in the function of the different detection lengths of the proposed optical device. The effective lengths which is the ideal length from the calculation were 38 to 46 times higher than the real detection length from the experiment. Thus, this meant the sensitivity of the optical detection was improved by the developed optical device. The increasing sensitivity of the proposed optical device attained by increasing the detection lengths. In this work, 5 mm of detection length of the proposed optical system was selected for using in the real application because of the highest enhancement of the sensitivity for 46 times.

a)

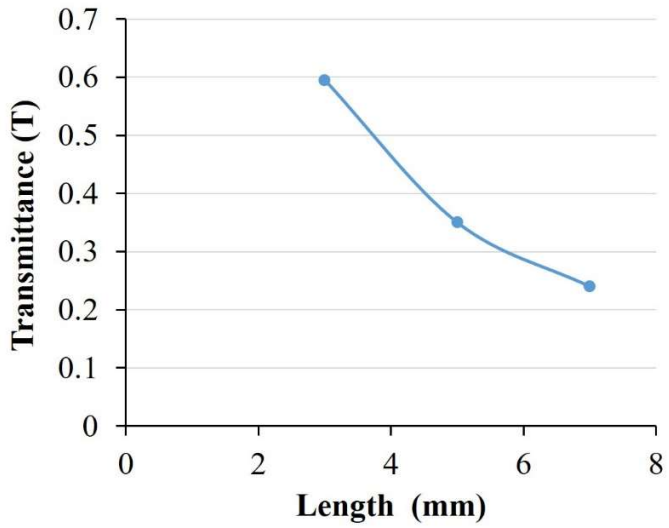

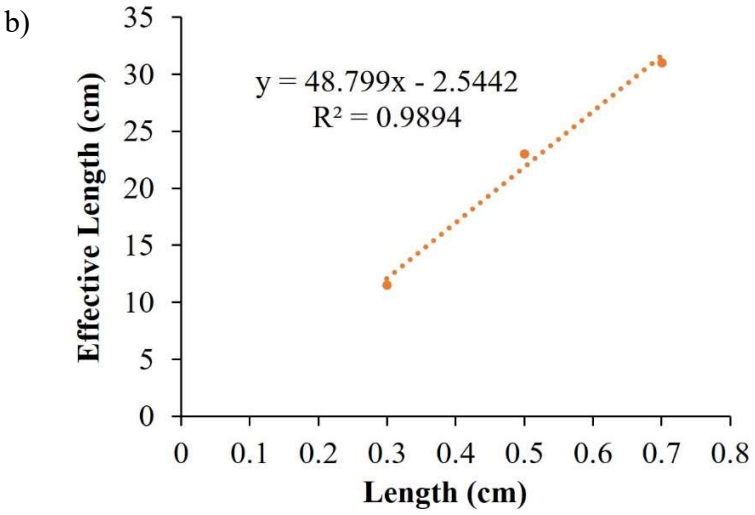

Fig. 7.4 a) Transmittance plotted as a function of detection length observed by the proposed optical device. b) Relationship between realistic length from the experiment versus effective length calculating via Beer-Lambert's law equation.

7.3.1.3 Reduction of noise effect of the proposed SOT-FIA optical device

The special optical property of the developed optical device for blocking any undesired light as noise effect was evaluated. The optimized optical device using 1 wt.% of W-PDMS with 5 mm of detection length was used to observe the RGB signals of the free air measuring in light room and dark room conditions for 2 minutes. The signal measurements were repeated 3 times to calculate the average signals. Then, the results of the average RGB signals between the light room and dark room were compared by calculation of the percentage difference of LED intensity. Table 7.2 presents that percentage differences of RGB signals between the light room and dark room was lower than 1% in all cases. Thus,

there was no effect of the noise background form the light room showing the success of trapping the external light of the proposed optical device. This indicated that the proposed optical device was confirmed its optical properties of low interfering noise signal which provided highly sensitive optical detection. Hence, the proposed optical device was able to use for chemical applications of trace analysis.

Table 7.2 Noise effect results obtained by the proposed optical device using with the simple LED detection system. The RGB signal of blank air sample were compared measuring in light room versus dark room.

LED	Light room (16 bit Intensity ± SD)	Dark room (16 bit Intensity ± SD)	% difference ± RSD
R	120 ± 2	121 ± 1	0.55 ± 0.03
G	153 ± 2	154 ± 2	0.87 ± 0.02
B	137 ± 1	138 ± 2	0.49 ± 0.02

Table 7.3 PTFE tube scattering effect by the proposed optical device using with the simple LED detection system. The RGB signal of blank air sample were compared measuring with a PTFE tube versus without a PTFE tube.

LED	With PTFE tube (16 bit Intensity ± SD)	Without PTFE tube (16 bit Intensity ± SD)	% difference ± RSD
R	121 ± 1	120 ± 1	0.84 ± 0.02
G	154 ± 2	154 ± 1	0.22 ± 0.02
B	138 ± 2	137 ± 1	0.24 ± 0.01

The PTFE tube was entered into the flow channels of the developed optical device without any joining material due to the adjustability of the proposed optical device. Thus, the effect of insertion of PTFE tube to the scattering light was observed. The free air sample was used to measure initial RGB signals with and without the PTFE tube. Table 7.3 shows the different percentages of RGB signals under condition of with and without PTFE tube. The results showed that the effect of PTFE tube could be negligible caused lower 1% of the percentage difference.

7.3.2 SOT-FIA optical system for Fe(II) determination in real sample

Quantitative analysis of iron in drinkable tap water samples were evaluated using the compact SOT-FIA optical system. 100 µL of 10 to 150 µg L^{-1} Fe(II) solution was injected to mix with the reagent stream of 0.025% w/v o-phenanthroline at a flow rate of 1 mL/min. The B intensities of the RGB signal at different Fe(II) concentration were measured 3 times repeatedly to calculate the average B intensities at different Fe(II) concentrations. The average B signals was then calculated the absorbances via the previously mentioned equation.

a)

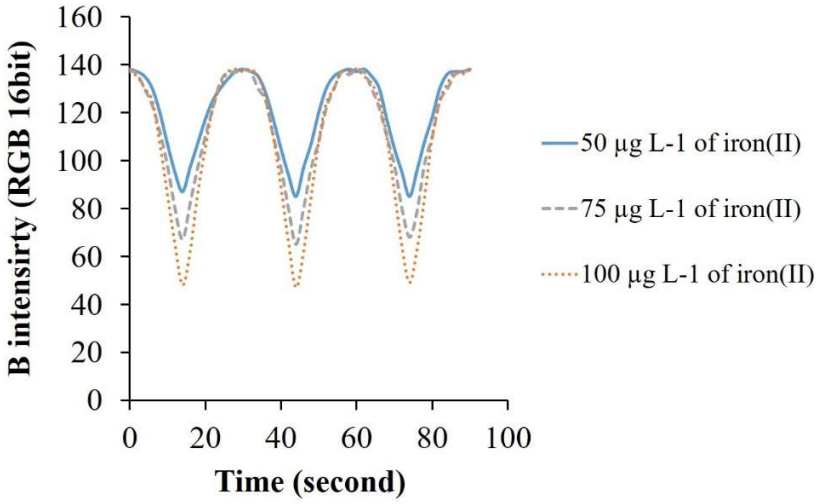

b)

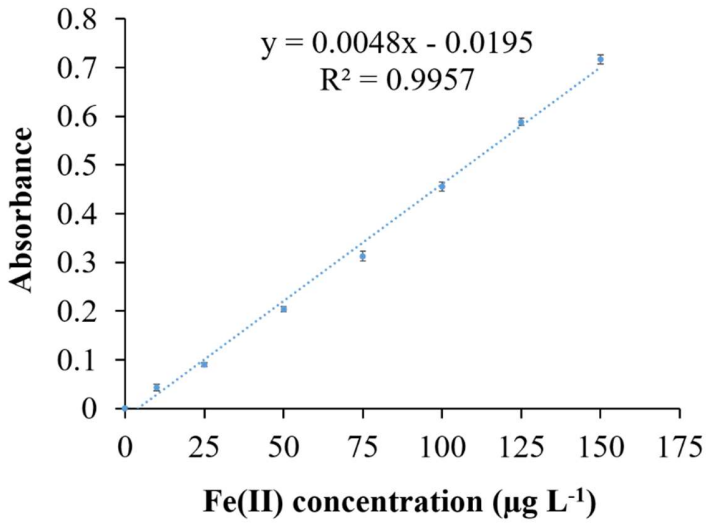

Fig. 7.5 a) Flow profiles of colorimetric determination of iron using the proposed optical system. b) Calibration curve of standard iron concentration obtained by using the proposed optical system.

Figure 7.5 a) presents the flow profile of 50, 75, and 100 µg L^{-1} of the Fe(II) solution using the proposed optical device within 90 seconds of analysis time. Figure 7.5 b) shows the calibration curve of iron analysis by plotting the Fe(II) concentration with the absorbance using the developed optical system. The analytical characteristics, precision, accuracy, and method validation were evaluated to confirm the ability of the proposed optical system.

7.3.2.1 Analytical characteristics of the developed method

From the calibration curve of the Fe(II) colorimetric determination presented in Figure 7.5 b), the linearity of quantitative analysis of Fe(II) was ranged from 10 to 150 µg L^{-1} of iron concentration. The linear equation was y = 0.0048x - 0.0195; $R^2 \geq 0.99$ (n = 3, standard deviation ≤ 1). The results of analytic parameters of the developed method such as

working range, detection limit (LOD), and quantification limit (LOQ) are presented in Table 7.4 with comparison the previous spectrophotometric method for iron determination using o-phenanthroline in tap water [14]. Also, the developed optical device was compared with the SOT optical device that was the same design without 1 wt.% of W-PDMS. The results showed that the wider working range was observed and LOD and LOQ of the developed optical system were 20 times lower than the previous method and the previously proposed K-PDMS optical device.

Table 7.4 Comparison of analytical parameters of previous spectrophotometric method, the proposed optical device using K-PDMS, and this proposed W-PDMS optical device.

Parameter	FIA with UV-Vis spectrophotometric method [14]	Black PDMS SOT-FIA module	This proposed SOT-FIA module
Working range ($\mu g\ L^{-1}$)	200-1,000	35-100	1.5-150
Detection limit ($\mu g\ L^{-1}$)	10	10	0.5
Quantification limit ($\mu g\ L^{-1}$)	35	35	1.5
Sample throughput (h^{-1})	120	120	120
Reagent consumption (mmol)	2.8	1.4	1.4

The power of LED light source in the detection system limited the enhancement of sensitivity that cannot reach increase for 46 times as mentioned above. However, the proposed method can improve the sensitivity for 20 times presenting in the LOD values. Thus, the iron determination using this developed optical system was better analytical performance compared to the previous research.

7.3.2.2 Accuracy of the developed method

The percentage of iron recovery was normally used for assessing of the accuracy of the method. 50, 75, and 100 µg L^{-1} of Fe(II) standard solution were added into 6 tap water samples and % recovery was calculated by comparison of the observed Fe(II) concentration recovered from the sample and nominal concentration.

Table 7.5 Percentage recovery of iron determination from drinkable tap water samples.

Drinkable tap water sample[a]	**% Recovery**		
	Fe(II) spiked concentration (µg L^{-1})		
	10	25	50
1	109 ± 2	100 ± 1	98 ± 1
2	107 ± 1	103 ± 1	101 ± 0
3	114 ± 2	107 ± 1	101 ± 1
4	105 ± 2	101 ± 0	99 ± 0
5	104 ± 1	108 ± 1	105 ± 1
6	104 ± 1	105 ± 1	99 ± 1

[a] Measured five times repeatedly for each sample (n = 5).

The results in Table 7.5 showed that % recovery was ranged from 98% to 114% which indicated that the results from the proposed method was accurate and reliable due to observing high % recovery.

7.3.2.3 Precision of the developed method

The precision of the method was assessed using intra-day variation which is the measuring results in the same day and inter-day variation which is the results on different conservative days. The six tap water samples were evaluated 5 times a day and 5 conservative days for intra-day and inter-day studies. % relative standard deviations (%RSD) were calculated for each replicate and the results are shown in the Table 7.6.

Table 7.6 Intra-day and inter-day variation of iron determination from drinkable tap water samples.

Drinkable tap water sample[a]	**Intra-day variation**		**Inter-day variation**	
	Mean ± SD	% RSD	Mean ± SD	% RSD
1	10.49 ± 0.10	0.96	10.64 ± 0.13	1.20
2	15.75 ± 0.18	0.94	15.69 ± 0.20	1.25
3	54.27 ± 0.14	0.25	54.79 ± 0.22	0.40
4	11.58 ± 0.10	0.87	11.70 ± 0.20	1.71
5	36.10 ± 0.07	0.19	36.21 ± 0.29	0.81
6	39.74 ± 0.11	0.29	39.90 ± 0.22	0.54

[a] Measured five times repeatedly for each sample (n = 5).

The %RSD of lower than 2% were presented in all cases of samples. Thus, the precision of the method was confirmed the stability and reproducibility of the proposed SOT-FIA optical system that can utilize in the chemical application.

7.3.2.4 Method validation

Table 7.7 presents the results of iron contents in the samples that were evaluated using the proposed method and the traditional spectrophotometric method (λ = 510 nm). The results from two methods were compared to the % deviation which showed that lower 3.5% of the % deviation was observed. Thus, there is no significant different results between the developed method and the conventional method.

Table 7.7 Validated results of the iron contents in drinkable tap water samples observed by the proposed optical system and a traditional spectrophotometric method.

Drinkable tap water sample[a]	**Fe(II) concentration (μg L^{-1})**		**% Deviation**
	UV-Vis spectrophotometer	FIA-SOT optical system	
1	10.28 ± 0.10	10.49 ± 0.10	2.05
2	15.54 ± 0.06	15.75 ± 0.15	1.38
3	53.36 ± 0.12	54.27 ± 0.14	1.70
4	11.22 ± 0.03	11.58 ± 0.10	3.20
5	35.08 ± 0.09	36.10 ± 0.07	2.93
6	38.40 ± 0.06	39.74 ± 0.11	3.49

[a] Measured five times repeatedly for each sample (n = 5).

This showed that the proposed optical system was validated and was able to use instead of the conventional spectrophotometric method with benefits of compact and potentially on-site analysis.

7.4 Conclusion

The rapid and simple on-demand fabrication using digital 3D printing with casting PDMS method was successfully demonstrated for development of the SOT-FIA optical device. The SOT structure of core transparent PDMS and cladding of carbon dispersed PDMS was enhanced the sensitivity of detection via adding the light scattering layer of the TiO_2 pigments in micron size dispersed in PDMS. The optical alignment for FIA system and the compact LED detection system was created and then printed via 3D printer to obtain the 3D printed mold and frame for fabrication of the developed optical device. The white pigment of the TiO_2 resulted in improvement of the optical sensitivity due to the scattering light effect of the TiO_2 particles. Also, the increase in detection length could enhance 38 to 46 times of the sensitivity of the detection. Due to the SOT concept, the ability of reduction of noise effect was confirmed that the interfered signal from the noise background of the measurement environment was lower than 1% in cases of comparison of the light room and the dark room. The proposed optical system using the handheld LED detection system was applied in real application of the FIA system for colorimetric determination of iron in drinkable tap water samples. Good analytical performances included wide chemical analysis range, low detection limit, and low quantification limit showed the developed optical system was highly sensitive

detection for trace chemical analysis. The abilities of high accuracy, good precision, and validation were also confirmed. This compact, simple fabricated, inexpensive, portable, and flexible optical device was achieved for chemical analysis application in trace level.

References

[1] H. Higuchi, H. Yoshioka, H. Nomada, Y. Oki, K. Morita, Carbon–polydimethylsiloxane-based integratable optical technology for spectroscopic analysis, Talanta. 166 (2015) 428–432.

[2] C. Malasuk, K. Nakakubo, S. Tsuru, H. Yoshioka, K. Morita, Y. Nakashima, Y. Oki, Silicone Optical Technology: Quasi Spatial Filter and Its Application for Multichannel Absorption Analysis, in: CLEO Pacific Rim Conf. 2018, Optical Society of America, Hong Kong, 2018: p. W3A.79.

[3] Y. Nakashima, M. Kounoura, C. Malasuk, K. Nakakubo, N. Watanabe, S. Iwata, K. Morita, Y. Oki, S. Kuhara, K. Tashiro, Y. Nakanishi, Continuous cell culture monitoring using a compact microplate reader with a silicone optical technology-based spatial filter, Rev. Sci. Instrum. 90 (2019).

[4] C. Malasuk, K. Nakakubo, H. Yoshioka, K. Morita, Y. Oki, 3D printing optical devices based on silicone optical technology (SOT) and its application on analytical chemistry, Opt. Components Mater. XVI. (2019) 66.

[5] C. Malasuk, K. Nakakubo, R. Ishimatsu, Y. Nakashima, H. Yoshioka, K. Morita, Y. Oki, Compact and on-demand 3D-printed optical device based on silicone optical technology

(SOT) for on-site measurement: Application to flow injection analysis, Rev. Sci. Instrum. 90 (2019).

[6] A.J. Capel, R.P. Rimington, M.P. Lewis, S.D.R. Christie, 3D printing for chemical, pharmaceutical and biological applications, Nat. Rev. Chem. 2 (2018) 422–436.

[7] M.R. Hartings, Z. Ahmed, Chemistry from 3D printed objects, Nat. Rev. Chem. 3 (2019) 305–314.

[8] M. Michalec, Ł. Tymecki, 3D printed flow-through cuvette insert for UV–Vis spectrophotometric and fluorescence measurements, Talanta. 190 (2018) 423–428.

[9] Y. Liang, Q. Liu, S. Liu, X. Li, Y. Li, M. Zhang, One-step 3D printed flow cells using single transparent material for flow injection spectrophotometry, Talanta. 201 (2019) 460–464.

[10] I. El Sharaa, K.S. El-turki, Iron determination of drinking water wells in Benghazi City, J. Res. Environ. Earth Sci. 3 (2017) 47–53.

[11] C. Steinbach, Titanium Dioxide - Material Information. https://www.nanopartikel.info/en/nanoinfo/materials/titanium-dioxide, 2020 (accessed 21 January 2020).

[12] S. Kawakubo, A. Naito, A. Fujihara, M. Iwatsuki, Field determination of trace iron in freshwater samples by visual and spectrophotometric methods, Anal. Sci. 20 (2004) 1159–1163.

[13] R.N.M.J. Páscoa, I. V. Tóth, A.O.S.S. Rangel, Sequential injection trace determination of iron in natural waters using a long-pathlength liquid core waveguide and different spectrophotometric chemistries, Limnol. Oceanogr. Methods. 7 (2009) 795–802.

[14] A.U. Rehman, A. Waseem, M. Yaqoob, A. Nabi, Flow injection spectrophotometric determination of total iron in fresh waters, using 1,10-Phenanthroline Reagent, J. Chem. Soc. Pak. 30 (2008) 836-839.

[15] C. Malasuk, R. Ishimatsu, K. Morita, H. Yoshioka, Y. Oki, Flow-through optical device based on Silicone Optical Technology (SOT) for determination of iron in drinkable tap water, Microchem. J. 157 (2020) 104897.

Chapter 8

Conclusion

Trend of devices in analytical chemistry has become small, portable, low cost, and versatile for on-site and real-time measurement applications. Thus, in this work focused on development of the miniaturized optical system using in the real applications of chemical and biological analysis. Based on the knowledge of silicone optical technology (SOT), the compact, lightweight optical device using for on-demand and on-site analysis with the optical properties of trapping the stray light and reduction of noise effect were proposed in various designs for the applications. The 3D printing technique with a simple coating and casting method was developed to fabricate the simple core/clad structure of SOT optical device. Thus, the SOT technology with digitally rapid fabrication of 3D printing was chosen for developing and improving of the FIA optical system to provide the benefits over the issues of large package, complex prototyping, and unavailable for on-site measurement. Hence, the objectives of this work are to develop SOT optical device for FIA system (SOT-FIA optical device) based on SOT concept, to evaluate the performance of SOT-FIA optical device as a low noise detection device, and to apply in FIA system for chemical and biological analysis.

The proposed compact microplate reader device was fabricated that consists of a 24 LED light sources, and 24 color sensors, and the SOT spatial filter in **Chapter 3**. The 24c-CMPL device was designed in the dimensions of culture microwell plate and fabricated by corresponding to SOT. The optical properties of the SOT spatial filter was investigated, and the results showed that the SOT spatial filter performed excellent ability to absorb the tiled incident light as interfered light form outside and the near LED light providing the low noise level detection. Thus, this device could perform monitoring of the culture environment in real time without any noise effect from the measurement environment by detecting changes

of cell behavior based on absorbance of 24c-CMPL device with high accuracy. The pH of the culture medium, changes in cell activity, and the ammonium concentration during the cell culture were successfully monitored without changing the culture cell environment using the fabricated device for biological application.

The first-time fabrication of a small, light-weighted, and flexible optical device by combining 3D printing and SOT-QSF planting for using in the analytical chemistry application to FIA system was proposed in **chapter 4**. The rapid and digital fabrication of silicone optical module was demonstrated by using 3D printable UV-cured-PDMS frame and injection coating of optical trapping layer. The facile coating method was demonstrated using syringe dispenser and the results of physical properties of coated surface showed proper and satisfied properties which able to use as the surface of optical channel. A simply fabricated SOT optical modules from 3D printed frame and coated quasi special filter showed 99.9% trapping performance on tilted light incidence, by introducing black PDMS internal baffles. This proposed SOT optical device provided the new idea for fabrication of the newly developed optical device using for FIA system.

In **chapter 5**, the design of SOT-FIA optical module was developed for more suitable use in real chemical analysis application by using a rapid digital 3D printing fabrication. The UV-curable silicone 3D printing was used for printing the optical module for the FIA system. A simple injection coating method performing the carbon black dispersed PDMS or black PDMS cladding and hand injecting method performing the transparent PDMS core were used to create the core and clad structure of the SOT theory. The coated surface of the black PDMS

was investigated that the coating process using syringe dispenser could provide the smooth and uniform surface that was suitable and appropriate to use as the optical channel. The optical properties of the fabricated optical module were confirmed that a 99.8% trapping efficiency for trapping tilted incident light was observed in case of adding black PDMS internal baffles and the noise effect was reduced to 0.5% observing in different environment of light room and dark room. The proposed optical device coupled with FIA system and compact LED detection system was applied in real application of iron determination in the natural water. The SOT-FIA optical device was ensured the robustness and chemical resistance with acid, base, and organic solution. The colorimetric assay of iron using o-phenanthroline reagent was performed showing good analytical performances with accurate chemical analysis. The proposed method was validated with the conventional spectrophotometric method. The results can indicate that the proposed SOT-FIA are potential use for chemical analysis with benefits of compact device for on-site measurement with low-noise detection.

The SOT-FIA optical module fabricated by following chapter 5 method was used as the optical device for biological application for determination of 3-phenoxybenzoic acid (3PBA) with its monoclonal antibody (anti-3PBA mAb) in **chapter 6**. A flow competitive enzyme-linked immunosorbent assay (ELISA) was proposed using enzymatic reaction of polyaniline in the presence of H_2O_2 and HRP benefited in shorten analysis time. The lighr absorption detection was demonstrated using the previous proposed optical device providing the advantage of low noise level detection. The absorbance changes by the enzymatic reaction was depended on the HRP concentration. In addition, the FIE competitive ELISA

was successfully investigated to confirm the ability of quantitative analysis of the 3PBA in range of 0.2 to 2 ppm concentration. The matrix effect of artificial urine showed no significant effect on the antigen-antibody interaction.

In **chapter 7**, the newly rapid and simple fabrication of SOT-FIA optical device was successfully developed using 3D printing and a simple casting method of PDMS. The 3D printing was used to fabricate the frame and mold for casting the SOT structure for application in FIA system. The TiO_2 pigment dispersed PDMS was used to create the optical scattering layer which could confirmed its optical property for enhancing the sensitivity of the detection. Also, the carbon black dispersed in PDMS as the optical trapping layer was used to cover the developed optical device for reducing the noise background. The sensitivity of the developed optical device was increased from 38 to 46 times compared to the calculation form Beer-lambert's law. The noise signal was lower than 1% assessing by the different signals between light room and dark room. The colorimetric determination of iron in drinkable tap water samples was investigated using the proposed optical device integrated with the FIA system and the handheld LED detection. It was confirmed that the developed optical system was able to monitor the iron contents in trace level analysis which good analytical characteristics overcome the previous spectrophotometric method. In addition, the accuracy and the precision of the method were guaranteed. The results of the iron contents in real samples were validated with conventional spectrophotometric method. The proposed compact and highly sensitive optical device was useful in real chemical application.

Acknowledgements

Firstly, I would like to express my sincere gratitude and deepest appreciation to my kind major advisor, Prof. Dr. Yuji Oki, who has given me the opportunity to do the research, valuable guidance, and warm encouragement throughout my doctor's degree study. Moreover, I am thankful for his kind support and advice in my life besides research.

I owe a deep sense of gratitude to my co-advisors, Asst. Prof. Dr. Hiroaki Yoshioka, our laboratory's teacher, Asst. Prof. Dr. Yuta Nakashima from Faculty of Advanced Science and Technology, Kumamoto University, and Asst. Prof. Dr. Ryoichi Ishimatsu from Department of Applied Chemistry, Faculty of Engineering, Kyushu university for their comments, kind suggestions, and assistance. Besides my advisor and co-advisors, my grateful appreciation is expressed to Prof. Dr. Kenshi Hayashi and Prof. Dr. Kazutoshi Kato from Graduate School of Information Science and Electrical Engineering, the external examiners of this thesis examination for their valuable discussion and suggestions, and also their kindness for spending valuable time for my thesis examination.

My sincere acknowledgements are extended to the scholarships from the Japan International Cooperation Agency (JICA) innovative Asia program, Japan Society and Technology Agency (JST), and Thailand Research Fund for monoclonal antibody production (No. TRG6080007) for the financial support of my doctor's degree study. I also wish to acknowledge Prof. Dr. Daisuke Nakamura of Kyushu University for experimental support with the scanning electronic microscope (SEM) and the Department of Electrical and

Electronic Engineering, Graduate School and Faculty of Information Science and Electrical Engineering (ISEE), Kyushu University for support of equipment and laboratory facilities.

I would like to give thanks to all members of Oki Laser Laboratory (Oki Lab), especially SOT group's members for support, training, suggestions, and friendship throughout my graduate study. I am also grateful to all Thai friends (Ruam Daek group), especially Dr. Chitiphon Chuaicham, Ms. Onchanok Juntarasakul, Ms. Nattanee Dechnarong, Mr. Rachanon Chaiuppala and Ms. Phatchada Santawaja in Ito campus and Chikushi campus of Kyushu University for their kind assistance, great friendship, and encouragement during my study.

Last but not least, I would like to express my endless gratitude to my dearest family for their unconditional love, encouragement and warm support throughout my life. Because of them, I always have passion to reach my goal and success.

Chacriya Malasuk